



QEX

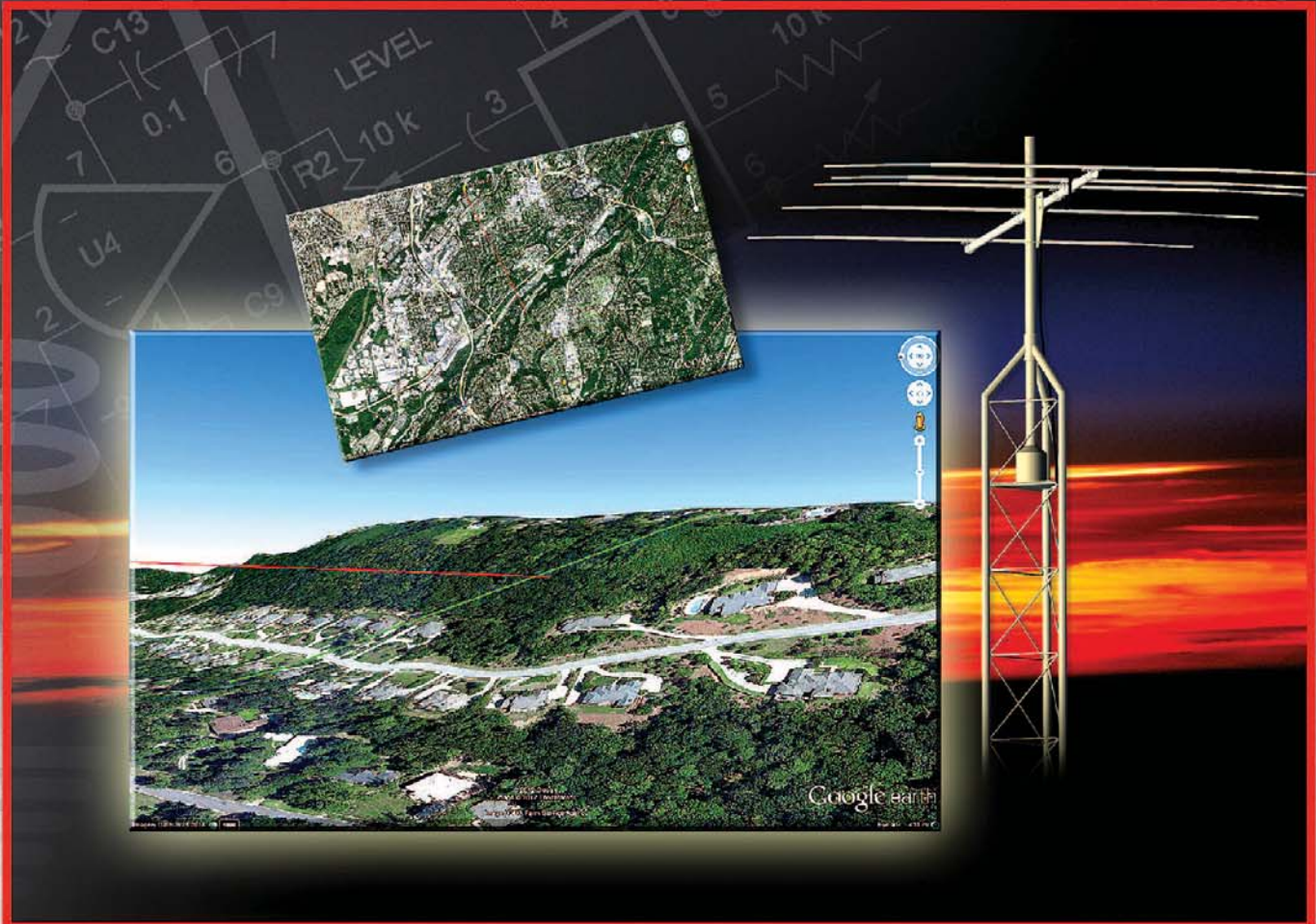
\$5

September/October 2013

www.arrl.org

A Forum for Communications Experimenters

Issue No. 280



WA4CWI uses Keyhole Markup Language programming to show us how to perform "Line of Sight Signal Path Analysis Using Google Earth." We can predict repeater coverage areas and simplex communications range with this powerful tool.

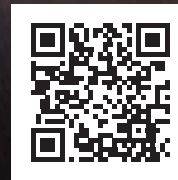
EVENT HORIZON OF DX TS-990S

Dual TFT Display & Dual Receiver HF/50 MHz Transceiver



The main receiver has an IP3 in the +40 dB class, and the sub receiver is the already famous TS-590S receiver. Capable of receiving two signals at once, on different bands. 7-inch and 3.5-inch color TFT displays allow displaying of independent contents. Simplification of complex operations at a glance. Make no mistake, this is not a toy. Finally a serious tool is available for getting the very most from your hobby, of course it's a Kenwood.

- Covers the HF and 50 MHz bands.
- High-speed automatic antenna tuner.
- USB, Serial and LAN ports.
- Various PC applications (free software): ARCP-990 enabling PC control, ARHP-990 enabling remote control, and ARUA-10 USB audio driver.
- Clean 5 to 200 W transmit power through the 50 V FET final unit.
- Built-in RTTY and PSK.
- Three Analog Devices 32-bit floating-point arithmetic DSPs.
- DVI output for display by an external monitor (main screen display only).



Scan with your phone to
download TS-990S brochure.

KENWOOD

Customer Support: (310) 639-4200
Fax: (310) 537-8235


www.kenwoodusa.com



ADS#11113



QEX (ISSN: 0886-8093) is published bimonthly in January, March, May, July, September, and November by the American Radio Relay League, 225 Main Street, Newington, CT 06111-1494. Periodicals postage paid at Hartford, CT and at additional mailing offices.

POSTMASTER: Send address changes to: QEX, 225 Main St, Newington, CT 06111-1494 Issue No 280

Harold Kramer, WJ1B
Publisher

Larry Wolfgang, WR1B
Editor

Lori Weinberg, KB1EIB
Assistant Editor

Zack Lau, W1VT
Ray Mack, W5IFS
Contributing Editors

Production Department

Steve Ford, WB8IMY
Publications Manager

Michelle Bloom, WB1ENT
Production Supervisor

Sue Fagan, KB1OKW
Graphic Design Supervisor

David Pingree, N1NAS
Senior Technical Illustrator

Carol Michaud, KB1QAW
Technical Illustrator

Advertising Information Contact:

Janet L. Rocco, W1JLR
Business Services
860-594-0203 – Direct
800-243-7768 – ARRL
860-594-4285 – Fax

Circulation Department

Cathy Stepina, *QEX Circulation*

Offices

225 Main St, Newington, CT 06111-1494 USA
Telephone: 860-594-0200
Fax: 860-594-0259 (24 hour direct line)
e-mail: qex@arrl.org

Subscription rate for 6 issues:

In the US: ARRL Member \$24, nonmember \$36;

US by First Class Mail: ARRL member \$37, nonmember \$49;

International and Canada by Airmail: ARRL member \$31, nonmember \$43;

Members are asked to include their membership control number or a label from their QST when applying.

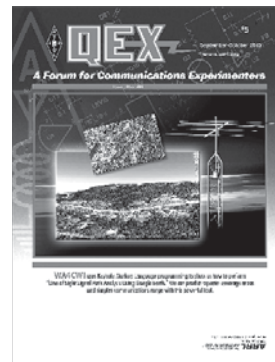
In order to ensure prompt delivery, we ask that you periodically check the address information on your mailing label. If you find any inaccuracies, please contact the Circulation Department immediately. Thank you for your assistance.



Copyright © 2013 by the American Radio Relay League Inc. For permission to quote or reprint material from QEX or any ARRL publication, send a written request including the issue date (or book title), article, page numbers and a description of where you intend to use the reprinted material. Send the request to the office of the Publications Manager (permission@arrl.org).

About the Cover

James McCullers, WA4CWI, uses Keyhole Markup Language (KML) programming to draw lines for “Line of Sight Signal Path Analysis Using Google Earth” images. He shows us how to predict repeater coverage areas and simplex communications range with this powerful tool. Google Earth 3D images clearly show mountains and terrain variations that can block line of sight signal paths.



In This Issue

Features

- 3 A 21 MHz Four Square Beam Antenna**
Garth Swanson, G3NPC
- 13 Frequency Synthesis and Impacts on Receiver Performance — Reciprocal Mixing and Blocking Dynamic Range**
Cornell Drentea, KW7CD
- 25 Frequency Dependence of Equivalent Series Resistance Measurement**
Dr Sam Green, W0PCE
- 28 Line-of-Sight Signal Path Analysis Using Google Earth**
Jim McCullers, WA4CWI
- 41 Blood Lead Levels in Australian Amateur Radio Operators—A Pilot Study**
Dr. Erich Siegfried Heinzle, VK5HSE
- 44 A Model for Sporadic E: Meteors+Wind Shear +Lorentz Force**
Flavio Egano, IK3XTV

Index of Advertisers

American Radio Relay League:.....	Cover III	Nemal Electronics International, Inc:.....	27
Arrow Solutions:	40	Quicksilver Radio Products.....	Cover IV
Down East Microwave Inc:.....	48	RF Parts:.....	43, 45
Kenwood Communications:	Cover II	Tucson Amateur Packet Radio:	27
National RF, Inc:	48		

The American Radio Relay League



The American Radio Relay League, Inc. is a noncommercial association of radio amateurs, organized for the promotion of interest in Amateur Radio communication and experimentation, for the establishment of networks to provide communications in the event of disasters or other emergencies, for the advancement of the radio art and of the public welfare, for the representation of the radio amateur in legislative matters, and for the maintenance of fraternalism and a high standard of conduct.

ARRL is an incorporated association without capital stock chartered under the laws of the state of Connecticut, and is an exempt organization under Section 501(c)(3) of the Internal Revenue Code of 1986. Its affairs are governed by a Board of Directors, whose voting members are elected every three years by the general membership. The officers are elected or appointed by the Directors. The League is noncommercial, and no one who could gain financially from the shaping of its affairs is eligible for membership on its Board.

"Of, by, and for the radio amateur," ARRL numbers within its ranks the vast majority of active amateurs in the nation and has a proud history of achievement as the standard-bearer in amateur affairs.

A *bona fide* interest in Amateur Radio is the only essential qualification of membership; an Amateur Radio license is not a prerequisite, although full voting membership is granted only to licensed amateurs in the US.

Membership inquiries and general correspondence should be addressed to the administrative headquarters:

ARRL
225 Main Street
Newington, CT 06111 USA
Telephone: 860-594-0200
FAX: 860-594-0259 (24-hour direct line)

Officers

President: KAY C. CRAIGIE, N3KN
570 Brush Mountain Rd, Blacksburg, VA 24060

Chief Executive Officer: DAVID SUMNER, K1ZZ

The purpose of *QEX* is to:

- 1) provide a medium for the exchange of ideas and information among Amateur Radio experimenters,
- 2) document advanced technical work in the Amateur Radio field, and
- 3) support efforts to advance the state of the Amateur Radio art.

All correspondence concerning *QEX* should be addressed to the American Radio Relay League, 225 Main Street, Newington, CT 06111 USA. Envelopes containing manuscripts and letters for publication in *QEX* should be marked Editor, *QEX*.

Both theoretical and practical technical articles are welcomed. Manuscripts should be submitted in word-processor format, if possible. We can redraw any figures as long as their content is clear. Photos should be glossy, color or black-and-white prints of at least the size they are to appear in *QEX* or high-resolution digital images (300 dots per inch or higher at the printed size). Further information for authors can be found on the Web at www.arrl.org/qex/ or by e-mail to qex@arrl.org.

Any opinions expressed in *QEX* are those of the authors, not necessarily those of the Editor or the League. While we strive to ensure all material is technically correct, authors are expected to defend their own assertions. Products mentioned are included for your information only; no endorsement is implied. Readers are cautioned to verify the availability of products before sending money to vendors.

Larry Wolfgang, WR1B

Empirical Outlook

Compatibility?

Are we compatible? Maybe the real question is, are we becoming more or less compatible?

Many of us have been involved in some aspect of the personal computer scene for many years. Perhaps you started learning about computers, as I did, by typing code statements on a key-punch machine that created a program deck of "IBM cards." These were fed to a terminal, which then linked to a remote computer that ran the program and returned a print-out of the results to a teleprinter machine. Eventually there were Sinclair, Commodore or Atari computers and cassette tape drives to store and run programs or data. Then came the now-famous Apple computers and the IBM Personal Computers, and some forms of disk operating systems with floppy disk drives. (I'm sure some readers have used floppy disks in all the variety of sizes, both physical and storage capability.) I guess the battle was on.

With any of those early "machines" you were pretty much limited to programs you wrote or that were designed for the particular hardware you were using. Deciding to build or buy a particular computer was determined mostly by what applications you wanted to run, and what software was available. The big choice became Apple or IBM, and while many companies began to assemble Personal Computers that used the IBM standards and ran some version of their disk operating system, the only way to get an "Apple compatible" computer that I am aware of was from Apple. Among the PCs, some sense of standards and compatibility began to sort out. While there were (and still are) arguments over which was better, more and more of the major software came with versions for either PC or Mac computers.

I won't claim that the two systems were becoming compatible, but graphical user interfaces moved us away from DOS commands and toward what for some, at least, is a more intuitive control system. On the Apple side, after they began using Intel processors, there has been a claim that Mac computers can run the *Windows* operating system or *Windows* (PC) programs directly. I took that into consideration recently when I had to upgrade my home computer and decided I liked many of the features of the iMac. What I have found so far, however, is that it may not be quite as simple as I was led to believe. Perhaps with some Apple tech support...

Of course there have been so many developments in personal computers in recent years. Laptops, Netbooks and various tablets (and even smart phones) have taken over many of the tasks that we used to depend upon our desktop computers to handle. With those developments come new variations. Now we have Android versus Apple and new Microsoft operating systems from which to choose. Will any of them play nice together? Certainly programmers are scrambling to write applications that will work on your choice of operating system, but at this point it seems to me that each requires its own version.

I don't know if the various systems are hardware specific, so whether each set of hardware requires the different operating system. For the manufacturers, there must be some advantage to the proprietary systems, but I think that for consumers there would be more advantages to being able to choose a particular operating system (at a specific time) for our favorite hardware, and perhaps being able to select a different operating system for that same hardware under other conditions. Is there any chance we could influence the market to go that way? Probably not, but we can dream, can't we?

We can follow similar progressions with our Amateur Radio equipment, where each manufacturer provides similar features with very different operating approaches. We learn to appreciate (or accept) one manufacturer's menu system over another, and so we often choose a radio based on how well we can navigate the various control features of the radio. One manufacturer's implementation of an operating protocol may provide features we like, but often to get the most out of that feature we are limited to other operators using the same manufacturer's equipment. Again I have to wonder if this is best serving the needs and interests of all Amateur Radio operators.

When we build our own equipment and program the microprocessors that control that equipment, we may be able to make our homemade equipment "play nice" with the commercial manufacturer's radios. I guess I am thinking here about APRS applications and the way several manufacturers have implemented features to use advanced features of the protocol, or with digital voice systems that would be compatible with D-Star, for example.

What do you think? Can we become more compatible?

A 21 MHz Four Square Beam Antenna

Achieving gain on 15 meters within a relatively small space.

The four square beam antenna is a square array of four vertical elements whose radiation pattern can be rapidly switched in direction by altering the relative phases of the four driving currents. The main beam relies on constructive interference of the signals from the elements where the relative phase of each is made up of the phase shift of the driving signal and the phase shift associated with the additional path length due to its spatial separation from the lead element.

At low frequencies where mechanical rotation is difficult for large structures phase control is an attractive possibility and is sometimes used on 80 meters. Typically, though not necessarily, the elements are positioned at the corners of a quarter wavelength square. At 21 MHz the antenna proves to be compact and can be easily accommodated in smaller yards and does not require a tower or a rotator. The array maintains the low angle radiation characteristic of a simple quarter wave vertical monopole but is able to manifest forward gain and reject noise and unwanted transmissions that would otherwise be received outside the main lobe.

This article considers design choices and explains how to design a practical feed system that takes into account the measured interactions between the four elements. The direction control system is also described. Far field measurements are presented that show the switched polar patterns to allow the actual performance to be compared with a theoretical model. A companion article in the September 2013 issue of *QST* presents a practical description of a 21 MHz four square antenna. That article can be found at www.arrl.org/this-month-in-qex.

Design Choices

A design requires a basic decision as to whether the array is to be broadside or diagonally firing; each requires a different set of driving currents. A first order comparison can be made by considering the simple summation of four unit-amplitude plane waves launched with the specified phases from the element locations. See Table 1.

Figure 1 shows the expected polar variations of power gain for broadside and

Table 1

Element Driving Current Phasings Required for Broadside and Diagonal Firing

	NW	NE	SW	SE
Broadside (S Firing)	0	0	-90	-90
Diagonal (NE Firing)	-90	-180	0	-90

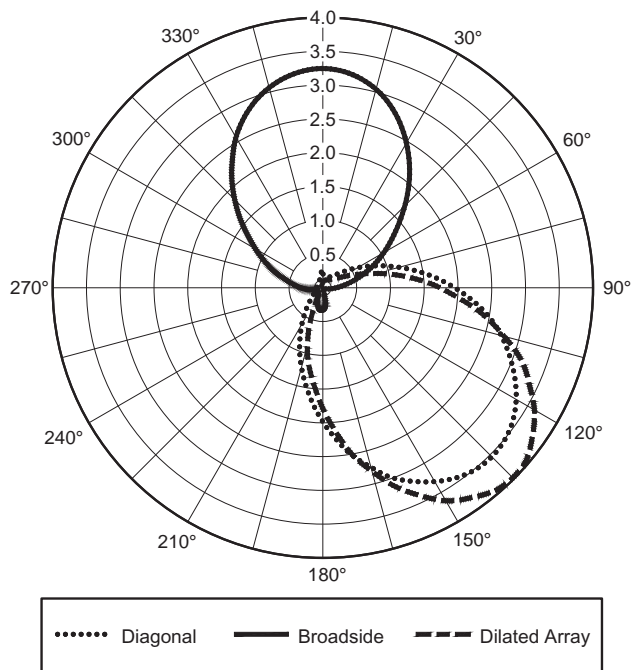


Figure 1 — A simplified comparison of the energy density (P) polar patterns of broadside and diagonally firing four square antennas based on a quarter wavelength square, showing the effect of dilation by a factor of $\sqrt{2}$.

diagonal firing from a quarter-wave square array. Diagonal firing gives about 10% more gain than broadside, but with a half power beamwidth of 90°, wider by 6°. Dilating the square by a factor of $\sqrt{2}$ makes the diagonal length an exact half wavelength and allows waves in that direction to perfectly reinforce. The dashed-line plot shows that this leads to a further increase of gain of about 10% and narrowing of the beamwidth to 84°.

In view of the limited space available, the extra space taken by the enlarged array and its slightly poorer reverse response, I decided to base a design on the smaller diagonally firing array bounded by a quarter-wave square.

The Antenna Array

The array was formed of four quarter wave vertical monopoles, each connected to its own set of quarter wavelength radials lying on the ground. See Figure 2. This basic element of the array was thoroughly characterized and reported in an article in the July 2011 issue of *RadCom*.¹ That study showed that a maximum radiation efficiency of 80% could be achieved with 13 or more ground radials. Purely for convenience, eight radials per monopole were selected for this design, reducing the radiation efficiency to 65%, equivalent to a small eventual loss of 0.9 dB. Figure 3 shows the parallel electrical response of one of the elements in isolation, with no coupling to its neighbors — this was ensured by open circuiting the neighboring driving points.

The design was centered on a frequency of approximately 21.2 MHz using monopole

elements adjusted to be resonant in isolation with a length of 3.34 meters. The side length of the array was 3.55 meters, a quarter wavelength in free space. In order to ensure as far as possible that the coupling between the elements was only electromagnetic, their radial systems were not connected directly to each other; each radial set was returned to its own ground mounting.

It is important to emphasize that because elements in an array interact electromagnetically their properties cannot be

considered to be independent of each other. Currents flowing in a particular element will induce voltages in its neighbors, causing components of current to flow in them and modifying any previously established terminal currents. The coupling between a pair of elements A and B can be expressed through a mutual impedance, Z_{ABm} . Equation 1 calculates the mutual impedance, Z_{ABm} , in terms of the measurements described below.

$$Z_{ABm} = \sqrt{Z_{BB} (Z_{AB} - Z_{AA})} \quad [\text{Eq 1}]$$



Figure 2 — The disposition of the elements, feeders and sets of eight quarter wavelength radials.

¹Notes appear on page 12.

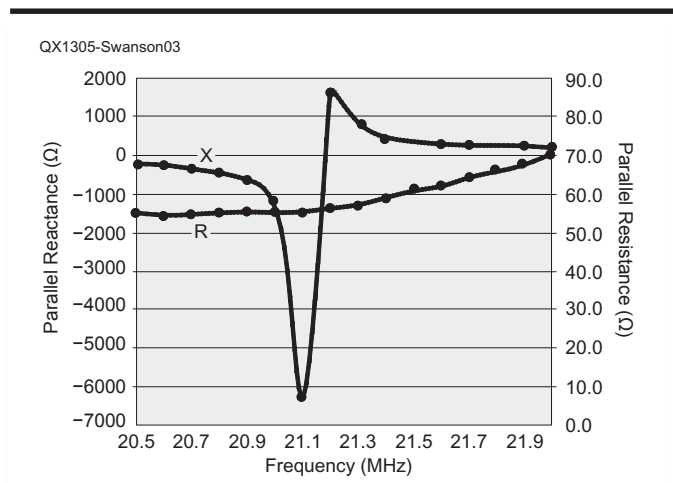


Figure 3 — The parallel electrical response of one of the elements with eight ground level radials when its three neighboring elements were open circuited.

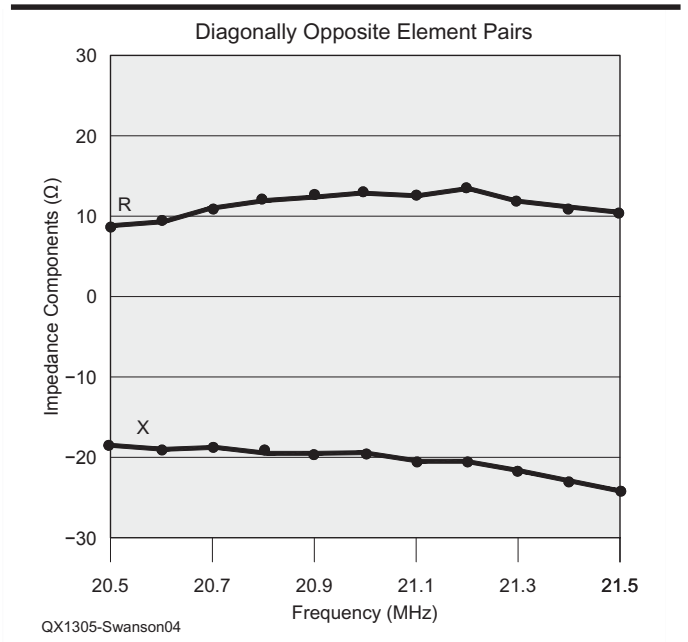


Figure 4 — Averaged measured components of the mutual impedance between pairs of diagonally opposite elements.

The inference of mutual impedances makes use of the principle of superposition, which permits its determination for a particular pair of elements in the absence of the others. As an example, if the mutual impedance between an element A and another element B is to be inferred, the driving point impedance of element A is first measured in isolation with all other driving points open circuited; this gives the value Z_{AA} . Likewise for Z_{BB} . Then Z_{AB} is the impedance of A in the presence of B alone, when the latter is short circuited at its driving point and all other elements are open circuited.

Clearly, coupling to an element A in an array of four requires the determination of Z_{AB_m} , Z_{AC_m} and Z_{AD_m} . A similar statement can be made when element B is considered, and in turn three more values have to be ascertained when each of elements C and D are considered. Three mutual impedance values must be ascertained for each element, a total of 12.

These parameters vary with frequency so the procedure has to be repeated at every frequency at which the mutual impedance is required. Actually the determination of the necessary values is less laborious than it sounds. If the four elements are identical in structure and tested at the same location then $Z_{AA} = Z_{BB} = Z_{CC} = Z_{DD}$ and if pairs A and C and B and D are diagonally opposite, their mutual impedances will be the same. The same reasoning is applicable to the side pairs. So one only needs to measure the isolated impedance values and ascertain the mutual impedances for an edge pair and a diagonally opposite pair. Of course this must be done at each frequency of interest.

The measurements were made with an MFJ-269 Antenna Analyzer remotely connected to the antenna by a length of RG58 coaxial cable, allowing the observer to stand well away from the antenna. The transforming effect of the coaxial cable was removed mathematically by taking into account its characteristic impedance, length, velocity factor and specific attenuation, all of which had been measured independently and found to be: 46 Ω , 10.52 meters, 0.657 and 0.06 dB/m respectively.

A spreadsheet allowed the raw data to be converted into the series elements of driving point impedance. Care was required in order to differentiate between positive(inductive) and negative(capacitive) reactance observations. Measurements were made point by point with frequencies set with an accuracy of ± 10 kHz. Figures 4 and 5 show the inferred components of the mutual impedances for diagonally opposite and edge pairs of elements. These are presented as averaged values; there were relatively small differences between the values obtained for

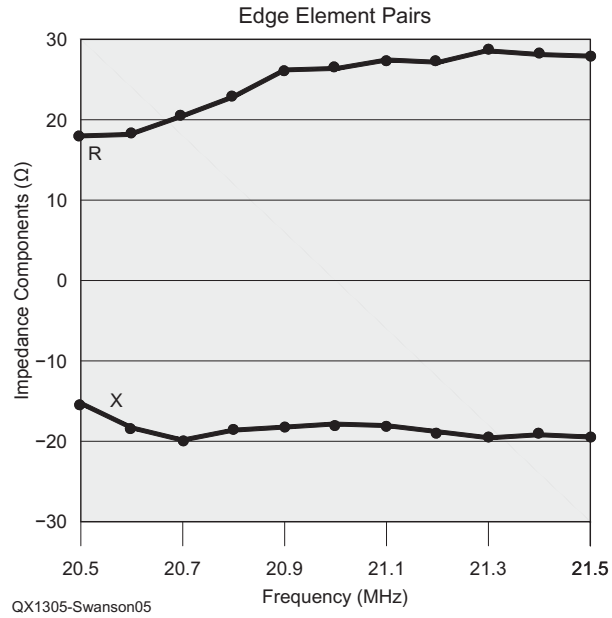


Figure 5 — Averaged measured components of the mutual impedance between pairs of elements at adjacent corners of the array.

particular pairs, perhaps because of small differences in their local environment. I used these averaged values in the design of the RF feed system.

The Feed System

A prerequisite for the design of the feed system of any antenna array is to know the driving point impedance of each element at the frequency of interest when every element is energized. The driving impedance of a particular element is affected by the mutual coupling with all other elements and is related to the mutual impedances by Equation 2, written here for element A.

$$Z_A = Z_{AA} + \frac{i_B}{i_A} Z_{AB_m} + \frac{i_C}{i_A} Z_{AC_m} + \frac{i_D}{i_A} Z_{AD_m} \quad [\text{Eq 2}]$$

Thus the impedance of an element is controlled by the currents in its neighbors, which are set by the required radiation pattern of the array. The problem then becomes how to deliver these currents into the four driving point impedances.

Systems for driving arrays have been reviewed by John Devoldere, ON4UN, in *Low Band DXing*.² A particularly straightforward method that has been chosen here is to make use of a transmission line of an appropriate length to transform the current feeding an antenna element into a voltage that can be preset at the feeder input. The method is sometimes called “current forcing,” because the length of the feeder, the

load impedance and the feeder input voltage completely define the voltage distribution along the feeder and at its termination. It is this terminating voltage that forces the required current to flow into the element driving point. The first step is to calculate the driving point impedances using the four complex currents necessary for a particular radiation pattern.

The four elements have to be individually driven and four separate feeders are needed to provide the transformations that deliver the complex currents required at the driving points. The necessary feeder input voltage will depend on its length. Al Christman, KB8I (now K3LC), pointed out that the feeders, having different lengths, could only be brought together at a common node if the four voltages were equal in magnitude and phase.³ In order to apply the Christman method, we need to be certain that points fulfilling these conditions will actually exist.

Based on the measured impedance parameters at 21.2 MHz, calculations of the four line voltage distributions have been made. Unit currents with the required phase shifts for diagonal firing will have defined the driving point impedances. The complex variations of line voltage are shown in Table 2. It is clear that in this case the magnitude and phase do not match simultaneously at any point. Having applied this method to a broadside firing four square array and a simple two element beam, the Christman method failed in those cases, too. John Devoldere also noted occasional failures of

the Christman method in *Low Band DXing*. See Note 2.

Nevertheless, the method provides a useful basis since points do exist here where the phases match well. These locations along the feeders are highlighted with bold type in Table 2. It requires only transforming the voltages at these equi-phase points to a unique voltage to be able to drive the four feeders from the same source. In this way the equi-phase and equi-voltage conditions would be met. This elaboration of the Christman method is novel and that is what I successfully implemented with my antenna.

Notice that the range of lower feeder lengths, up to 2.4 meters, is not useful because the cables would be too short to reach the four elements from a central point. Notice also that the two central, off axis, feeders require the same current, so only three feeder types are shown in this tabulation.

Table 2 shows the lengths of RG58 feeders that are required to establish the driving point current magnitudes and phase shifts for diagonal firing: they are 3.0 meters for the rear element, 5.2 meters for each of the central elements and 6.9 meters for the leading element. They will deliver the required complex currents to the element driving point impedances, which of course embody the mutual components arising from inter-element coupling. These impedances are shown in Table 3.

This design procedure is a key step in the design of this four square array. The modified Christman method has also been applied successfully to a practical two element design and theoretically to a broadside-firing four square array.

Arranging an Array Common Feed Point

Each element therefore has its own feeder with a length chosen so that it delivers the appropriate complex current to its element and has an input voltage that is in phase with the three other feeder input voltages. Because the feeder input voltage magnitudes differ, it is necessary to transform them to the same voltage, maintaining the same phase so that the array can be fed at a common node. The extent of the voltage adjustment is shown by Table 4.

There is a 3% difference in voltage between the required feeder input voltages for the rear and lead elements. The discrepancy is comparable with the accuracy of the calculations, so these feeder inputs could be simply paralleled. The two central element feeders have the same voltage and phase distributions, so their inputs can be paralleled together. These require a voltage about 20% larger, so scaling down was necessary and an

RF transformer was constructed to do this.

The combined impedance looking into the common feed-point must provide an acceptable match to the 50 Ω line from the transmitter, so not only was voltage scaling required but impedances needed to be scaled too.

An initial attempt to accomplish this using a transformer with two secondary windings was abandoned because it proved

very difficult to neutralize the inductive leakage reactances that were reflected from the secondaries to the primary winding to add to its leakage reactance. Because the two secondary windings shared the same primary winding there was an awkward interaction between the two neutralization steps.

It proved preferable to construct two transformers and to parallel their primary windings. The global leakage

Table 2

Voltage and Phase Along the Three Types of Feeder Showing the Locations of the Equal Phase Points in Bold Type.

Length(meters)	Lead Element Feeder		Central Elements Feeder		Rear Element Feeder	
	Mag	Phase	Mag	Phase	Mag	Phase
0	108.7	-135.5	68.8	-105.8	31.2	-88.2
0.2	112.2	-133.2	66.8	-100.6	24.7	-87.6
0.4	113.8	-131.0	64.1	-95.1	17.8	-86.5
0.6	113.5	-128.9	61.0	-89.0	10.5	-83.9
0.8	111.3	-126.6	57.5	-82.2	3.2	-69.4
1	107.2	-124.3	53.9	-74.4	4.6	75.8
1.2	101.4	-121.6	50.5	-65.6	12.0	84.7
1.4	94.0	-118.6	47.5	-55.5	19.1	86.8
1.6	85.1	-114.9	45.3	-44.2	26.0	87.8
1.8	75.2	-110.4	44.1	-32.0	32.4	88.4
2	64.5	-104.3	44.3	-19.5	38.2	88.8
2.2	53.7	-95.8	45.7	-7.4	43.3	89.2
2.4	43.6	-83.0	48.1	3.7	47.6	89.5
2.6	36.1	-63.9	51.3	13.6	51.0	89.7
2.8	33.5	-38.7	54.9	22.3	53.5	90.0
3	37.2	-14.2	58.6	30.0	55.0	90.3
3.2	45.3	3.7	62.2	36.7	55.6	90.5
3.4	55.6	15.6	65.4	42.8	55.1	90.8
3.6	66.6	23.7	68.0	48.3	53.6	91.2
3.8	77.2	29.5	70.1	53.6	51.2	91.5
4	87.1	33.9	71.4	58.5	47.8	92.0
4.2	95.8	37.6	71.9	63.4	43.5	92.5
4.4	103.1	40.6	71.6	68.3	38.5	93.2
4.6	108.7	43.4	70.6	73.3	32.7	94.2
4.8	112.6	45.9	68.8	78.5	26.4	95.6
5	114.7	48.3	66.4	84.1	19.6	98.0
5.2	114.8	50.7	63.4	90.2	12.6	103.1
5.4	113.1	53.1	60.1	96.9	5.6	121.2
5.6	109.5	55.7	56.6	104.5	4.0	-137.1
5.8	104.2	58.5	53.2	113.1	10.6	-105.8
6	97.2	61.7	50.2	122.8	17.7	-99.0
6.2	88.8	65.5	47.9	133.6	24.6	-96.1
6.4	79.3	70.2	46.6	145.3	31.0	-94.4
6.7	63.7	80.0	46.8	163.4	39.7	-92.9
6.8	58.5	84.4	47.5	169.3	42.2	-92.5
7	48.6	96.1	49.6	-179.5	46.7	-91.8
7.2	40.9	113.1	52.5	-169.4	50.4	-91.2
7.4	37.3	135.4	55.9	-160.5	53.1	-90.6
7.6	39.3	158.7	59.5	-152.6	54.9	-90.1
7.8	46.1	177.4	63.0	-145.6	55.6	-89.6
8	55.5	-169.4	66.3	-139.2	55.4	-89.0
8.2	66.0	-160.2	69.0	-133.4	54.2	-88.5
8.4	76.5	-153.6	71.2	-128.0	51.9	-87.8
8.6	86.4	-148.5	72.6	-122.8	48.8	-87.1
8.8	95.3	-144.4	73.3	-117.8	44.7	-86.2
9	102.8	-140.9	73.2	-112.7	39.9	-85.1
9.2	108.8	-137.9	72.4	-107.6	34.3	-83.7
9.4	113.1	-135.1	70.8	-102.3	28.2	-81.7
9.6	115.5	-132.4	68.6	-96.7	21.6	-78.3
9.8	116.2	-129.8	65.9	-90.6	14.7	-72.0
10	114.9	-127.2	62.7	-84.0	8.1	-54.7

Table 3
Calculated Driving Point Impedances for Diagonal Firing.

Element	Driving Point Impedance (Ω)
Leading	77.5 + j76.2
Central(off-axis)	66.2 - j18.7
Rear	1.0 - j31.1

reactance of each could be independently neutralized, ensuring that phase shifts in both transformers were zero. The ratio of their secondary turns was determined by the required voltage scaling ratio, in this case, nominally, 0.84. The absolute number of turns in the secondary windings was then determined by the number of primary turns. In practice 20 turns were selected for each transformer because these fit conveniently onto the chosen ferrite toroids. The numbers of secondary turns for the two transformers were then adjusted mathematically to achieve a suitable value for the paralleled primary reflected impedances, always preserving the required ratio between the two secondaries. This procedure led to a common node input impedance of (51 - j29) Ω . The details of the transformers are shown in Table 5.

The transformers were constructed on Type 61 ferrite toroids having an outside diameter of 6 cm and an inside diameter of 4 cm. The primary windings were formed from a single strand of 22 SWG enameled copper wire and the secondaries were of four plaited strands of the same wire wound compactly onto the toroid in the same sense and interleaved with the primary turns. [Note that SWG is British Standard Wire Gauge, with a wire diameter of 0.028 inch. This is roughly equivalent to number 21 American Wire Gauge (AWG), with a diameter of 0.0285 inch. — *Ed.*] Care was taken to begin the ground ends of the two windings at the same position. This helped to minimize the local potential differences between the windings, ensuring that capacitive currents between the windings were minimized. The table shows that more primary turns were required than had been anticipated by a simple view of transformer design. This could be due to winding end effects where the end turns coupled inefficiently to the core. Careful adjustment of the number of turns was made as measurements checked the open circuit voltage ratio. Small errors in achieving the specification are due to an inability to realize fractional turns.

Figure 6 shows the interconnection of the two transformers and the placement of series preset 150 pF neutralizing capacitors. With the secondary short circuited, an oscilloscope was used to observe the primary voltage and current waveforms, and the neutralizing capacitor was adjusted until they

Table 4
Electrical Parameters at the Equal Phase Points.

Position of Feed Point (meters)	Lead Feeder		Central Feeder		Rear Feeder	
	(V)	(degs)	(V)	(degs)	(V)	(degs)
3.0					55.0	90.3
5.2			63.4	90.2		
6.9	53.5	90.3				
Input Z of feeder (Ω)	16.6 - j15.5		46.3 - j21.3		21.0 - j161.6	

Table 5
Details of the Two Transformers Used for Voltage Scaling and Impedance Matching.

	Theoretical Designs		Actual Designs	
	Lead/Rear	Center	Lead/Rear	Center
Primary Turns	20	20	23	23
Secondary Turns	8.4	10	8	10
Combined Input Z	51 - j29 Ω			
OC Voltage Ratio	2.4	2.0	2.3	2.0
	Required	Required	Measured	Measured

Table 6
The Hybrid Ground Electrical Parameters Used for Simulation.

	Relative Permittivity	Electrical Conductivity (S/m)
Inner zone	73	0.75
Outer zone	42	0.088

Table 7
The Actual Drive Currents.

Beam Heading	Measured Elemental Drive Currents (Normalized Magnitude and Phase Angle With Respect to the Rear Element)			
	NE	SE	SW	NW
NE	1.0, -180°	0.67, -90°	1.0, 0°	0.77, -90°
SE	0.93, -105°	1.04, -165°	0.89, -90°	1.0, 0°
SW	1.0, 0°	0.69, -97°	0.97, -192°	0.70, -90°
NW	0.86, -90°	1.0, 0°	0.71, -90°	1.07, -180°

were in phase. The procedure was repeated for the second transformer; there was no interaction between these adjustments. The attenuation of each transformer was about 1.2 dB, equivalent to an efficiency of 76%. The paralleled connection of their primaries provided the driving point of the array.

The actual complex currents flowing into the four elements for the four different beam headings are shown below in Table 7 and discussed later.

The Direction Control System

Figure 7 shows the topology of a switching matrix for routing the three possible phase-shifted feeds to the appropriate elements for a particular direction of fire. The switches used were RF latching reed relays with

a carry current of 1.5 A and a switching time of 2 ms. They were chosen because of their ability to maintain a particular setting without being continuously energized and because they were hermetically sealed and suitable for operation outside. The switches had an actuation current of 16 mA, suitable for control by TTL pull-down devices. This matrix was built on glass-epoxy strip board.

The switch module required five control lines, one to reset the entire switch array and four to select the directions of fire. The direction control lines were routed to the inputs of 2-input NOR gates that energized the appropriate switches for a chosen firing direction. Energy for the switches and NOR gates was supplied by a 9 V battery from a hand held remote controller.

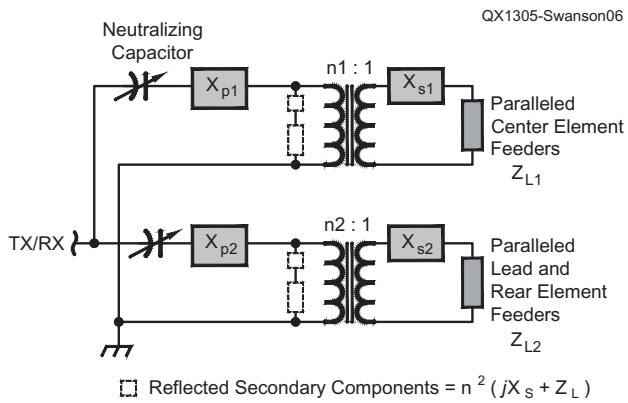


Figure 6 — The interconnection of the feeder transformers.

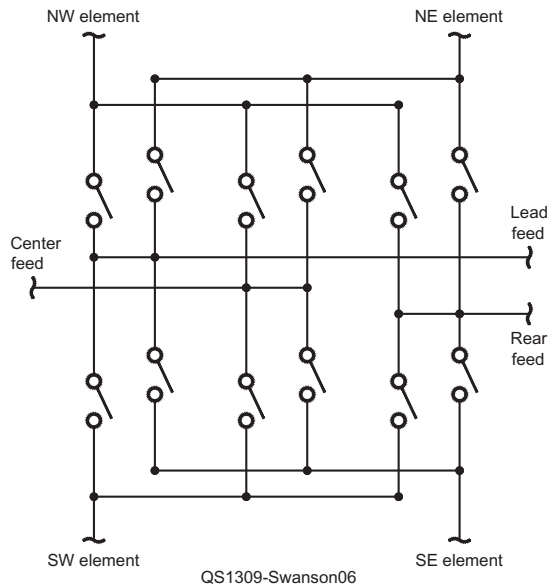


Figure 7 — The router switch array.

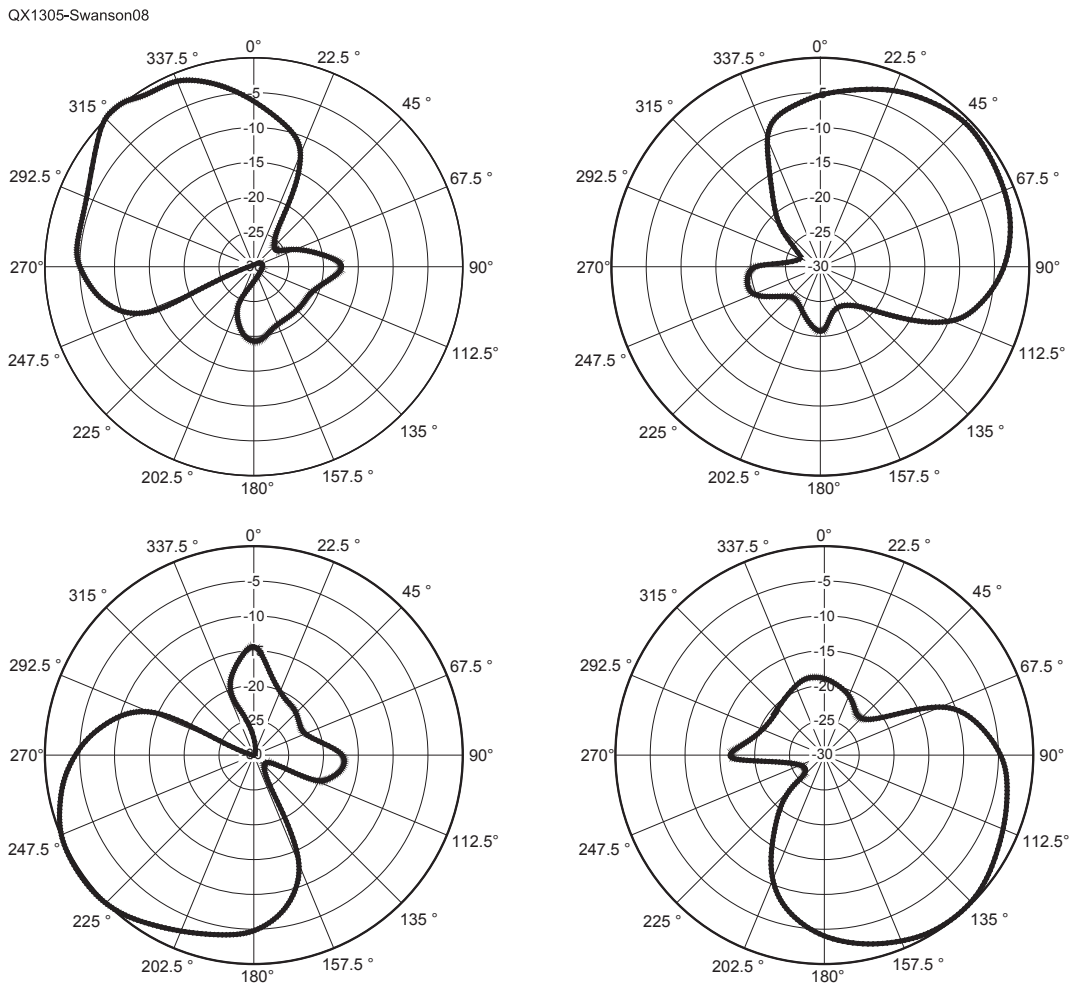


Figure 8 — Measured polar radiation patterns for the four diagonal beam headings.

The antenna design depends critically on transmission lines that have definite lengths, 3.0 meters, 5.2 meters and 6.9 meters. Locating the switching module centrally required that the lengths of the feeders connecting the switch module to the elements should be no less than 2.5 meters, leaving lengths of 0.5 meters, 2.7 meters and 4.0 meters between the module and the common driving point. The latter lengths of feed line were housed with the switch matrix and transformer power splitter modules in a weather-proof box located on the ground centrally between the elements.

The beam is steered by resetting the switches and then briefly energizing the appropriate direction control line to set the required switch configuration. All switching is carried out in the absence of RF excitation to avoid the possibility of contact damage caused by arcing. The system has been in use for two years without any degradation. In principle, the direction of fire could be changed in as little as 4 ms.

The overall measured RF loss from the power splitter output to the elements via the switching matrix was no greater than 0.8 dB and depends slightly on the selected direction. Thus, from the power splitter input to the element inputs there is a loss of about 2 dB, a feed system efficiency of 63%. Since the elements each have a radiation efficiency of about 70% the effective radiation efficiency of the antenna array measured at its feed point is 42%.

Directional Behavior

Polar radiation patterns of an antenna should be measured in the far field of the antenna so that phase differences between signals arriving from parts of the antenna that are off axis are small compared with the phase shifts that would have occurred had they been on the axis. If Δ is the off-axis deviation and R is the range, the phase error in degrees is given by Equation 3.

$$\text{Phase Error (Degrees)} = \frac{180 \Delta^2}{\lambda R} \quad [\text{Eq 3}]$$

The site available for these measurements allowed a range of 38 meters. For this four square array at 21.2 MHz, the maximum phase error at this distance would be no more than 2°. Distortions in the pattern to be measured would therefore be negligible.

Stations were established at 22.5° intervals at a radius of 38 meters from the array center. Measurements were made using a tripod mounted field strength meter with a dynamic range of 90 dB. At each location in turn the received signal — a relative measure of the signal strength — was recorded for each of the four beam headings, with good reproducibility.

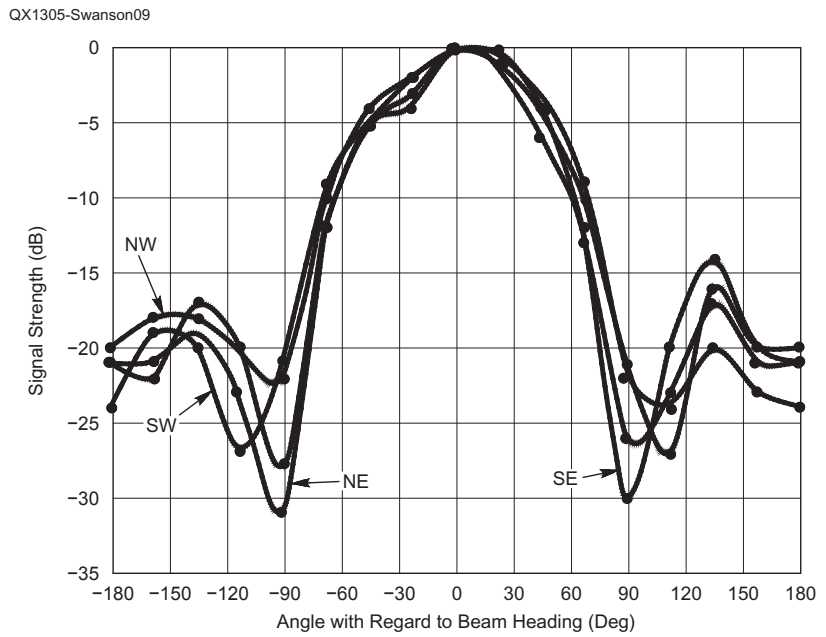


Figure 9 — The four measured patterns overlaid for comparison.

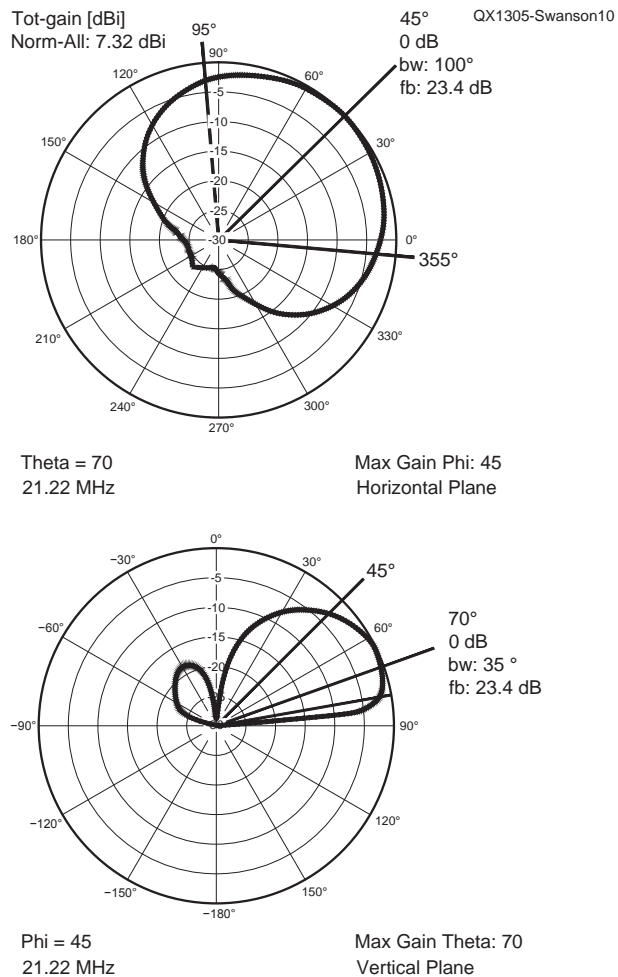


Figure 10 — Computed ideal radiation patterns on the hybrid ground with perfectly defined driving currents.

Figure 8 shows the observed polar patterns for each beam heading. Each is formed from sixteen measured points and data smoothing has been used to help visualize the patterns. Caution is required in interpreting some of the finer angular detail. They are very similar and show clear evidence that switching occurred as intended. They are plots of relative field strength and do not reveal

that the maximum signal strength at each diagonal angle was actually the same, ± 1 dB. The front to back ratio for each pattern was at least 20 dB. These are logarithmic plots, which intrinsically exaggerate detail in the rear sectors; remember that these features are about a hundred times smaller than the main lobes. The half-power beamwidths were about 90° in each case, very close to that

anticipated from a first order analysis earlier in this article. See Figure 1.

Figure 9 represents the superimposed data on rectilinear axes to aid comparison. There is significant and consistent detail in the rear sector. The overall impression is of similarity in the main lobes for the four beam headings.

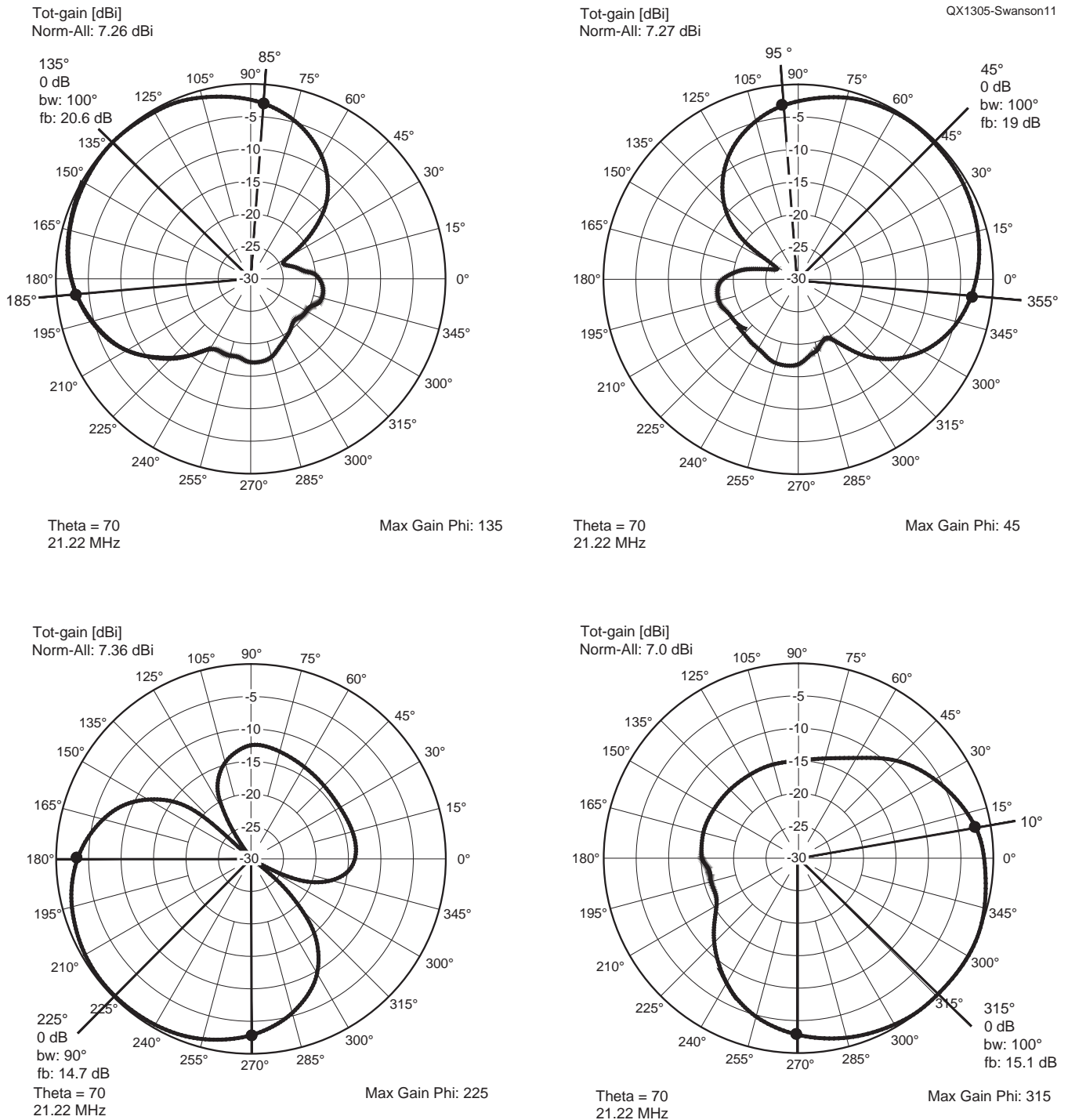


Figure 11 — Computed radiation patterns with the actual driving currents using the hybrid ground. These are all horizontal plane radiation patterns.

Simulation and Modeling

A valid computer model allows experiment and refinement without the effort and time involved in making alterations and new measurements. The *4NEC2* package based on the *NEC2* electromagnetic modeling code offers the advantage of setting current as well as voltage excitations, and is freely available.

The model of the four square antenna that is used here is built on the behavior of independent monopoles, each with their own set of radial wires lying on the ground. This basic unit has been thoroughly characterized and was described in my July 2011 *RadCom* article. See Note 1. Because the *NEC2* code cannot model structures with ground based radial conductors, the ground system has been modeled as a hybrid ground with two concentric ground regions, each with defined electrical parameters. It is convenient that modeling of hybrid concentric grounds is a feature of *4NEC2*.

The electrical parameters of the outer zone, extending to infinity, were obtained by measuring the terminal parameters and resonance frequency of one of the monopoles without any radials at all. Optimization was carried out using the simulator to adjust the ground parameters until the required terminal parameters were obtained. See Note 1.

The central region, a quarter wavelength in radius, is made quasi-metallic by the radials. The optimizer was used again, in this case with the two-zone model, to adjust the parameters of this inner zone until the measured terminal impedance of the element with its eight radials was obtained,

the outer zone parameters being set at the values that had already been determined. The appropriate two-zone parameters for the hybrid ground are stated in Table 6. They represent the behavior of the monopole with eight radials operating at 21.2 MHz on the imperfect ground.

Figure 10 shows the computed behavior of the antenna on the hybrid ground when driven with a perfectly defined set of drive

currents. It provides a basis for comparison when the actual currents were used. The actual complex drive current for each element was measured at each directional setting and used in the simulation to arrive at calculated polar patterns for the four directions, again on the hybrid ground. The normalized currents, which sometimes deviated from the intended values, are listed in Table 7.

The modeled polar patterns using the

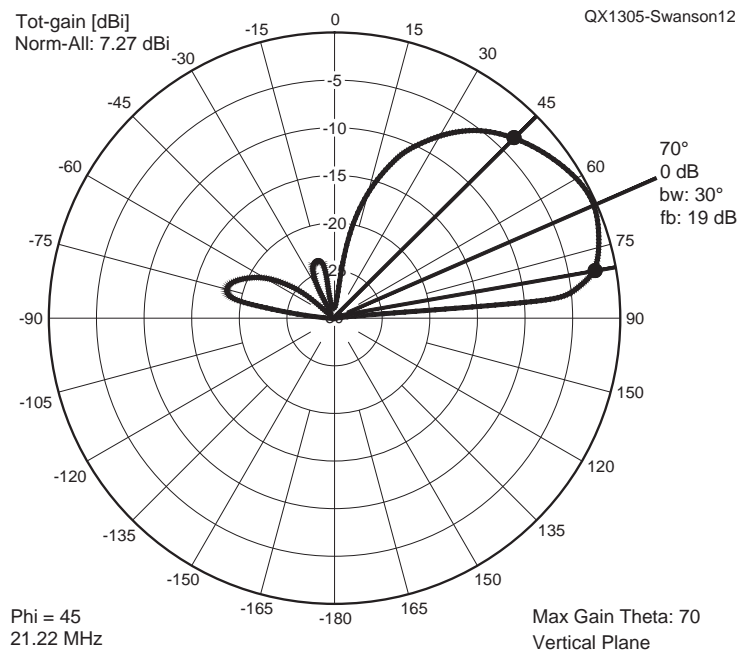


Figure 12 — Computed vertical radiation pattern with the actual driving currents using the hybrid ground.

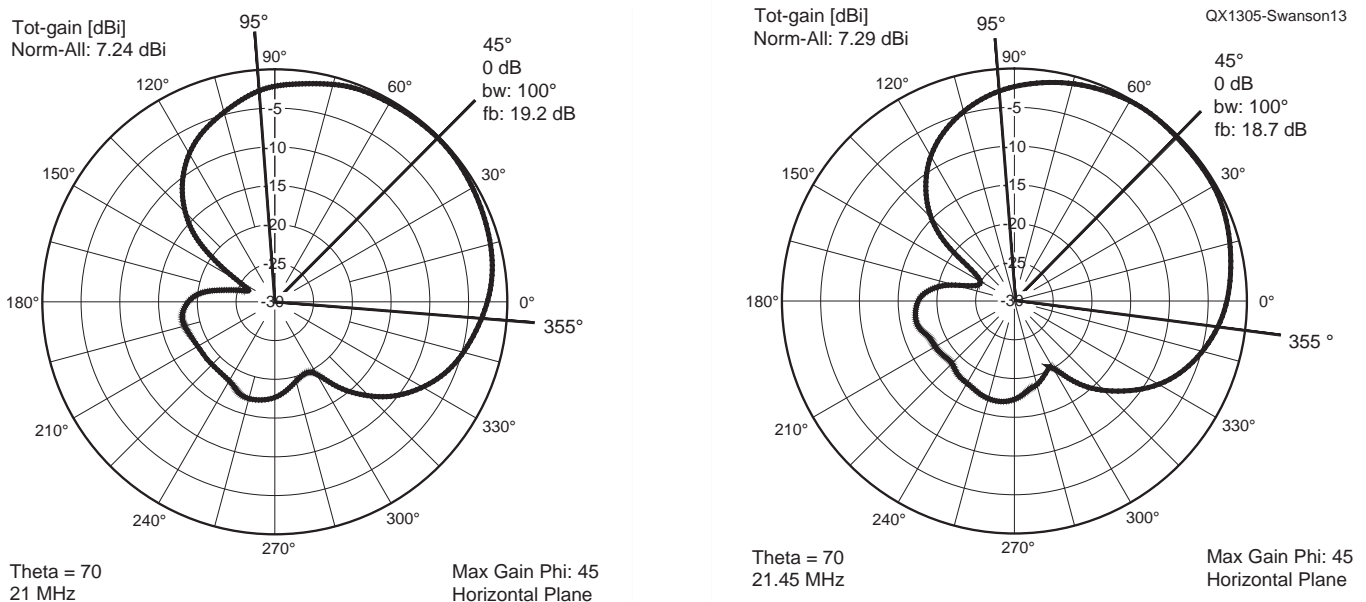


Figure 13 — The computed horizontal radiation patterns at the extremities of the 21 MHz band using the hybrid ground.

actual drive currents are shown in Figure 11. There is good agreement between these and the measured plots shown in Figure 8. The front to back ratios span the range from 20.6 to 14.7 and are somewhat smaller and less consistent than the actual values. See Figure 8. The beamwidths are in very good agreement with the measurements. Predicted, but not measured, are the forward gains; these are very similar for the four directions, ranging between 7.00 and 7.36 dBi.

The simulation also provides the elevation of the main lobe above the horizon. Although the only pattern presented here — Figure 12 — is for the NE direction the elevation is close to 20° for all beam headings, with a half power vertical beamwidth of 35°.

A very useful indication of the insensitivity to frequency as the 21 MHz band was traversed is provided by the two NE polar patterns shown in Figure 13. This 2% change of frequency caused a change of only 0.5 dB in the front to back ratio and a negligible change in gain of only 0.05 dB.

Discussion

The antenna behavior on the hybrid ground, but with a perfect set of drive currents, provides a basis for discussion. See Figure 10, which shows that the forward gain is 7.32 dB, the highest attainable value on this practical ground. The behavior in the rear section is determined by the degree of cancellation of the fields from the four elements. It is here that small differences between the field components become apparent and reflect imperfections in the array and its feed system that result in errors in the drive currents.

Despite the discrepancies between the actual drive currents and those intended, they were used in the simulation and the predicted gain values come close to the maximum attainable on the hybrid ground. Compare Figures 10 and 11. The observed front to back ratios were at least 20 dB on this ground and Figure 10 suggests that an improvement by 3 to 4 dB might be achievable. Although appreciable, it is questionable if this improvement would have practical value when the ratio was already 20 dB. It is interesting to note that with a perfectly defined set of drive currents and a perfect ground the best possible gain and front to back ratio would be 10.8 dBi and 29.8 dB.

In Table 5 the off-axis element drive currents are highlighted. They are invariably low compared with the on-axis elements. It should be relatively easy to correct this by increasing the number of secondary turns of

the appropriate transformer and should lead to an improved front to back ratio. This will undoubtedly disturb the transformation of the central element feeder impedances, however, and measures will be needed to ensure that the transformed impedances combine in parallel to approach 50 Ω.

Harder to understand are the off-axis current asymmetries. These elements are driven from the same secondary winding through two feeders that have the same lengths and should deliver very similar drive currents. The asymmetries are not reversed or replicated when the beam heading is oppositely directed. Had they been due to different local environments for the pair of axis elements the asymmetry would have persisted when the feeders were interchanged, but this did not occur.

No account was taken in the design of the delays introduced by the switching matrix. Although they would be relatively small, the path lengths through the matrix were not equal for the four signals and depended on the pattern of switch closures. It is possible that this is a source of asymmetry and a careful study of these pathways is needed.

There are strong indications from modeling on a practical ground that the forward gain is between 7 and 8 dBi, but this needs to be confirmed by measurement and will require reference to a standard antenna.

Conclusions

An electronically steerable four square phased array antenna has been realized for use at 21 MHz. The antenna has a diagonal fire configuration with a main beam that can be switched rapidly to one of four orthogonal directions. The antenna makes use of a novel feed system that uses two RF transformers to ensure that the element feeders are driven with the same voltage and phase. The overall loss from the array feed point to the element inputs was 2 dB. This elaboration of the Christman method allows it to be used universally in situations where only equi-phase points exist on the set of feeders.

On an imperfect practical ground the antenna achieved a measured front to back ratio in excess of 20 dB — a value consistent with listening and on-air use that showed differences of between 3 and 4 S units. I have not yet measured the forward gain; however, based upon computer modeling using a hybrid model to represent the practical ground, its gain is estimated to be 7 to 8 dBi. The horizontal and vertical half power beamwidths are 90° and 35° respectively with a vertical beam elevation of 20°. Modeling has also predicted that the

antenna characteristics vary only slightly across the operating bandwidth of 0.45 MHz at 21 MHz. The directional properties of the antenna accorded well with computer modeling, which points the way to further improvement.

The performance of another four element beam, the four-element Yagi, provides an interesting comparison. Modeling of the Yagi indicates a gain of 11 dBi, a front-to-back ratio of 20 to 25 dB and a half power beamwidth of 60°.⁴ Practical corresponding values claimed for the four element 21 MHz SteppIR antenna are 10.2 dBi, 27 dB and 60°.⁵

In comparison with the Yagi, the diagonally firing four square antenna at 21 MHz is likely to have a gain 2 to 3 dB lower; it has a similar FB ratio and a half power main beamwidth that is 30° wider. While there is scope for further refinement of this implementation of the four square antenna it is doubtful if the resulting improvements would significantly affect the gain and beamwidth but could improve the observed front-to-back ratio by 3 to 4 dB.

J. Garth Swanson was born in 1941 and obtained a full transmitting license at the age of 16. He graduated from Imperial College London with a BSc (Engineering) in 1963 where he was awarded a PhD in Electrical Engineering in 1967.

He then worked at the Westinghouse Research Laboratory in Pittsburgh, PA for four years, working on thin film electronic devices. On returning to the UK he spent a year in industry and then moved to a career in academia. Garth eventually became chairman of the Electrical Engineering department at King's College in the University of London, where he was a Professor of Physical Electronics with research interests in electronic and optoelectronic materials. He has spent two sabbatical periods at French research laboratories. On his retirement in 2001 he became Professor Emeritus at King's College and has pursued an interest in phased array HF antennas.

Notes

¹Garth Swanson, G3NPC, "The Ground Mounted Quarter Wave Vertical Antenna," *RadCom*, July 2011, pp 60-64.

²John Devoldere, ON4UN, *Low-Band DXing*, 2nd edition, ARRL, 1995.

³Al Christman, KB8I (now K3LC), "Feeding Phased Arrays — An Alternate Method," *Ham Radio*, May 1985, p.58.

⁴ARRL *Antenna Book*, 16th edition, 1991.

⁵SteppIR Antennas Inc, 2112 116th Ave NE, Bellevue, WA, USA. www.steppir.com/ 4-element-yagi

Frequency Synthesis and Impacts on Receiver Performance — Reciprocal Mixing and Blocking Dynamic Range

A top expert in the field of receiver design performance explains some important receiver performance measurements.

The topic of reciprocal mixing and phase-noise-limited minimum discernible signal (MDS) has been a confusing and controversial subject for many years. Analysis in this area has been very limited. Most of what has been reported is “test results” rather than a complete design approach to the problem.

In this article, we will attempt to explain how synthesizer composite phase noise and spurious problems affect the dynamic range performance of receivers from a designer’s point of view. We will begin with the reciprocal mixing, which is caused by the phase noise impacts on the minimum discernible signal and will conclude with a brief discussion on the blocking dynamic range (BDR). I hope that this material will be beneficial to amateur receiver and transceiver builders, as well as to professional RF engineers involved in commercial or military receiver or transceiver design.

Introduction

If you ever looked at a modern superheterodyne receiver test report, you probably noticed on occasion the statement: “MDS — phase noise limited.” This means that the minimum discernible signal cannot be tested because the phase noise of the receiver overwhelms the sensitivity of the radio. You probably questioned how one can prevent this from happening before

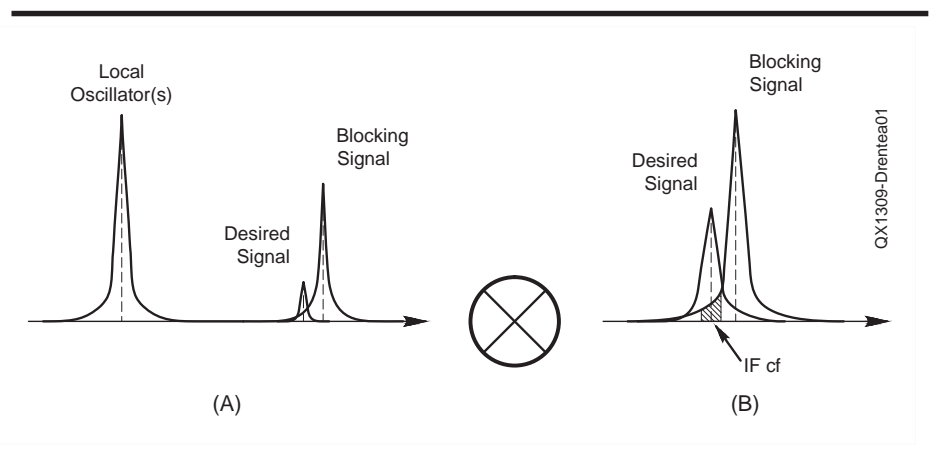


Figure 1 — Reciprocal mixing occurs when the phase noise from any or all local oscillators in a receiver mix with a strong adjacent blocking signal, and its phase noise sidebands, as shown in Part A. The resulting IF signal is blocked at the receiver’s MDS level as shown in the shaded area of Part B.

a receiver design becomes a reality. The answer is rather complex and it depends on the particular implementation of the receiver, but especially its synthesizer. The final results will depend on how much phase noise (PN) performance is delivered by each of the local oscillators (LO) in the synthesizer. This phase noise is injected into the mixers, and is then translated into the IF (or IFs) bandwidth of interest. In a well designed receiver, it is essential that all LOs

be equal in their phase noise performance otherwise the worst one will prevail, blocking signals at the MDS.

To combat the above problem, certain topologies and design choices have to be considered early in the planning stages of designing the receiver and its synthesizer. The phase noise requirements for any LO have to be such that MDS signals would be above their level when translated into baseband and as seen through the receiver’s

conversions. This would improve on the receiver “reciprocal mixing” performance.

Setting design requirements for phase noise performance in receiver design is not an easy task. The problem becomes more complicated as phase noise, intermodulation distortion (IMD) and the five kinds of dynamic range are not treated in concert.¹ There is no real connection between their basic definitions and an accurate mathematical model of the phase noise requirements as a function of all other dynamic range factors.

Instead, defacto technological limitations have dictated current synthesizer design and performance. This, in turn has produced radios with “phase-noise-limited minimum discernible signal” due to the phenomenon called “reciprocal mixing.”

Reciprocal Mixing

So, what is reciprocal mixing? Reciprocal mixing occurs in a superheterodyne receiver or in a direct sampling software defined radio (SDR) when the noise sidebands of any local oscillator mix with a strong adjacent signal and its noise sidebands. This creates unwanted noise products in-band of the last intermediate frequency (IF), and/or an equivalent DSP filter, blocking the receiver’s minimum discernible signal (MDS). This is different than the single-tone blocking dynamic range phenomenon which is compression driven as offset in frequency from the center of a received signal. We will discuss blocking dynamic range later on in this article. Figure 1 shows how reciprocal mixing happens.

In other words, reciprocal mixing occurs when the resulting intermodulation distortion products produced by mixing the noise sidebands of the LO(s) with the blocking signal obscure a desired signal at the receiver’s MDS level. In a modern receiver, the noise sidebands of the synthesized local oscillator(s) are usually the main culprit, as we do not have control over the interferer’s (jammer) radio performance. Consequently, the reciprocal mixing impacts a receiver’s dynamic range at the MDS as a function of multiple noises, jitter and spurs created mainly by the synthesized LOs as mixed with external carrier and anomalies from an adjacent channel.

Phase Noise

In order to understand the problem better, let’s now take a more in-depth look at phase noise. Any local oscillator exhibits a finite amount of instability that can be characterized by two components; long term and short term. It is short term instability

that produces phase noise. Much more on this subject can be found in Chapter 16 of *Modern Communications Receiver Design and Technology*.¹

Any practical local oscillator signal is not a perfect pure sine-wave; instead it has noise sidebands known as phase noise. Several factors govern the amount of phase noise generated. For an open loop resonant oscillator, the Q , or quality factor of the resonating tank circuit is the most important contributing factor to its phase noise performance.

In the context of resonators, Q is defined in terms of the ratio of the energy stored in the resonator to the energy supplied by a generator, per cycle, in order to keep signal amplitude constant, at the resonant frequency (f_r), where the stored energy is constant with time. This is shown in Equation 1.² The 2π factor in the equation allows Q to be expressed easier as a second-order differential equation, which describes most electrical or mechanical resonant systems.

$$Q = 2\pi \times \frac{\text{Energy Stored}}{\text{Energy dissipated per cycle}}$$

$$= 2\pi f_r \times \frac{\text{Energy Stored}}{\text{Power Loss}} \quad \text{Eq 1}$$

Leeson’s equation is used to anticipate a tuned resonant oscillator phase noise as shown in Figure 2. As can be seen in the figure, an oscillator’s phase noise performance is governed by three independent criteria:

1) Closest to the center frequency of a signal, flicker noise with a $1/f$ characteristic is combined with the resonator’s noise to produce a tapered response as shown.

2) Further away from the center frequency, the Q of the resonator dictates the noise floor. The response shown in Figure 2 results from the filtering affect of the resonating tank circuit.

3) Far away from the center frequency, the noise remains constant as shown. This represents the broadband noise floor of the oscillator.

Today, state-of-the-art receivers no longer use free running oscillators. They use a variety of closed loop synthesis to generate frequency multiples of a master reference oscillator. Synthesizers using phase-locked loops reduce the phase noise produced by a tuned oscillator close to the carrier within the loop bandwidth to a level approaching that of the phase noise of a multiplied reference oscillator. Farther away from the carrier, however, and beyond the loop’s bandwidth corner frequency, the PLL synthesizer usually adds a minute amount of additional noise. Depending on how tight the loop bandwidth is positioned, the intersection of the two phase noise levels creates the so-called “hump” sometimes seen in phase noise performance plots. The hump can be cured by widening the loop bandwidth of the PLL at the cost of decreasing the close-in phase noise performance. A new form of synthesizer which will be discussed later in this article, the DDS-driven PLL does remedy the problem through using a high granularity DDS running at a high frequency to steer a PLL.

The problem is more complicated than this, however. All analog elements of a receiver such as amplifiers, mixers, and active filters exhibit some nonlinearity because there is a maximum signal they can process. These introduce distortion to both the wanted and any unwanted signals. This can lead to the creation of new interfering distortion products occurring at new frequencies. If these occur at critical frequency points within the receiver’s IF, it will affect the SNR needed for an adequate carrier to noise (C/N) advantage at the demodulator.

In a real receiver, multiple stages are cascaded, and intermodulation products developed in one stage are fed to the next

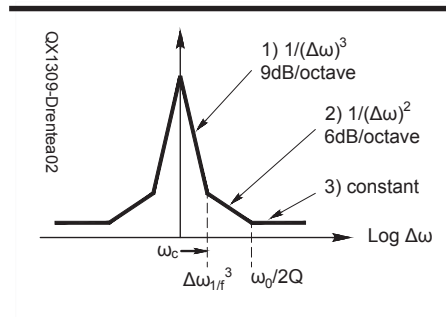


Figure 2 — Local oscillator phase noise according to Leeson.

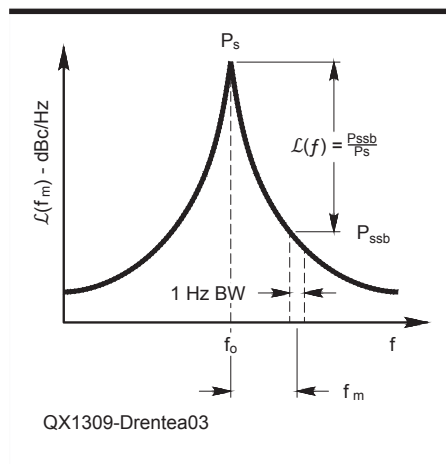


Figure 3 — How phase noise is measured. The single sideband (SSB) phase noise is observed in one of the LO’s sidebands. It is measured in dBc/Hz (in a 1 Hz bandwidth) at a delta offset from the carrier center.

¹Notes appear on page 23.

stage, adding cumulatively at each stage. Consequently, the later stages must be able to handle these larger signals. This can be seen clearly through a chain analysis of the system, which accounts for IMD. The earlier stages, which are intended to handle small and large RF input signals from the antenna also have to employ strong components by definition. The net result is that the entire receiver has to employ high dynamic range components throughout, such as class A amplifiers and class III mixers. (See Note 1.) This requires high DC power consumption and also the means to remove the additional heat produced. A practical balance of power usage has to be maintained throughout the design, which is usually a compromise dictated by the particular application and cost. Before any circuit design begins, it is the system designer who must take all these factors into account.

How Does Phase Noise Enter the Receiver

At this point, we need to stop and briefly refresh our phase noise definitions. As is well known, single sideband (SSB) phase noise is observed in one of the LO's sidebands as shown in Figure 3. It is measured in dBc/Hz (in a 1 Hz bandwidth) at a delta offset from the center corresponding to its frequency response of interest, translated in the ultimate bandwidth of a receiver's baseband response.

To better understand how a coherent multiple LO synthesizer can impact the MDS of a receiver, let's now look at Figure 4. These show how phase noise from a LO transfers directly into a receiver's IF, dB per dB, impacting the receiver's MDS.^{1,3}

This means that in a multiple conversion superheterodyne receiver, the phase noise performance of all coherently synthesized LOs have to be compatible with each other. Otherwise the worst performing LO in the scheme will spoil the MDS of the receiver.

Designing for a similar phase noise performance at several synthesizer ports in a multiple conversion receiver is not a trivial thing to achieve. Disregarding this fundamental rule will result in phase noise limited minimum discernible signal at a point of no return in the design cycle. Providing equal phase noise performance at all LOs in a synthesizer involves complex mathematical calculations and considerable design intuition.

Shown in Figure 5 is the coherent system design of the Star-10 transceiver depicting the impact of its synthesizer at every LO port of the double conversion approach and its baseband conversion (LO1, LO2, LO3).^{9, 10, 11} As previously stated, the phase noise performance of each LO source has to be compatible with all the other LOs in order for the receiver to avoid reciprocal mixing,

Consequently, all LOs have almost identical phase noise performance (-137 dBc/Hz).

To achieve good performance, the system and/or circuit designer starts out with the design of the master reference unit (MRU) shown at the bottom right of Figure 5. The MRU serves as the reference for LO2 and LO3 and determines the phase noise performance of these LOs. This design takes in consideration the degradation of phase noise performance through multipliers such as DDS-driven phase-locked loop and dividers as impacted only by the devices' noise floor. (See Note 1.) Thus, the improvement or degradation in phase noise performance is estimated through the use of the $\pm 20 \log N$ equation.

The process of ensuring equal phase noise performance in a coherent system is tedious work and should be followed rigorously with tests of every LO port of a brassboarded system. Only then can one proceed to the final version of the design and its actual implementation.

Complex Synthesizers and Composite Phase Noise

Although the performance of a high

probability of intercept receiver depends on a good noise figure, the proper frequency planning, and low distortion circuits, it is mainly affected by synthesizer phase noise and spurious performance interacting directly with the "weakly nonlinear behavior of linear circuits." (See Notes 1 and 2.) In addition, jitter — the timing aspect of the phase noise can also impact digital signal processing (DSP) in superheterodyne and especially in direct sampling software defined radios. Jitter is very important to sampling digital signals. Designers use complex mathematical analysis tools to determine how much phase noise is required in DSP processing.

To better understand the subject, we will now briefly recap solutions to frequency synthesis previously presented. For a more in-depth reading on synthesis, please refer to *Modern Communications Receiver Design and Technology*.¹ In addition, the reader is also directed to the many other references listed at the end of this article.

Today's superheterodyne and direct sampling software defined radios use a combination of several synthesizer forms to achieve a fully coherent approach to tunability

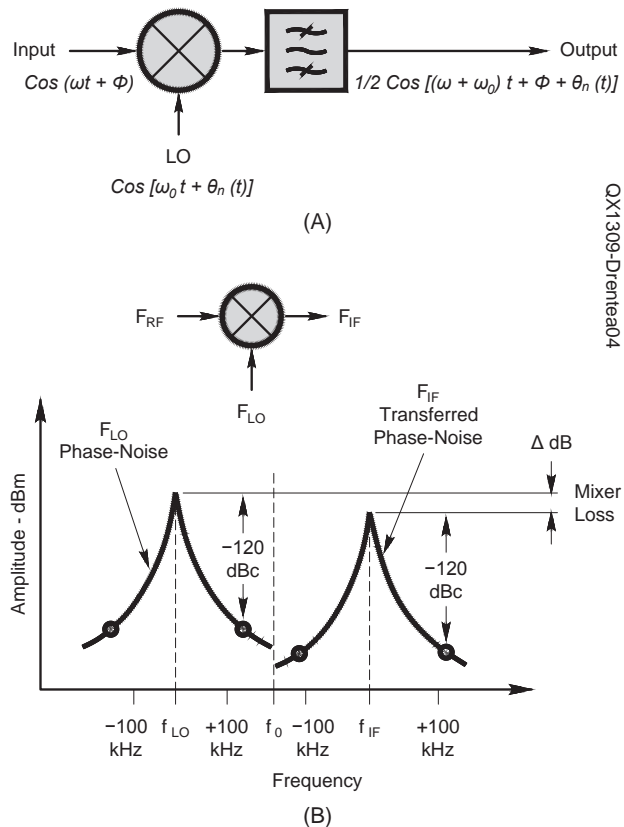
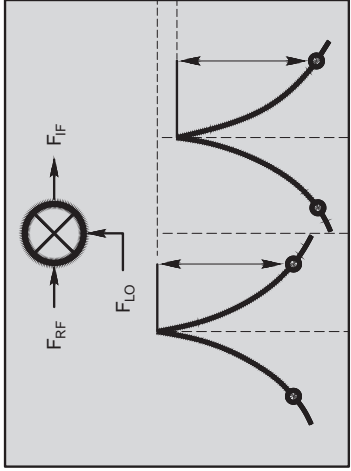
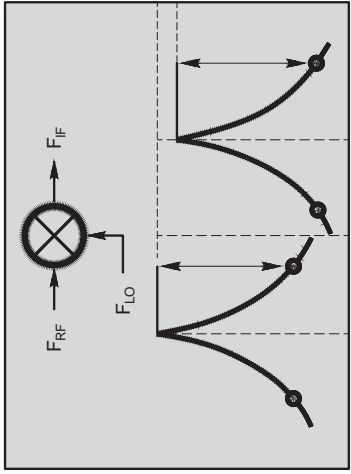


Figure 4 — Phase Noise of an LO is transferred to the IF of a superheterodyne receiver directly, dB per dB as impacted only by the mixer loss. The same is true for a quadrature mixer software defined radio (SDR), which is a form of superheterodyne, or a direct sampling software defined radio where the LO is the sampling clock.¹



Automatically Switched Half Octave Filter (8) Bank

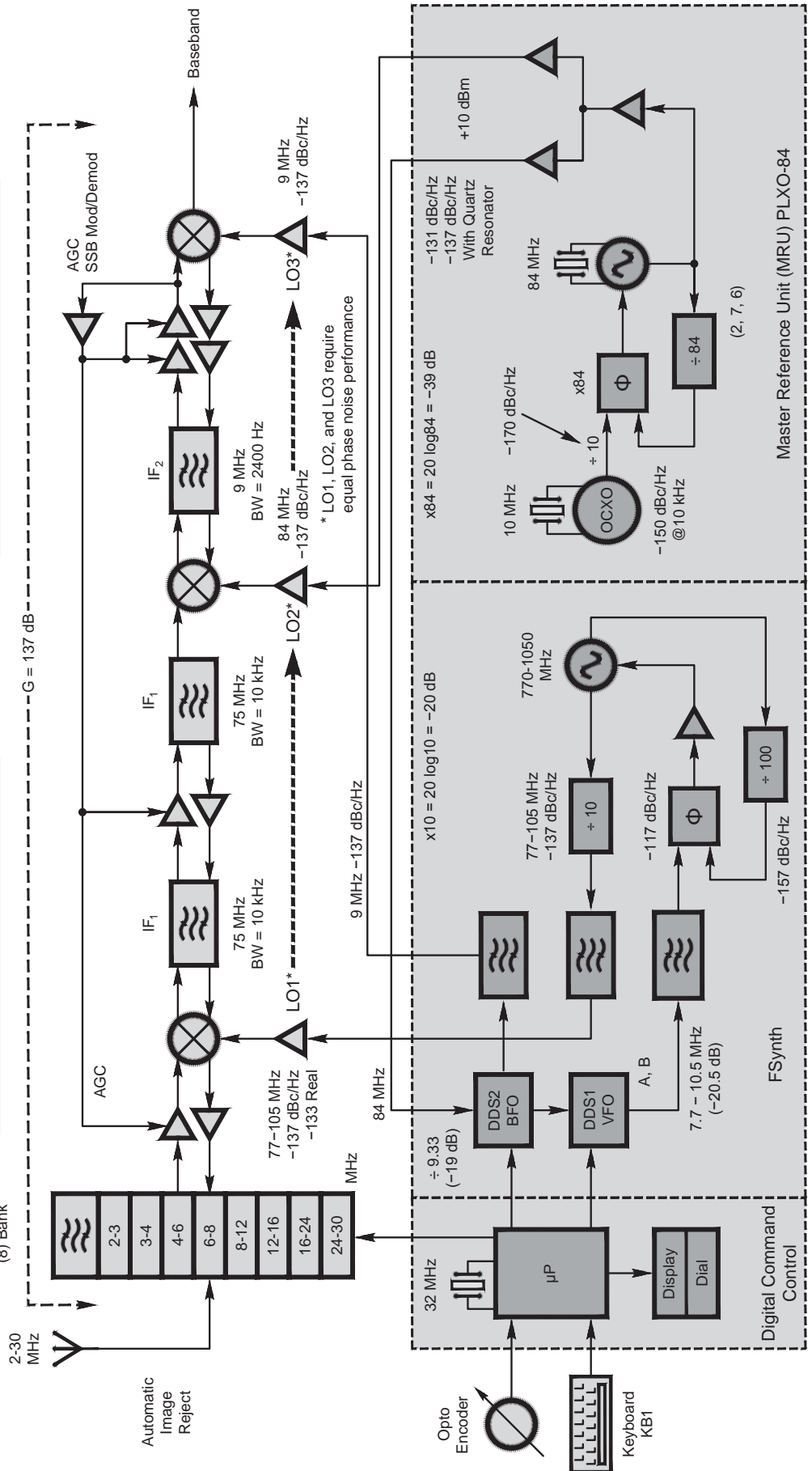


Figure 5 — Double conversion Star-10 transceiver's coherent synthesizer provides three LOs (LO1, LO2 and LO3) with near identical phase noise performance (-137 dBc/Hz) for equal signal processing of the receiver's MDS throughout all mixers. The receiver's MDS is therefore guaranteed (not phase noise limited) ensuring the entire processing gain for the receiver.

and demodulation.^{1, 4, 5, 6, 8, 9, 10, 11} They follow a judicious mathematical implementation of a combination of several “brute force” and “non-brute force” synthesizer forms as explained in Note 1. Choosing and combining the technologies and obeying strict intermodulation distortion rules is a complex and not always successful design process. If not done correctly, synthesizers can cause phase noise limited receiver dynamic range situations or worse. They can also produce systems with accidental in-band self jamming signals.

For optimum performance, one must pay full attention to phase noise degradation all the way from the system's master reference unit to the receiver's baseband output. This gets more complicated when designing high resolution complex synthesizers. Phase Noise degradation in these systems is not always predictable because of the fine granularity of the step resolution and also the unknown characteristics of some of the parts used in the design.

Using Multiplication Versus Division in Synthesizers

Another cause for inferior phase noise performance in synthesizers is the utilization of multipliers at frequencies where frequency division is totally possible. Some manufacturers today use multipliers in their synthesizers, which in turn degrade receiver performance by increasing phase noise. Frequency multiplication in LOs is justifiable only at microwave frequencies where digital division is not achievable. Despite this, it is not unusual to see frequency multipliers (doublers, triplers, or quadruplers) used in frequency synthesizers of modern HF radios. One of the reasons for using multipliers is that they are relatively easy to implement and are perceived as low cost. For instance, some master reference units in modern transceivers use quartz based oscillators operating at ~ 15 or ~ 32 MHz. These frequencies are being doubled, sometimes several times to provide fixed and/or variable references to PLLs, DDSs or DDS-driven PLLs. The idea is that by using lower frequency parts and multiplying up, a design is more economically produced. If a synthesizer uses frequency multipliers, however, the resulting phase noise is degraded in dB by the equation

$20 \log N$ where N is the multiplication factor. (See Note 1.)

Conversely, if a synthesizer contains digital dividers and division is performed from a higher frequency, the phase noise can be reduced according to the same equation. Obviously, this is the preferred method and consequently, multipliers should be avoided in HF or VHF synthesizer designs. They should be used only at microwave frequencies where divider technology is not yet available or is too expensive. Today, at least one radio company has adopted the divider methodology in its synthesizer designs, while others continue to use multipliers. The Ten-Tec model 599 (Eagle) transceiver uses a divided down VCO in its PLL synthesizer, which runs as high as 1.4 GHz.

Contrary to popular belief, the final cost of using multipliers in manufacturing can often be higher than that of dividers using digital techniques. Various digital dividers as well as IC PLL integrated circuits offer phase noise floor performance, which is not always evident in their specification sheets. In particular, IC phase locked loop integrated circuits have different noise floor capabilities ranging from unspecified to better than a measured -160 dBc/Hz at a 5 kHz offset. Some manufacturers claim a theoretical phase noise floor of better than -200 dBc/Hz. Usually referred to as the L1 Hz figure-of-merit (FOM) for the phase detector and charge pump, which is used to figure out the best in-band phase noise floor. For the ADF4111 (Analog Devices Single integer-N 1.2 GHz PLL), the L1 Hz figure of merit for the phase detector and charge pump is

-213 dBc/Hz, then the $L(fm)$ in band noise floor (dBc/Hz) = $L1$ Hz + $[10 \log_{10}(PFD \text{ frequency})] + [20 \log_{10}(N \text{ division})]$.

Knowing which PLL or divider integrated circuit chip to use can make the difference between success and failure. Because today's technology is changing so rapidly, a comprehensive study of the currently available devices and their performance backed by test data is always recommended before committing to a design. In addition, MRU technologies have to be carefully considered at microwave frequencies where quartz and surface acoustic wave (SAW) oscillator technologies present limitations. In the case of quartz, fundamental and overtone SC cut technologies stop at ~ 150 MHz while SAW technologies are limited to a maximum of ~ 1.5 GHz. MRU designs at these frequencies, should always be built into ovens.

At the start of a design, rather than venture on an unsure path, a conscientious designer needs to complete a thorough analysis of the topology and the candidate parts, backed by actual phase noise data. Although this is seldom considered because of schedule limitations, it can indeed pay off in the long run. Investing in a study of alternative paths (Plan B) using a decision making engineering matrix can pay for itself by making quality design decisions at the beginning rather than having to repair a poor performing product after the fact. Depending on how successful the designer is in coming up with a “best of the worst” frequency plan compatible with the synthesizer's topology, the phase noise impact on dynamic range can be minimized.

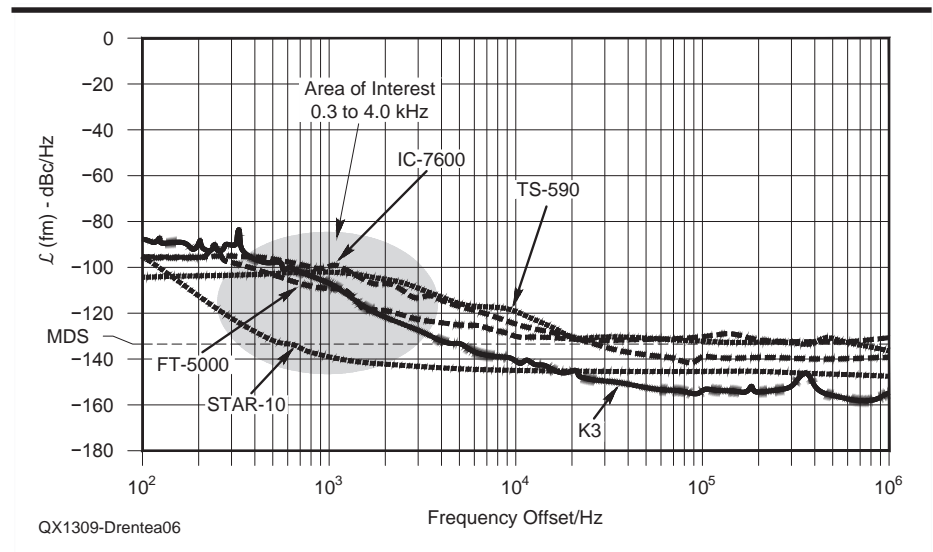
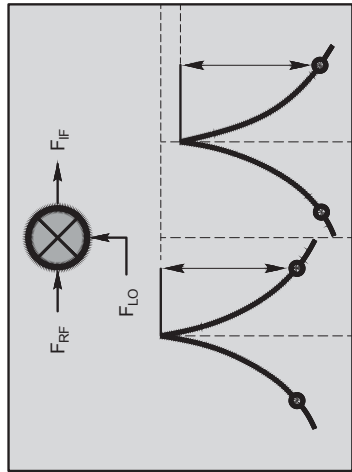
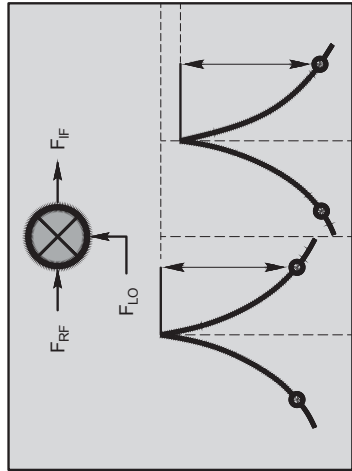
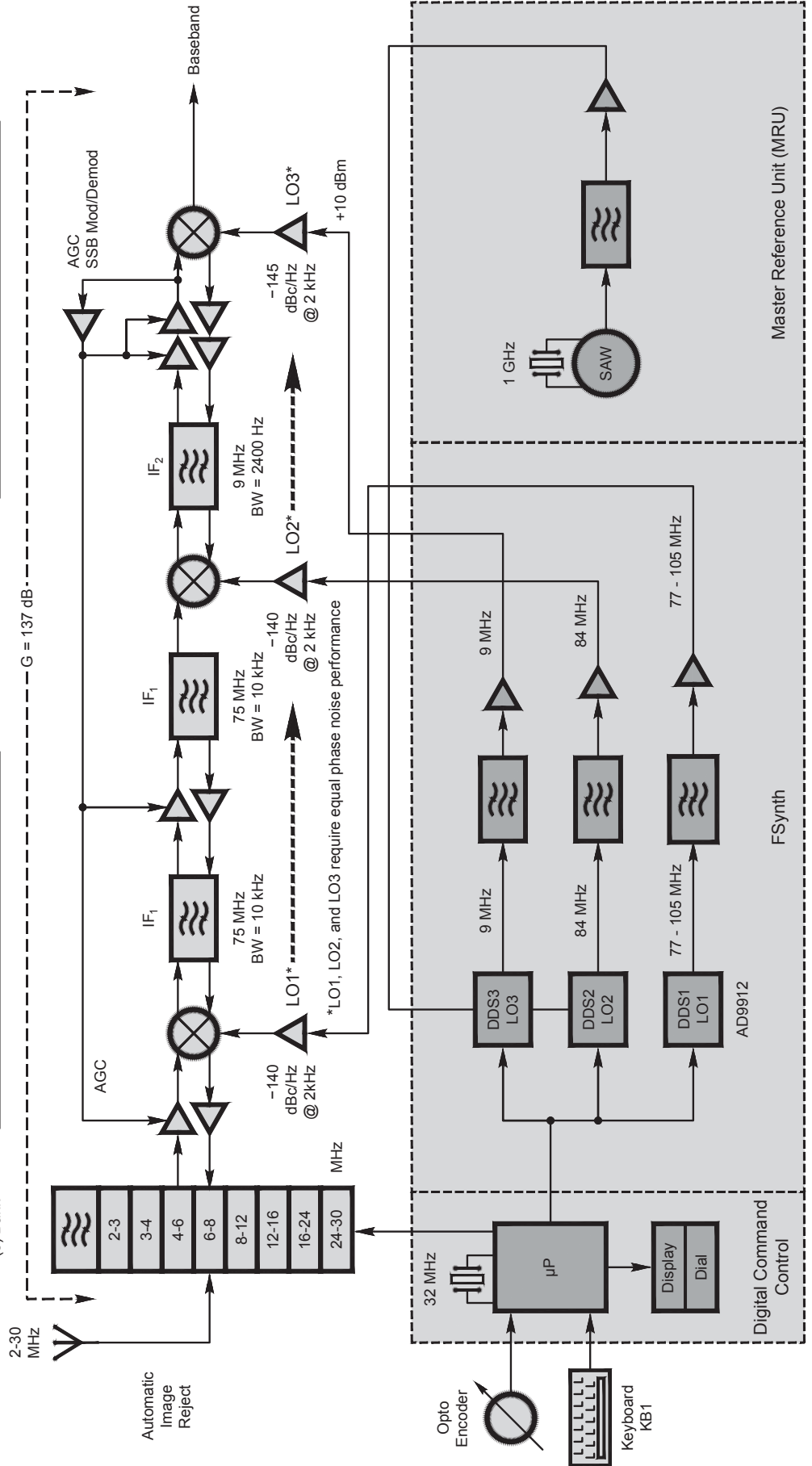


Figure 6 — Typical phase noise performance of several high performance HF transceivers as reported in QST, against the Star-10 phase noise performance. In single sideband (SSB) and KCW communications, the area of interest for phase noise is the frequency range between 300 Hz through 4 kHz (inside the oval circle) as phase noise folds into the passband of a typical receiver IF. (Source ARRL - QST, Technical Lab and Notes 11, 12, 13).



Automatically Switched Half Octave Filter (8) Bank



show up in the PLL's output. Running these PLL's at higher frequencies (1.5 GHz, for example) and dividing down as well as using modern Delta-Sigma modulators as noise cancellation filters, can improve this situation. This approach was used in the Ten-Tec Eagle's fractional-N PLL. More information on the fractional-N PLL can be found in Notes 1, 5, 6, 7, 8 and 12.

The fractional-N PLL can be noisier because it has built-in fractional compensation within its charge pump output. Switching between the two numbers (N and N+1) can cause additional phase noise and spurious problems which cannot be fully predicted. This problem becomes more complex when using more than one dual modulus fractional-N phase-locked loop in the system. This can occur when mixing the output of two or more fractional-N PLLs via a brute force synthesis approach. (See Notes 1, 5, 6, 7 and 8.) This relationship is sometimes empirically determined and has unpredicted effects on a transceiver's dynamic range unless established through laboratory testing and cured. Using a high VCO frequency (such as 1.4 GHz) and dividing down to obtain the LO frequencies, however, can ameliorate this problem. The fractional-N is generally noisier in a particular application due to the spurious tones. The fractional division process accumulates errors that cyclically repeat, resulting in tones (spurs). Fractional compensation approaches are used to counter the accumulating phase errors, and are useful. They reduce the spurs, but have numerous limitations. Newer (all digital) devices with delta sigma modulators achieve better results.

Several attempts have been made to quantify the theoretical digital switched phase noise performance of a fractional-N PLL as computed at the composite phase detector output. Among them, is a method described in Note 14. The extended rationale is based on a previous work performed by National Semiconductor. (See Note 12.) The noise analysis is validated through a condition that the total jitter is uncorrelated from sample-to-sample. This is another theoretical assumption that guarantees the removal of fractional spurs, leaving only the white noise.

The Direct Digital Synthesizer (DDS)-Driven PLL

By far the most popular synthesis method used today is the DDS-driven PLL. Initial publication of the DDS-driven PLL concept can be found in the 1987 book entitled, *Single-Sideband Systems & Circuits* by W. Sabin and E. Schoenike. (See Note 3.) The first practical implementation of a DDS-driven PLL has been reported on behalf of the Honeywell Corporation by this writer at the 1988 RF Technology-Expo Frequency

Synthesis Session B1 (Dr. Ulrich Rohde, Chair), in Anaheim, California on February 12, 1988. (See Note 4.) About 500 engineers were present in the audience and a year later, almost every HF radio on the market used this concept. A patent was granted in October 1990, following the two publications, to R. Gilmore of Qualcomm Inc, (Direct Digital Synthesizer Driven Phase Locked Loop Frequency Synthesizer Application — Patent # 4,965,533).¹³

Instead of manipulating the PLL N, and N + 1, as in a fractional-N PLL, the new synthesis method takes advantage of the fact that the DDS is a perfect fractional divider. A synthesizer's step resolution can then be addressed through the DDS as a variable reference to a PLL. The design of the PLL is greatly simplified using the DDS as a variable reference. This is due to the fact that the DDS's output frequency remains relatively high (for example ~10 MHz) while its resolution can be in the order of a milihertz. This minimizes the close-in reference feedthrough phase noise problems associated with low frequency references.

Modern HF transceivers today utilize this relatively new form of synthesizer to generate fine local oscillator (LO) frequency step increments derived from a single reference frequency standard, usually a temperature compensated quartz crystal oscillator (TCXO) or an oven controlled quartz crystal oscillator (OCXO). More information about DDS-driven PLL implementations can be found in Note 1.

We now see how the DDS-driven PLL, combined with various "brute force" synthesizer forms, simplifies complex synthesizer design. It utilizes direct digital synthesis as a variable high resolution fractional reference source running at relatively high frequencies, steering a fixed integer N, phase-locked loop with a low N multiplying number.

DDS-Only Synthesis

Recently, direct digital synthesizer (DDS) chips have been used alone as frequency synthesizers. I published an article series entitled "Beyond Fractional-N" in the Mar/Apr and May/June 2001 issues of *QEX*. (See Notes 5 and 6.) This work introduced the DDS-Driven PLL concept as the ultimate fractional divider and a replacement for the Fractional-N approach. In part two of that article, I went a step further and presented a practical DDS-Driven PLL synthesizer operating at ten times the frequency required by the LOs and divided by 10 for an improved phase noise performance due to percentage bandwidth improvements at the higher frequencies. This method was later used in the design of my Star-10 transceiver, as described in *QEX* in Notes 9,

10 and 11. It put the actual PLL operational frequencies at around 1 GHz, thus presenting a certain percentage bandwidth advantage and reducing the number of VCOs from four to one. This also achieved a 6 to 10 dB improved phase noise performance over the conventional multiplying methods. At least one manufacturer (Ten-Tec, Orion) followed this design idea in their new products while others continue to use multipliers.

My 2001 article series also introduced the DDS-only synthesizer method (no PLL) as a possible future of synthesizer design in radios. At that time, this idea attracted several negative letters of protest because of spurious problems associated with glitch energy, which was a characteristic of that DDS technology.

Over the past ten years, new noise canceling techniques have been implemented by the industry in DDS design and synthesizer costs have been cut by almost entirely eliminating the PLL. With the introduction by Analog Devices of new 14-bit GHz DDS devices, it is now possible to design complete digital synthesizers using no PLLs. While an argument can still be made in favor of the DDS-Driven PLL using the PLL loop filter as a spur reducing mechanism, today's new radios have been using DDS-only technology, which can greatly simplify the problem of obtaining similar phase noise performance from multiple LOs. Almost all new transceivers today use DDS-only technology, fulfilling the prediction of my 2001 article.

A new DDS-only brassboard synthesizer was recently created for the Star-10 transceiver. This replaced the DDS-driven PLL synthesizer with an AD-9912A. Several tests were performed by Constantin Popescu, KG6NK, regarding phase noise, spurs and MDS levels. An HP-3048A phase noise analyzer was used in these tests. The two oscillators correlation method was also used. A 1 GHz master reference unit was created by multiplying a 100 MHz OCXO (manufactured by PTI) by 10 (x5 and x2). This design produced excellent phase noise performance. Figure 8 shows a block diagram of a complete DDS-only synthesizer, which could be used in the Star-10 transceiver. A 1 GHz phase-locked SAW oscillator (built into an oven) could also be used as a reference instead of the multiplied 100 MHz OCXO.

Typical phase noise performance of each DDS-LO as demonstrated through the actual tests is shown in Figure 8. All LOs have nearly identical performance of -140 dBc/Hz at 2 kHz, fulfilling the equal phase noise performance LOs requirement for combating the reciprocal mixing problem discussed at the beginning of this article. Figure 9 shows Constantin Popescu (KG6NK) and his new phase noise setup using the HP-3048A phase

noise analyzer used in these tests.

Figure 10 shows the actual phase noise characteristics of the three AD-9912A DDSs configured for the Star-10 transceiver using a common 1 GHz master reference oscillator. Figure 11 shows typical spurious performance of the AD-9912A as used in the brassboard.

Conclusions

Whether you are a home brewer or a design engineer, the same attention to a complex system design is necessary before starting on the circuit design. The right mix of technologies and synthesis methods have to be considered. Using the proper mixer ratios in the “brute force” sections of synthesizers is

just as important as the receiver ratios for best intermodulation distortion performance. See Note 1. As seen from the above tests, the new DDS technology simplifies the challenge of obtaining similar phase noise performance at several LO ports in a coherent synthesizer design. Combating spurs in these DDSs continues to be challenging, but future

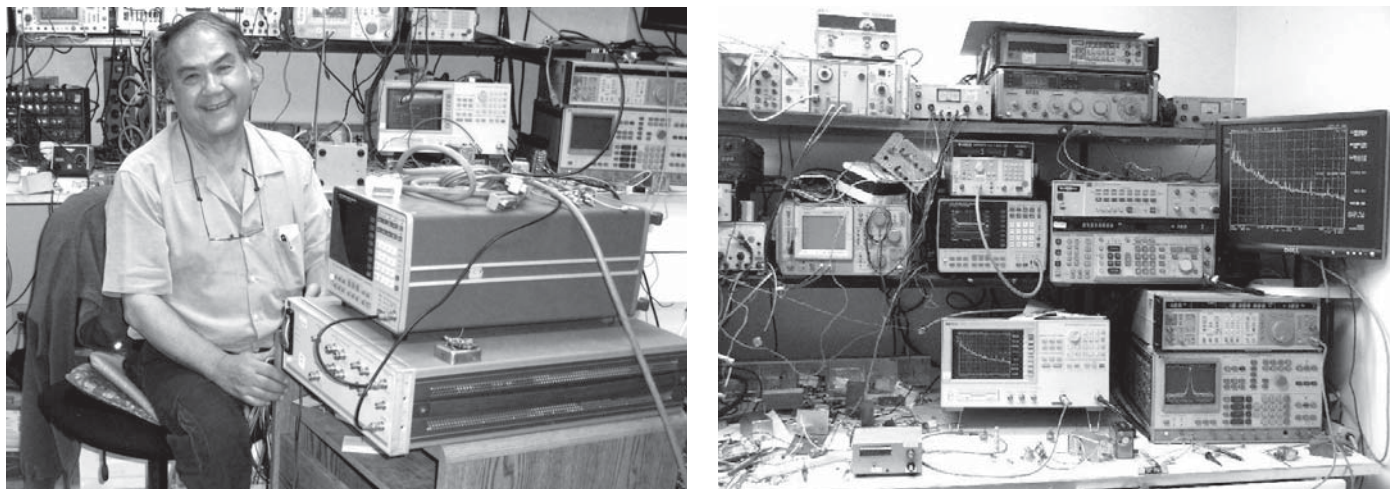


Figure 9 — The left photo shows Constantin Popescu (KG6NK) performing the phase noise and spurious tests for the Star-10 DDS-only synthesizer. The right photo is Constantin’s workbench and test equipment.

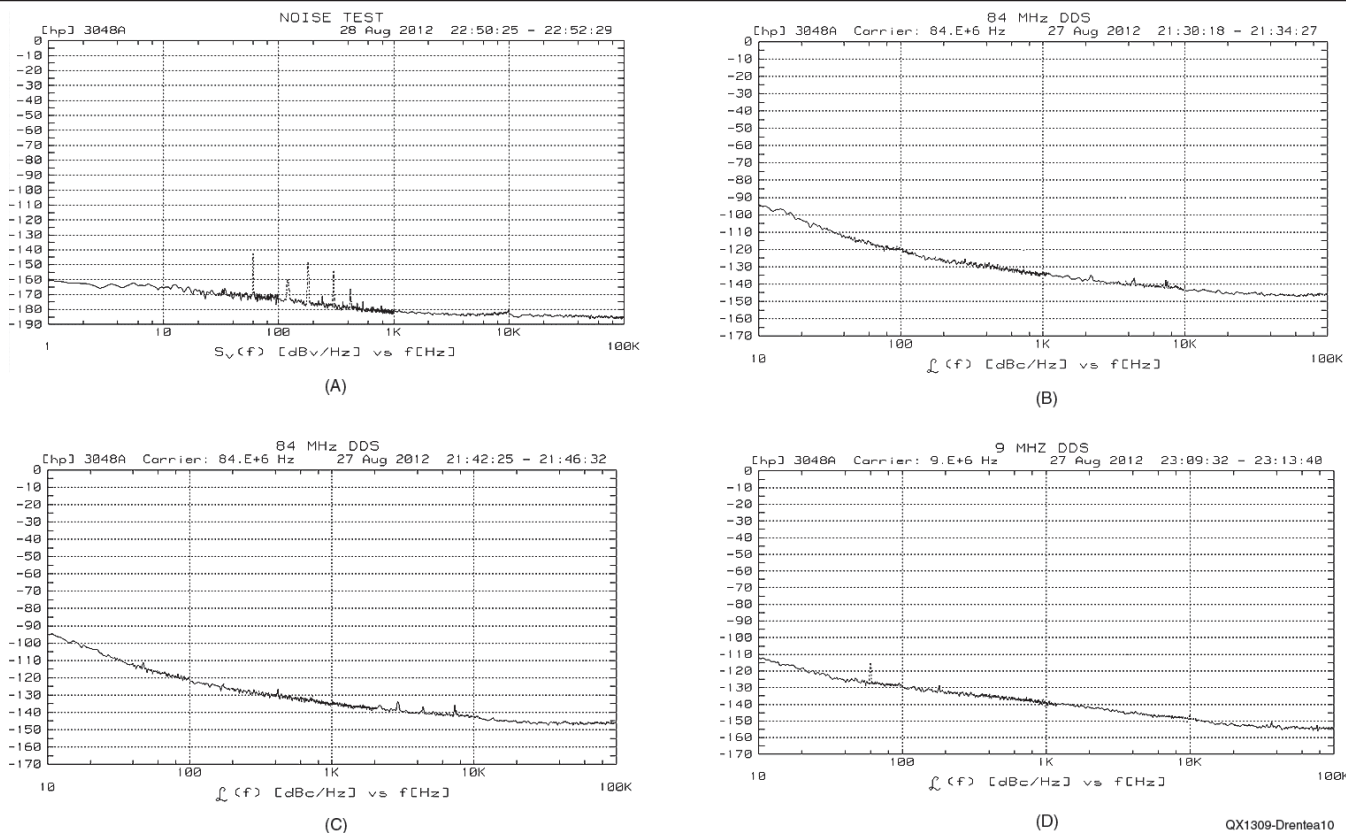


Figure 10 — Comparative phase noise performance tests of three DDS-only LOs in the Star-10 transceiver. See Figure 9. (Courtesy of KG6NK). Part A is the noise floor of the HP-3048 Phase Noise Instrument used in the tests. Part B shows the typical phase noise performance of the 77-107 DDS LO1 (measured at 84 MHz). Part C shows the typical phase noise performance of the 84 MHz DDS LO2. D is the typical phase noise performance of the 9 MHz DDS LO3.

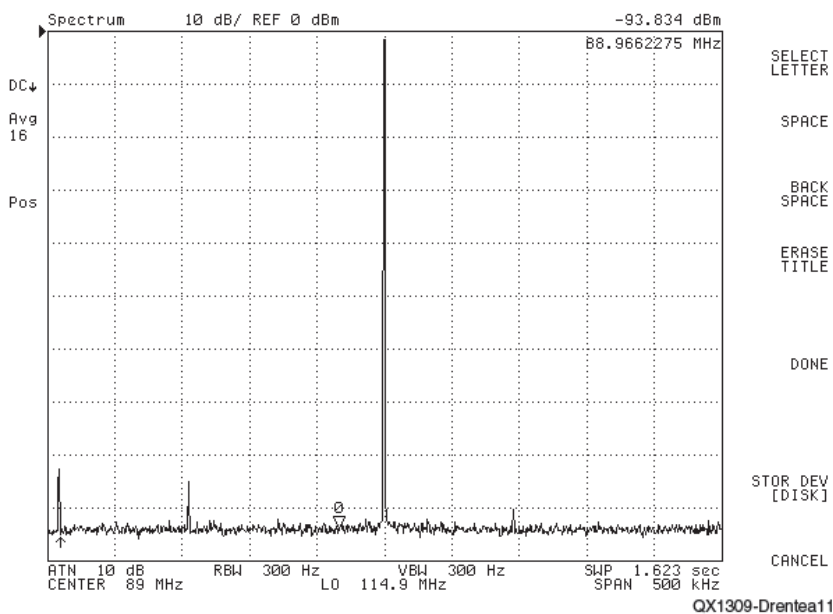


Figure 11 — Typical spurious performance of the AD-9912A. A few spurs exist at -85 dBc or less. For best spurious performance, the DDS reference should be no less than 8 times the Nyquist limit, in this case 1 GHz for 105 MHz maximum frequency out. (Test courtesy of KG6NK).

improvements should be expected. Still, making an entire system coherent while using proper ratios remains an art rather than a science and no computer program by itself can replace good engineering judgment.

Blocking Dynamic Range

The above discussion would not be complete without also discussing the blocking dynamic range phenomenon in receivers. We must differentiate between the two seemingly identical phenomena. Blocking dynamic range is considered to be a different problem than reciprocal mixing, although some common grounds exist. Blocking Dynamic range is usually treated as a system compression problem at an offset frequency from the center of the receiving frequency. Reciprocal mixing is a phase noise problem caused by mixing with an adjacent signal and creating intermodulation products. The two overlap in some hard to predict ways. While it is relatively simple to find the cascaded noise figure (NF) and the 1 dB compression point (P1dB) of a receiver using standard equations, it is usually not very clear how to use these numbers to predict the actual performance of a receiver in the presence of an adjacent blocking large signal. See Note 1.

As previously indicated, BDR is only one of several kinds of dynamic range, none of which entirely describes the performance of a receiver. It is for this reason that blocking dynamic range is usually determined empirically through tests. This is done by ramping up a jammer (blocker) signal at the RF input of a receiver and listening at some

predetermined offset frequency from the desired received MDS signal and finding at what level the jammer causes the received signal to be muted.

Then, the difference between the blocker signal level and the MDS level determines the blocking dynamic range at that offset frequency. The test is usually performed with the receiver's narrowest filter switched in and at an arbitrarily chosen offset which usually relates to the channel spacing as determined by the channelization allocations of spectrum to be received. In the high-frequency (HF) Amateur Radio Service, this number is just outside of the receiver's ultimate bandwidth as there is no predetermined channelization of these bands. This makes for stringent receiver requirements otherwise seen only in radar receivers that have to cope with severe clutter situations where a small Doppler modified signature of a flying object has to be detected against a large reflecting background such as a mountain.

For this reason, blocking dynamic range is usually considered to be the toughest test for a receiver. It encompasses a multitude of design parameters including, but not limited to, the linearity of many design elements such as front end and IF filters (including their shape factor effects), their switching mechanisms, the low-noise amplifier (LNA), the conversion mixers (dictated by their class and LO drives). Modeling for such a complex environment can be difficult. The problem can be even more complicated in direct sampling software defined radios.

Another suggested method for measuring BDR is to establish a predetermined large

level jammer signal and move its frequency closer and closer to the desired signal at the MDS. Then measure the delta frequency in hertz at which point the desired signal is muted. The smaller the delta frequency number is at the blocking point (closer to the desired signal at the MDS), the better the receiver is. This quantity is then compared with the channel spacing at hand to ensure immunity to adjacent interference. Again, in the case of Amateur Radio HF communications, this spacing is determined by an adjacent signal located just outside the narrowest bandwidth of the IF filter, considering its shape factor.

Final Conclusions

This article was written in response to requests from several ham operators asking to define some of the more elusive receiver parameters, such as reciprocal mixing and blocking dynamic range to help them and clarify some of their misconceptions. My motivation for this paper has been the clarification of these topics as they are continually presented in radio test reports. Although the topics are theoretically and mathematically very complex, I have described them in simple and practical design terms so that the article could be understood by both the Amateur Radio enthusiast as well as the professional RF engineer. We have learned that the design of a receiver's synthesizer and particularly its phase noise performance are two of the most important design considerations that we make. The two cannot be viewed as separate fields, however, because synthesizer phase noise directly impacts an entire receiver's performance, dB per dB. We also learned about the history of synthesizer design and the impact on phase noise performance by using multipliers or dividers in their designs. Finally, we learned about the current trends of direct digital synthesis using DDS-only synthesizers, which are now replacing Fractional-N PLL and DDS-driven PLL designs of the past.

Many thanks go to Stephen Heald of Tait Communications (New Zealand), Robert Zavrel, W7SX, Mike Lindsay, AD7RZ, Jason Cooper, KN7AZ, Bob Allison, WB1GCM, and Constantin Popescu, KG6NK, for their encouragements and contributions to these hard to explain topics. I hope this material inspires anyone involved in transceiver and receiver design, including home builders/enthusiasts as well as professional RF designers.

Cornell Dreentea, KW7CD, is an ARRL Member who serves as an advisor to the ARRL Receiver Test Review Committee. He is an accomplished RF technologist with fifty years of hands-on applied technology experience in the aerospace, telecommunications and electronics industry. He has been an engineer and scientist

at companies such as Honeywell, Hughes, and Raytheon. He holds five patents and has been involved in the design and development of complex airborne/space guidance and communications systems at frequencies of up to 100 GHz. During his career he has developed several products. This includes, but is not limited to ultra wide-band, high probability of intercept microwave receivers, Doppler agile space transceivers, and multi-function frequency synthesizers. He has published over 90 technical papers and articles in national and international magazines and is the author of two books. See Notes 1 and 8.

Notes

- ¹C. Drentea, *Modern Communications Receiver Design and Technology*, ARTECH House 2010, ISBN 13: 978-1-59693-309-5, ISBN 10: 1-59693-309-7.
- ²D. Weiner and J. Spina, *Sinusoidal Analysis and Modeling of Weakly Nonlinear Circuits*, Van Nostrand Reinold, 1980, ISBN 9-442-26093-8.
- ³W. Sabin and E. Schoenike, *Single-Sideband Systems and Circuits*, p 350, McGraw Hill 1987, ISBN 0-07-054407-7.
- ⁴C. Drentea, "Designing Frequency Synthesizers," Proceedings RF Technology Expo Symposium, 1988, Frequency Synthesis Session B1, (Session Chair Dr. Ulrich Rohde), Anaheim, California, Feb 10-12, 1988.
- ⁵C. Drentea, "Beyond Fractional-N, Part 1," *QEX*, Mar/April 2001.
- ⁶C. Drentea, "Beyond Fractional-N, Part 2," *QEX* May/June 2001.
- ⁷D. Banerjee, "Fractional N Frequency Synthesis," Application Note 1879, National Semiconductors.
- ⁸C. Drentea, *Radio Communications Receivers*, McGraw Hill 1982, ISBN 0-6306-1393-5.
- ⁹C. Drentea, "The Star-10 Transceiver (Part 1)," *QEX*, Nov/Dec 2007.
- ¹⁰C. Drentea, "The Star-10 Transceiver (Part 2)," *QEX*, Mar/Apr 2008.
- ¹¹C. Drentea, "The Star-10 Transceiver (Part 3)," *QEX*, May/June 2008.
- ¹²D. Banerjee, "PLL Performance, Simulation and Design," National Semiconductor 1998, www.national.com.
- ¹³R. Gilmore for Qualcomm Inc., Patent # 4,965,533, "Direct Digital Synthesizer Driven Phase Locked Loop Frequency Synthesizer," Oct 1990.
- ¹⁴P. White, "Understanding Phase Noise From Digital Components in PLL Frequency Synthesizers," Applied Radio Labs, DN 006.

Additional References

- D. Jiang, P. V. Brennan and J. Zhang, *Analyses of Intermodulation Effects in Fractional-N Frequency Synthesis*, Department of Electrical & Electronic Engineering, University College, London, WC1E7JE, United Kingdom.
- D. Redmayne, E. Trelewicz and A. Smith, "Understanding the Effect of Clock Jitter on High-Speed ADCs," *ANALOG & POWER*.
- A. Chenakin, "Frequency Synthesis Current Solutions and New Trends," *Microwave Journal*, May 2007, Horizon House Publications, Inc.

- D. Owen, "Fractional-N Synthesizers," Application Note, IFR, www.ifrsys.com.
- A. Tauro, Ph.D, "The Phase Locked Loop," *Politecnico di Bari Dipartimento di Elettrotecnica ed Elettronica*.
- P. White, "Techniques of Frequency Synthesis — Non-Ideal Behavior in PLL Frequency Synthesizers," peter@radio-labs.com, Applied Radio Labs: www.radio-labs.com.
- A. Kajiwara and M. Nakagawa, "A new PLL Frequency Synthesizer With High Speed Switching," *IEEE Transactions on Vehicular Technology*, Vol 41, Nov. 1992, pp.407-413.
- B. Zhang and P. Allen, "Feed-Forward Compensated With Switching Speed Digital Phase-Locked Loop Frequency Synthesizer," *Proceedings of the IEEE International Symposium on Circuits and Systems*, Vol 4, 1999, pp 371-374.
- A. M. Fahim and M. I. Elmasry, "A Fast Lock Digital Phase-Locked-Loop Architecture for Wireless Applications," *IEEE Transactions on Circuits and Systems*, Vol 50, Feb. 2003, pp 63-72.
- T. Aytur and J. Khoury, "Advantages of Dual-Loop Frequency Synthesizers for GSM Applications," *Proceedings of the IEEE International Symposium on Circuits and Systems*, 1997, pp 17–20.
- C. M. Yuen, C. N. Wong, and K. F. Tsang, "1 μ s Fast Acquisition 2.4 GHz Low Voltage Frequency Synthesizer for FH-CDMA Mobile Communications," *Proceedings of the IEEE Asia Pacific Microwave*, Vol 1, 1997, pp 317-320.
- H. Sato, K. Kato, T. Sase, I. Ikushima, and Shin-ichi Kojima, "Fast Pull-In PLL IC Using Two-Mode Pull-In Technique," *Electronics & Communications in Japan*, Part. 2, Vol 75, no. 3, pp 41–51, 1992.
- F. M. Gardner, *Phase Lock Techniques*, John Wiley and Sons, New York, 2nd edition, 1979.
- R. C. H. van de Beek, C. S. Vaucher, D. M. W. Leenaerts, E. A. M. Klumperink, and B. Nauta, "A 2.5-10 GHz Clock Multiplier Unit With 0.22-ps RMS Jitter in Standard 0.18 μ m CMOS," *IEEE Journal of Solid-State Circuits*, Vol 39, Nov. 2004, pp 1862-1872.
- B. Stilling, "Bit Rate and Protocol Independent Clock and Data Recovery," *Electronics Letters*, Vol 36, April 2000, pp 824-825.
- C. H. Park, and B. Kim, "A Low-Noise, 900 MHz VCO in 0.6- μ m CMOS," *IEEE Journal of Solid-State Circuits*, Vol 34, May 1999, pp 586-591.
- S. Sidiropoulos, D. Liu, J. Kim, G. Wei, and M. Horowitz, "Adaptive Bandwidth DLLs and PLLs using Regulated Supply CMOS Buffers," *2000 Symposium on VLSI Circuits*, June 2000, pp 124-127.
- J. G. Maneatis, "Low-Jitter Process-Independent DLL and PLL Based on Self-Biased Technique," *IEEE Journal of Solid-State Circuits*, Vol 31, Nov 1996, pp 1723-1732.
- J. Browne, "Frequency Synthesizers Tune Communications Systems," *Microwaves & RF*, March 2006.
- V. Kroupa, *Frequency Synthesis Theory, Design and Applications*, John Wiley & Sons Inc., Hoboken, NJ, 1973.
- V. Manassewitsch, *Frequency Synthesizers Theory and Design*, Third Edition, John Wiley & Sons Inc., Hoboken, NJ, 1987.
- U. Rohde, *Microwave and Wireless Synthesizers: Theory and Design*, John Wiley & Sons Inc., Hoboken, NJ, 1997.
- J. Klapper and J. Frankle, *Phased-locked and Frequency Feedback Systems*, John Wiley & Sons Inc., Hoboken, NJ, 1972.
- Rohde & Schwartz, "A 24 GHz Network Analyzer," *Microwave Journal*, Vol 48, No. 10, October 2005, pp 136–142.
- Z. Galani and R. Campbell, "An Overview of Frequency Synthesizers for Radars," *IEEE Transactions on Microwave Theory and Techniques*, Vol 39, No. 5, May 1991, pp 782–790.
- V. Kroupa, *Direct Digital Frequency Synthesizers*, IEEE Press, Piscataway, NJ, 1999.
- T. Endres, R. Hall and A. Lopez, "Design and Analysis Methods of a DDS-based Synthesizer for Military Space Borne Applications," *1994 IEEE International Frequency Control Symposium Proceedings*, pp 625–632.
- W. Egan, *Frequency Synthesis by Phase Lock*, John Wiley & Sons Inc., Hoboken, NJ, 2000.
- R. Best, *Phase-locked Loops—Theory, Design and Applications*, McGraw-Hill, New York, NY, 1984.
- U. Rohde, *Digital PLL Synthesizers: Design and Applications*, Prentice Hall, Upper Saddle River, NJ, 1983.
- A. Blanchard, *Phase-Locked Loops*, John Wiley & Sons Inc., Hoboken, NJ, 1976.
- F. Gardner, *Phaselock Techniques*, Second Edition, John Wiley & Sons Inc., Hoboken, NJ, 1979.
- "Fractional-N Synthesizer," Application Note, Synergy Microwave Corp., www.synergymicrowave.com.
- Valpey Fisher Corp., "A High Frequency Reference Module," *Microwave Journal*, Vol 48, No.4, April 2005, pp 142–144.
- S.M. Shajedul Hasan, Ph.D. Dissertation, "New Concepts in Front End Design for Receivers with Large, Multiband Tuning Ranges," Virginia Polytechnic Inst. and State University, April 2009: <http://scholar.lib.vt.edu/theses/available/etd-04142009-195430/>.
- S.M. Shajedul Hasan and S.W. Ellingson, "Multiband Public Safety Radio Using a Multiband RFIC with an RF Multiplexer Based Antenna Interface," *Software Defined Radio (SDR) '08*, Washington DC, October 2008: www.ece.vt.edu/swe/mypubs/Hasan_SDR08_Paper.pdf.
- S.M. Hasan and S.W. Ellingson, "Multiband Public Safety Radio Using a Multiband RFIC with an RF Multiplexer Based Antenna Interface," (presentation slides), IEEE International Antennas and Propagation Symposium, San Diego, CA, July 10, 2008. See Technical Report #25 (above) for paper: www.ece.vt.edu/swe/chamrad/crdocs/Hasan_VT_APS08.pdf.
- S. Ellingson and S.M. Hasan, "Multiband/Multimode Radio" (presentation slides), NIJ Commtech Technical Working Group Meeting & Program Review, Boulder, CO, April 2, 2008: www.ece.vt.edu/swe/chamrad/crdocs/080402_NIJ_TWG_Ellingson_Long.pdf. Also available: Quad Chart, www.ece.vt.edu/swe/chamrad/crdocs/080402_NIJ_TWG_Ellingson.pdf.
- S. Ellingson, "Multiband/Multimode Radio," International Wireless Communications Expo (IWCE), Las Vegas, NV, Feb 27, 2008: www.ece.vt.edu/swe/chamrad/crdocs/080227_IWCE_Ellingson.pdf.
- T. Tsou, P.J. Balister, J.H. Reed, "Latency Profiling for SCA Software Radio," SDR Forum Technical Conference, Denver, CO, Nov 2-4, 2007: www.ece.vt.edu/swe/chamrad/crdocs/0711_SDRF_Thomas_Tsou1.pdf.
- P.J. Balister, C. Dietrich, J.H. Reed, "Memory Usage of a Software Communications Architecture Waveform," SDR Forum Technical Conference, Denver, CO, Nov 2-4, 2007: www.ece.vt.edu/swe/chamrad/

- crdocs/0711_SDRF_Thomas_Tsou1.pdf.**
- S.W. Ellingson, "Design Techniques for Multiband / Multimode Radios, Presentation - Bradley Dept. of Electrical and Computer Engineering, Virginia Polytechnic Institute & State University, www.ece.vt.edu/swe/mypubs/0806_MultibandRadio_Ellingson.pdf.
- S.W. Ellingson and S.M. Hasan, "Multiband/Multimode Radio," (presentation slides), NIJ CommTech PI Meeting, Arlington, VA, Oct 24, 2007: www.ece.vt.edu/swe/chamrad/crdocs/071024_NIJ_PIM_Ellingson.pdf.
- S. Ellingson, "Multiband Radio (Update from Spring 2006)," (presentation slides), NIJ / Commtech Technical Working Group Meeting & Program Review, Las Vegas, NV, April 24, 2007: www.ece.vt.edu/swe/chamrad/crdocs/070424_Ellingson_Rev1a.pdf.
- S. Ellingson, "All-Band All-Mode Radio for Public Safety," (presentation slides), International Wireless Communications Expo (IWCE), Las Vegas, NV, March 28, 2007: www.ece.vt.edu/swe/mypubs/070328_IWCE_SE.pdf.
- S.W. Ellingson, "All-Band All-Mode Radio for Public Safety," (presentation slides), NIJ CommTech PI Meeting, Irvine, CA, Jan 11, 2007: www.ece.vt.edu/swe/chamrad/crdocs/070111_NIJ_VirginiaTech_SE_b.pdf.
- S.M. Hasan et al., "A Low Cost Multi-Band/Multi-Mode Radio for Public Safety," SDR Forum, Orlando FL, Nov 2006: www.ece.vt.edu/swe/chamrad/crdocs/SDR06_SM_Hasan.pdf.
- S.M. Hasan et al., "A Low Cost Multi-Band/Multi-Mode Radio for Public Safety Applications," (poster), 2006 Wireless Personal Communications Symposium, Jun 2006: www.ece.vt.edu/swe/chamrad/crdocs/01hasan.pdf.
- S. Ellingson and J. Reed, "Multi-Band Multi-Mode Radio for Public Safety," (presentation slides), International Wireless Communications Expo (IWCE), Las Vegas, NV, May 19, 2006: www.ece.vt.edu/swe/chamrad/crdocs/NIJ_060519_IWCE.pdf.
- S. Ellingson and J. Reed, "A Low Cost All-Band All-Mode Radio for Public Safety: Kickoff Meeting at Virginia Tech," (presentation slides), Oct 13, 2005: www.ece.vt.edu/swe/chamrad/crdocs/051013_NIJCT_Kickoff_VT.pdf.
- S.-J. Park and G.M. Rebeiz, "Low-Loss Two-Pole Tunable Filters With Three Different Predefined Bandwidth Characteristics," *IEEE Transactions on Microwave Theory and Techniques*, Vol 56, No. 5, May 2008, pp 1137-48.
- R. Paulsen and M. Spencer, "Miniaturization of Fixed and Tunable Filters — Where and When to Use Integrated Passive Devices," SDR Forum Technical Conference, 2007.
- B.G. Perumana et al., "Resistive-Feedback CMOS Low-Noise Amplifiers for Multiband Applications," *IEEE Transactions on Microwave Theory and Techniques*, Vol 56, No. 5, May 2008, pp 1218-25.
- J.H. Reed, *Software Radio: A Modern Approach to Radio Engineering*, Prentice-Hall, 2002.
- B. Razavi, "Design Considerations for Direct-Conversion Receivers," *IEEE Transactions on Circuits and Systems II*, Vol 44, No. 6, Jun 1997, pp 428-435.
- B. Razavi, *RF Microelectronics*, Prentice-Hall, 1998.
- E. Ranu and S.W. Ellingson, "A Low-Cost Wideband UHF Downconverter with 5:1 Tuning Range," *IEEE Transactions on Instrumentation and Measurement*, Vol 51, No. 5, Oct 2002, pp 1080-1084.
- A. Rofougaran et al., "A Single-Chip 900-MHz Spread-Spectrum Wireless Transceiver in 1-mm CMOS — Part I: Architecture and Transmitter Design," *IEEE Journal of Solid State Circuits*, Vol 33, No. 4, Apr 1998, pp 515-34.
- W. E. Sabin, "Diplexer Filters for an HF MOSFET Power Amplifier," *QEX*, Jul/Aug 1999, pp 20-26.
- W. E. Sabin & E.O. Schoenicke (eds.), *HF Radio Systems and Circuits*, Rev 2nd ed, Noble, 1998.
- C. W. Tang and S. F. You, "Design Methodologies of LTCC Bandpass Filters, Diplexer, and Triplexer with Transmission Zeros," *IEEE Transactions on Microwave Theory and Techniques*, Vol 54, No. 2, Feb 2006, pp 717-723.
- A. Tasic et al., "Design of Adaptive Multimode RF Front End Circuits," *IEEE Journal of Solid-State Circuits*, Vol 42, No. 2, Feb 2007, pp 313-322.
- Virginia Tech, "Multiband/Multimode Radio for Public Safety Applications," Project website: www.ece.vt.edu/swe/chamrad/.
- K.L. Wu and W. Meng, "A Direct Synthesis Approach for Microwave Filters With a Complex Load and Its Application to Direct Diplexer Design," *IEEE Transactions on Microwave Theory and Techniques*, Vol 55, No. 5, May 2007, pp 1010-1017.
- Z. Zhou and K.L. Melde, "Frequency Agility of Broadband Antennas Integrated with a Reconfigurable RF Impedance Tuner," *IEEE Antennas and Wireless Propagation Letters*, Vol 6, 2007, pp 56-59.
- R. Groshong, *The Application of DSP Technology in HF/VHF Radio Systems*, Rockwell Collins, Advanced Technology Center, 1998 International Symposium on Advanced Radio Technologies.
- C. Azeredo-Leme, "Clock Jitter Effects on Sampling: A Tutorial," *IEEE Circuits and Systems Magazine*, 1531-636X/11/ IEEE THIRD QUARTER 2011.
- D. Redmayne, "A Practical Guide to Designing A/D Converter Driver and Clock Circuitry," Linear Technology, IEEE IMS 2001, Baltimore, USA.
- J. A. Crawford, "Advanced Phase-Lock Applications," 2010-2011, AMI ALC, www.am1.us.
- D. Jiang, P.V. Brennan and J. Zhang, "Analyses of Intermodulation Effects in Fractional-N Frequency Synthesis," Department of Electrical and Electronic Engineering, University College London, United Kingdom, 0-7803-8834-8/05/\$20.00 ©2005 IEEE; djiang@ee.ucl.ac.uk.
- P. V. Brennan, H. Wang, D. Jiang, P. M. Radmore, "A New Mechanism Producing Discrete Spurious Components in Fractional-N Frequency Synthesizers," *IEEE Transactions on Circuits and Systems*, Vol 55, No. 5, June 2008.
- J. Carlini, "Practical Developments Using Today's Fractional Synthesizers," *High Frequency Electronics*, Sep 2009 Copyright © 2009, Summit Technical Media, LLC.
- D. Banerjee, "Fractional N Frequency Synthesis" National Application Note 1879, Dec 10, 2008.
- D. Owen, "Fractional-N Synthesizers," IFR Application Note: www.ifrsys.com.
- D. Redmayne, E. Trelewicz and A. Smith, "Understanding the Effect of Clock Jitter on High-Speed ADCs," Linear Technology, ECE April 2007.
- E. McCune, Earl McCune RF Communications Consulting, "Physical Relationships Along the Power Amplifier Continuum," IEEE Microwave Theory and Techniques Society.
- D. Butterfield and B. Sun, "Prediction of Fractional Spurs for UHF PLL Frequency Synthesizers," QUALCOMM, Inc., San Diego, CA, 0-7803-5152-5/99/ 0 1999 IEEE.
- Ira A. Fulton School of Engineering, Arizona State University, Tempe, AZ 85287 USA, 2008 IEEE Radio Frequency Integrated Circuits Symposium.
- P. White, "Understanding Phase Noise From Digital Components in PLL Frequency Synthesizers," www.radiolab.com.au, DN006 20 Dec 2000.
- S. Meninger, M. H. Perrott, *Sigma-Delta Fractional-N Frequency Synthesis*, Massachusetts Institute of Technology (MIT), June 7, 2004.
- P. P. Sotiriadis, *Principles of Cascaded Diophantine Frequency Synthesis*, 978-1-4244-1795-7/08/\$25.00 ©2008 IEEE; pps@ieee.org.
- "Smart Selection of ADC/DAC Enables Better Design of Software-Defined Radio," Texas Instruments, Application Report SLAA407, April 2009.
- Chao-Ching Hung, Shen-Iuan Liu, "A Noise Filtering Technique for Fractional-N Frequency Synthesizers," *IEEE Transactions on Circuits and Systems — II: Vol 58, No. 3, Mar 2011*.
- A. Chenakin, "Frequency Synthesis: Current Solutions and New Trends," *Microwave Journal*, May 2007.
- Petr Vagner, Petr Kutin, "X-Band PLL Synthesizer," *Radio Engineering*, Vol 15, No. 1, April 2006, Department of Radio Electronics, Brno University of Technology, Brno, Czech Republic.
- L. Åsbrink, "Blocking Dynamic Range in Receivers," *QEX*, Mar/Apr 2006, pp 35-39.
- E. Ngompe, "Computing the LO Phase Noise Requirements in a GSM Receiver," *Applied Microwave and Wireless*.
- R. G. Meyer, A. K. Wong, "Blocking and Desensitization in RF Amplifiers," *IEEE Journal of Solid-State Circuits*, Vol .30, No 8, Aug 1995.
- B. Razavi, *RF Microelectronics*, Prentice Hall Communications Engineering Series, 1998.
- "ADC Parameters for Your Wideband Telecommunications Receiver," Maxim, Application Note 3717.
- Chao-Huang, Li-xiang Ren, Er-ke Mao and Pei-kun He, *A Systematic Frequency Planning Method in Direct Digital Synthesizer (DDS) Design*, 978-1-4244-5668-0/09/\$25.00 © 2009 IEEE, Beijing Institute of Technology, Beijing, China.
- T. Neu, "Impact of Sampling-Clock Spurs on ADC Performance," Texas Instruments Data Acquisition.
- Doug Smith, KF6DX, "Improved Dynamic-Range Testing," *QEX* Jul/Aug 2002, pp 46-52.
- Peter Chadwick, G3RZP, "HF Receiver Dynamic Range: How Much Do We Need?" *QEX*, May/June 2002, pp 36-41.
- Mike Tracy, KC1SX, *ARRL Test Procedures Manual*, ARRL, Rev G, Jan 2002.
- W. Domino, N. Vakilian and D. Agahi, "Polynomial Model of Blocker Effects on LNA/Mixer Devices," *Applied Microwave and Wireless*.
- B. Sklar, *Digital Communications Fundamentals and Applications*, ISBN 0-13-084788-7, Prentice Hall 2001.
- M. K. Simon, S. M. Hinedi and W. C. Lindsey, *Digital Communications Techniques, Signal Design and Detection*. ISBN 0-13-200610-3, Prentice Hall 1995.
- E. Ngompe, Conexant Systems, Inc., "Computing the LO Phase Noise Requirements in a GSM Receiver," *Applied Microwave and Wireless*.
- C. A. Barnes, A. Hati, C. W. Nelson and D. A. Howe, "Residual PM Noise Evaluation of Radio Frequency Mixers," National Institute of Standards and Technology Boulder, CO, USA.

Frequency Dependence of Equivalent Series Resistance Measurement

With a little encouragement from his friends, the author finds a better way to test the equivalent series resistance of capacitors in or out of a circuit.

Doug is one of the experts behind the counter at Gateway Electronics in St Louis, MO.¹ Folks from a wide area seek his advice on repairing electronic stuff, so Doug has seen a lot of failed electrolytic capacitors in the past several years. (It seems that some Chinese manufacturers used inferior materials in the capacitors they manufactured.)

Doug had Mark Kreske build an equivalent series resistance (ESR) meter to check out suspect capacitors. Mark is a college student pursuing a degree in electronics. Mark and I are two of Doug's "groupies." Doug was troubled that Mark's meter identified some but not all bad capacitors. In particular, Doug had some known bad devices on a computer motherboard that checked okay with Mark's meter.

Doug set out to interest me in this problem and gave me some bad capacitors to evaluate. I measured the transmission of signals through the capacitor under test as a function of frequency with my DDS Sweep Measurement System and saw the behavior in Figure 1.² A good electrolytic capacitor of moderate value behaves like the short circuit baseline reference over most of the frequency range.

The results clearly show small differences between good and bad capacitors around 100 kHz, and a substantial difference at low audio frequencies. Strangely, all the ESR meter designs I find on the Internet operate in

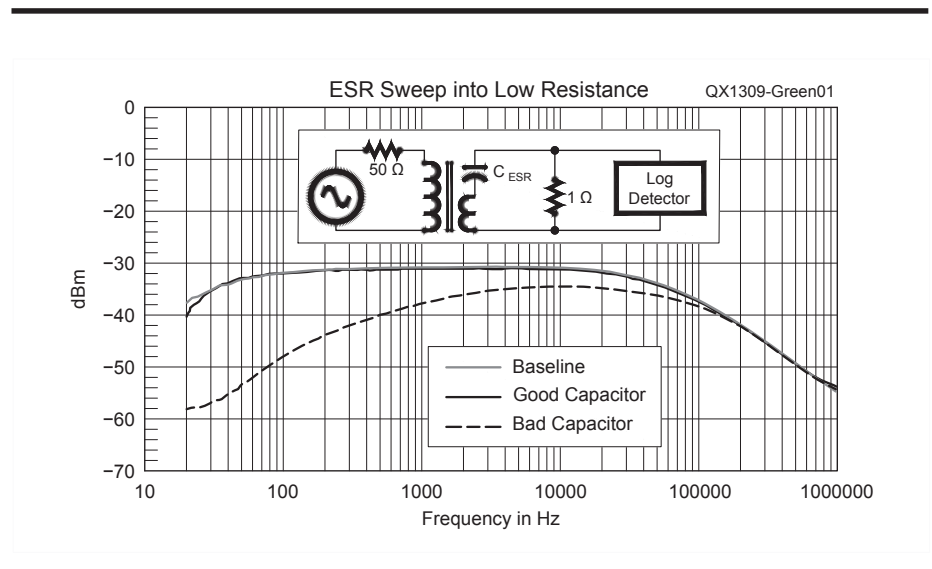


Figure 1 — Transmission through good and bad electrolytic capacitors versus frequency.

the neighborhood of 100 kHz.^{3,4,5,6,7,8,9} This has to be wrong!

Mark used the schematic diagram shown in Figure 2 to build his ESR meter. This circuit came from a meter described at Note 3. I built the same meter, with some simplifications, and modified it to work at two frequencies to enable comparisons.

The first simplification is to use three AAA cells for power rather than a regulated 5 V supply.

The second simplification is to tie the five buffer outputs together and use a

single 130 Ω resistor in place of five 680 Ω resistors.

The dual frequency modification involves changing R1 from 1 k Ω to 1 M Ω to lower the operating frequency below 100 Hz. Then I switch a 1 k Ω resistor in parallel with the 1 M Ω resistor to operate at the higher frequency.

I increased capacitors C2 and C3 from 0.01 μ F to 10 μ F and C6 from 0.1 μ F to 1 μ F in order to enable operation at the lower frequency. C5 (0.47 μ F at 400 V) is difficult to increase. Instead, I omitted C5

¹Notes appear on page 27.

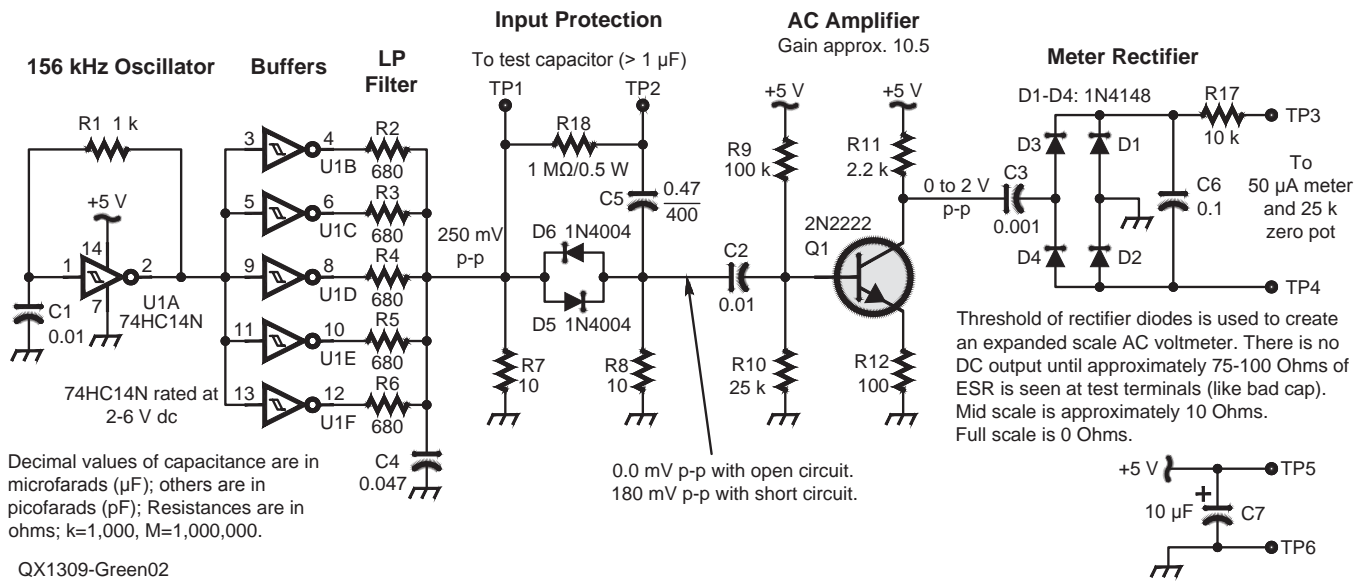


Figure 2 — ESR Meter schematic diagram from the Electronics DIY website, as listed in Note 3.

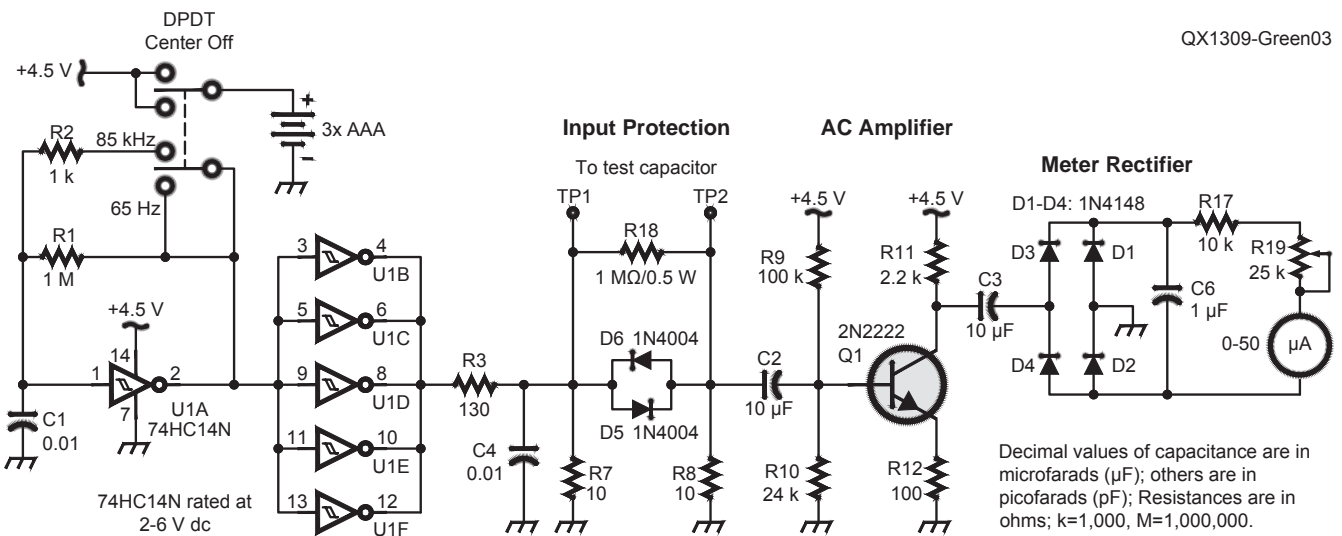


Figure 3 — ESR Meter with modifications for dual frequency operation.

by replacing it with a short circuit. The intent of C5 is to protect the circuitry from rapidly discharging a charged capacitor. I discharge my capacitors prior to testing.

Figure 3 shows my final circuit. I used a DPDT center-OFF switch to connect three AAA cells to provide the +4.5 V supply. One ON position selects the 1 M Ω timing resistor for 65 Hz operation. The other ON position shunts the 1 M Ω timing resistor with the 1 k Ω timing resistor for 85 kHz operation.

This circuit, in low frequency mode, correctly identified the known bad capacitors on Doug's motherboard. I suggest that ESR meter users modify their instruments in this manner to improve their ability to identify bad components.

Dr Sam Green, WØPCE, is a retired aerospace engineer. Sam lives in Saint Louis, Missouri. He holds degrees in Electronic Engineering from Northwestern University

and the University of Illinois at Urbana. Sam specialized in free space optical and fiber optical data communications and photonics. He became KN9KEQ and K9KEQ in 1957, while a high school freshman in Skokie, Illinois, where he was a Skokie Six Meter Indian. Sam held a Technician class license for 36 years before finally upgrading to Amateur Extra Class in 1993. He is a member of ARRL, a member of the Boeing Employees Amateur Radio Society (BEARS), a member of the Saint

Louis QRP Society, and breakfasts with the Saint Louis Area Microwave Society. Sam is a Registered Professional Engineer in Missouri and a Life Senior Member of IEEE. Sam holds seventeen patents, with one more patent application pending.

Notes

¹The Gateway Electronics web site is www.gatewayelectronics.com/.

²Sam Green, W0PCE, "A Full Automated DDS Sweep Generator Measurement System — Take 2," Sep/Oct 2012 *QEX*, pp 14-24.

³The ESR meter that we started with is described by Lawrence Glaister, VE7IT, on the Electronics_DIY website at: electronics-diy.com/electronic_schematic.php?id=949

⁴An ESR meter that was first described by Manfred Mornhinweg, XQ6FOD, is presented on the MZ Entertainment website at: www.mzentertainment.com/studio_workshop_test_equipment_esr_meter.html.

⁵Lee Davison describes a similar ESR meter at mycorner.no-ip.org/misc/esr/esr_04.

⁶For a description of a five transistor ESR meter, see: www.eevblog.com/forum/projects/5-transistor-esr-meter-design/.

⁷For information about an ESR meter kit see: www.users.on.net/~endsodds/.

⁸There is an ESR meter that uses a 555 timer IC described at: koti.mbnet.fi/hsahko/elek/kv/esr/index.en.shtml.

⁹For an ESR meter circuit that uses a resistor bridge design, go to: kakopa.com/ESR_meter/.

We Design And Manufacture To Meet Your Requirements

*Prototype or Production Quantities

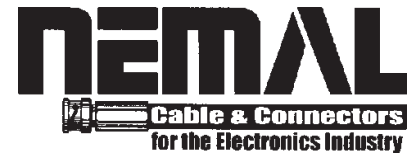
800-522-2253

This Number May Not Save Your Life...

But it could make it a lot easier! Especially when it comes to ordering non-standard connectors.

RF/MICROWAVE CONNECTORS, CABLES AND ASSEMBLIES

- Specials our specialty. Virtually any SMA, N, TNC, HN, LC, RP, BNC, SMB, or SMC delivered in 2-4 weeks.
- Cross reference library to all major manufacturers.
- Experts in supplying "hard to get" RF connectors.
- Our adapters can satisfy virtually any combination of requirements between series.
- Extensive inventory of passive RF/Microwave components including attenuators, terminations and dividers.
- No minimum order.



NEMAL ELECTRONICS INTERNATIONAL, INC.

12240 N.E. 14TH AVENUE
NORTH MIAMI, FL 33161

TEL: 305-899-0900 • FAX: 305-895-8178

E-MAIL: INFO@NEMAL.COM

BRASIL: (011) 5535-2368

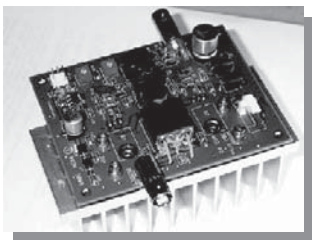
URL: WWW.NEMAL.COM



HPSDR is an open source hardware and software project intended to be a "next generation" Software Defined Radio (SDR). It is being designed and developed by a group of enthusiasts with representation from interested experimenters worldwide. The group hosts a web page, e-mail reflector, and a comprehensive Wiki. Visit www.openhpsdr.org for more information.

TAPR is a non-profit amateur radio organization that develops new communications technology, provides useful/affordable hardware, and promotes the advancement of the amateur art through publications, meetings, and standards. Membership includes an e-subscription to the *TAPR Packet Status Register* quarterly newsletter, which provides up-to-date news and user/technical information. Annual membership costs \$25 worldwide. Visit www.tapr.org for more information.

NEW!



PENNYWHISTLE
20W HF/6M POWER AMPLIFIER KIT

TAPR is proud to support the HPSDR project. TAPR offers five HPSDR kits and three fully assembled HPSDR boards. The assembled boards use SMT and are manufactured in quantity by machine. They are individually tested by TAPR volunteers to keep costs as low as possible. A completely assembled and tested board from TAPR costs about the same as what a kit of parts and a bare board would cost in single unit quantities.

HPSDR Kits and Boards

- **ATLAS** Backplane kit
- **LPU** Power supply kit
- **MAGISTER** USB 2.0 interface
- **JANUS** A/D - D/A converter
- **MERCURY** Direct sampling receiver
- **PENNYWHISTLE** 20W HF/6M PA kit
- **EXCALIBUR** Frequency reference kit
- **PANDORA** HPSDR enclosure



TAPR

PO BOX 852754 • Richardson, Texas • 75085-2754

Office: (972) 671-8277 • e-mail: taproffice@tapr.org

Internet: www.tapr.org • Non-Profit Research and Development Corporation

Line-of-Sight Signal Path Analysis using Google Earth

The author shows us how to use this powerful new tool to check the coverage areas of our repeaters or simplex operation.

As operating frequencies increase into the UHF and gigahertz range the importance of clear line-of-site paths between operating points becomes a major concern. The use of directional antennas and lower power at these frequencies requires a direct and uninterrupted signal path. Determining if communication is possible along a selected path or attempting to discover why a signal cannot reach a desired location requires knowledge and analysis of the terrain along the path. Tools that can analyze a path between two communication points are a necessity especially for long distances and uneven terrain, but these prove cost prohibitive for the Amateur Radio community.¹

Fortunately there is an available solution incorporating the resources and programming language of Google Earth that provides a method to visualize line-of-site signal paths and analyze the paths to determine if restrictions exist that could block signal propagation. This article will show how Google Earth, accompanied by a small bit of ingenuity can be incorporated to create a zero cost signal path analysis tool.

Figure 1 illustrates the classic line-of-site path view where the line of site is determined by a line from the antenna height to the horizon. Unless the area covered by the antenna is on a large body of water or flat plains this view is largely theoretical. Figure 2 illustrates the problems encountered in mountainous or uneven terrain where the line-of-site path can be obstructed by terrain features between the antenna sites that interrupt the direct signal path. The problem in determining if a clear line-of-site path exists

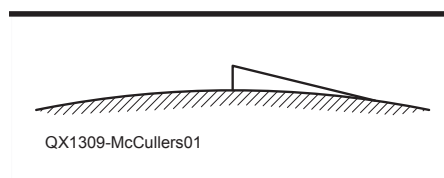


Figure 1 — Classic view of line-of-site path.

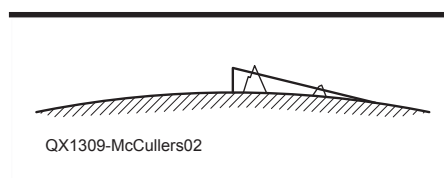


Figure 2 — Line-of-site path illustrating terrain obstructions.

between two points is discovering the restrictions that exist along the path that could block a signal. It is difficult to examine terrain between two points to determine if natural features such as hilltops could disrupt the signal path. This is a particular problem in areas of uneven terrain where the constantly changing terrain increases the difficulty in recognizing and locating specific features.

Birmingham Alabama is an example of this environment. Located in the foothills of the Appalachian Mountains in the north central part of the state, Birmingham is in an area of rolling hills with peaks exceeding 1200 feet and valleys averaging 500 feet

above sea level. Often, a signal path between two hilltop peaks will cross one or more ridge tops even along short paths. The numerous peaks offer many excellent venues for locating communication facilities, but the uneven terrain creates problems in obtaining clear line-of-site paths. Additionally, the steep terrain changes create problems with signals in valleys sheltered by the peaks. It is not uncommon to find locations where a small change in either height or location can make a difference in communicating. Multi-path problems and signal dropout are persistent problems for amateur, commercial two-way and broadcast services.

The Birmingham Amateur Radio Club (BARC) operates multiple repeaters, both analog and D-STAR, providing coverage for a multi-county area.² Attempting to provide adequate coverage given the features of the local terrain is difficult. In 2010 an interference problem resulting from close spacing of an antenna to a newly installed strobe beacon at an analog 2 meter repeater site required temporarily swapping to a borrowed antenna at a slightly lower level on the tower. Complaints soon began to flow in describing reduced coverage, and in several instances loss of coverage, some within relative short distances from the repeater site.

During the “What?” analysis phase, the process of visualizing the problematic signal paths proved unsuccessful, primarily due to the terrain changes between the repeater site and the reporting locations. At the same time, plans were being made to add D-STAR repeaters at other sites. It was desirable to know if communication would be possible between the repeater sites. For both situations, tools were needed to visualize and analyze the signal paths.

¹Notes appear on page 40.

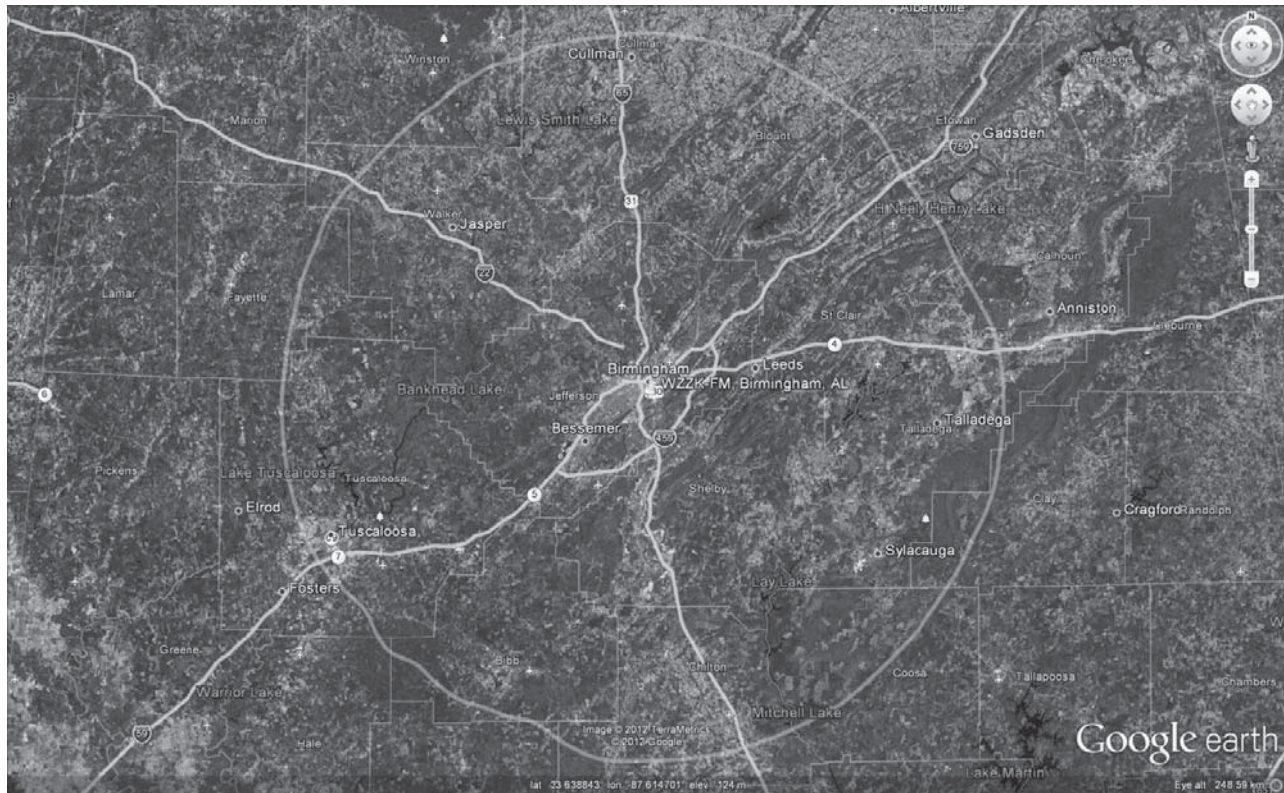


Figure 3 — FCC FM Broadcast 60 dBu Service Contour plotted by using KML.

Aware that the FCC was replacing drawn maps of broadcast coverage contour plots with maps based on Google Maps, I decided to explore the mechanism used to draw the plots.³ Figure 3 shows an FCC contour plot for a local FM broadcast station. [For color versions of the Google Earth screen shots from this article, go to www.arri.org/qxfiles and look for the file **9x13_McCullers_Images.zip**.⁴ — Ed.] Examining the plotting data for the contour map revealed the plot was drawn using KML, the programming language of Google Earth. I was familiar with the use of Keyhole Markup Language (KML) with Google Earth to plot three-dimensional paths of high-altitude balloon flights and the use of KML by the FM Fool and TV Fool sites to plot broadcast coverage area using the Longley-Rice Irregular Terrain model.⁵ With these uses of Google Earth as examples, the next step was to create a plot of a signal path that allowed for visual inspection of the path. This proved interesting but time consuming and cumbersome because it was necessary to survey the entire path searching for potential trouble spots. When Google Earth introduced Elevation Profile, which displays a terrain slice between two points, the combination of terrain profiling and a visual view combined to make Google Earth an excellent signal path analysis tool.

Becoming Familiar with Google Earth

First introduced in 2005, Google Earth is available free for *Windows*, *Apple Mac OS* and *Linux*.⁶ For best result, Google Earth should be run on a fast processor with ample memory. A good video/graphics card greatly improves 3D rendering and a fast internet connection assures smoother transitions when scrolling the map image. Google Earth is also available for free for the Apple iPhone, iPad and Android based devices. These versions are not useful for analyzing signal paths, however, because they can only access KML files from web sites.

It is important to download the latest version of Google Earth before experimenting with the examples in this article, because earlier releases of the Elevation Profile contained minor problems, in which elevations were not always displayed correctly. The examples in this article have been tested on *Windows XP*, *Windows 7* and *Mac OS 10.8* using Google Earth 6.6.2 and 7.1.1. All images included in this article are the property of Google and its providers and are used by permission.⁷

Google Earth is simple to use but requires a bit of practice and experience to make manipulation of the imagery smooth and effortless. Three basic controls are included in the upper right hand quadrant of the image display. They are normally semi-

transparent and are activated when the mouse cursor hovers over them. The controls from top to bottom are Rotation, Movement and Zoom. Movement is also available by holding down the left mouse button and moving the mouse across the map image. If the mouse is equipped with a scroll wheel, the wheel allows zooming on the image, which is smoother to use than the zoom slider. An image tilt function is activated by holding down the space key on the keyboard and using either vertical movement of the mouse or operation of the mouse scroll wheel to tilt the image from 0° to 90° where 0° is a vertical, downward view and 90° is a horizontal, perpendicular view. If mouse movement is used to control tilt, the image can also be rotated at the same time with horizontal movement of the mouse. The tilt function is useful when viewing signal paths as well as while examining terrain changes in 3D.

Individual preferences are set on the Options dialog found on the *Windows* version by clicking “Tools” on Google Earth’s menu bar, then “Options”. On *Mac OS X*, Options is found by clicking “Google Earth” on the menu bar followed by “Preferences.” Options allow Google Earth to be optimized based on computer speed, memory and graphic capabilities. Other options allow for tailoring Google Earth to individual likes as well as activating features that support signal path analysis. The options required to use

Google Earth as a signal path tool are listed in Table 1.

An Introduction to KML

KML is an abbreviation for Keyhole Markup Language. Keyhole, Inc. created the software that became Google Earth, and was purchased by Google in 2004. KML is an XML (Extensible Markup Language) derived language used to draw images and provide notations on Google Earth map images. XML is a markup language created to allow a common basis for information exchange between computing systems that is both human and machine readable. A markup language differs from a procedural language such as *BASIC*, *C* or *Java* in that it describes an object as opposed to performing an action such as calculating or controlling an activity. A program written in a procedural language such as *C* or *Java* interprets a document written with a markup language, and based on predetermined definitions completes an activity. XML provides a basic structure and set of rules a markup language must adhere to.

Markup languages are extensively used in Business-To-Business transactions to describe documents such as order information, banking request and health information. Markup languages grew out of GML (Generalized Markup Language) invented by IBM in the 1960s to allow document formatting control information to be included in text based documents. The most widely known markup language is HTML (Hypertext Markup Language), the basis for browser screen formatting on the World Wide Web.

This article is not intended to be a KML reference, but will demonstrate how KML can be used to produce a signal path image that allows visual analysis of the path and provides input to Elevation Profile. KML is feature rich and well documented. The complete KML reference can be found at the Google web site.⁸

KML Tags and Elements

In KML, text enclosed in angle brackets <like this> are markup instructions known as Tags. Tags are written in pairs, a start or open tag <tag> followed by an end or close tag </tag>. Each start tag must have a corresponding end tag or the document will be declared in error. The text between the start and end tag is known as an element, which describes the content of the element. Elements in KML may contain text or other elements. Elements may be nested where each nested level further describes the preceding higher level element. A third tag type is known as an empty-element tag or empty tag. As the name implies, an empty tag does not contain an element but performs a set function with no modifiers. Empty tags are represented

Table 1

Options set in Google Earth to Produce the Images and Examples for This Article.

The Options dialog is found on the Windows version by clicking “Tools” on Google Earth’s menu bar, then “Options”. On Mac OS X, Options is found by clicking “Google Earth” on the menu bar followed by “Preferences”.

- Map coordinates expressed in Decimal Degrees as selected in “Show Lat/Long” on the Option 3D tab.
- “Terrain” selected in the Terrain Quality Box.
- “Terrain Quality” set to optimize the available computer resources.
- “Do not automatically tilt while zooming” set in the Navigation box on the Options Navigation tab.
- Elevation Exaggeration is interesting and allows changes in terrain elevations to be more or less visible. The default is 1.0. The images in this article were created with a setting of 1.5. The highest setting 3.0 allows very small elevation changes to be highlighted but over exaggerates large changes making them appear unrealistic.
- The Options Navigation tab contains sliders to set the Fly-To-Speed Rate and the Mouse Wheel rate. Fly-To-Speed determines the rate of movement when a destination is selected in the left sidebar Places and Search boxes. Fly-To-Speed also determines the rate of movement on the global view when Google Earth is started.

by a start tag immediately followed by an end tag <tag></tag> or more commonly, a special empty-tag of the form <tag />. KML elements are case sensitive and mixed cases are used within the specification. KML elements beginning in upper case are features while lower case elements describe the feature in greater detail. Nesting of feature elements and reuse of descriptive elements are allowed. The KML reference for a feature describes the feature elements that can be internally nested along with the appropriate descriptive elements.

The following is a simplified illustration of a nested element describing a “Placemark” that will be used later:

```
<Placemark>
  <name>Red Mountain Repeater</name>
  <Point>
    <coordinates> -86.870192,33.475133,0</coordinates>
  </Point>
</Placemark>
```

The information describing the Placemark is contained between the starting and ending Placemark tags. The name element provides a name for the Placemark, while the Point element provides the geographic coordinates of the Placemark using the <coordinates> element.

Note the use of indentation in the Placemark description. Indentation and white space make the KML document more human readable and should be used for clarity even though indentation requires more horizontal space. Indentation and white space are ignored during computer processing of the document.

Listing 1 shows a basic KML document, which illustrates the minimum elements required to build a KML document. Again, note that white space is allowed and recommended for reading clarity. The first and second lines are required and describe the document as XML based and supplies text encoding information to the XML parser. The “<?xml” start tag must begin in column one on the first line. The specifics of these lines are not important but they must begin each KML document. [The Listing text files for this article are available for download from the ARRL *QEX* files website. We have printed the first 4 listings here for your reference, but to save page space we did not print listings 5 through 10.⁹ — Ed.]

Building a Signal Path File using KML

With an understanding of markup language basics and KML, it is time to show how to use KML elements to construct the visual elements needed to use Google Earth as a signal path analysis tool.

If a picture is worth a thousand words, a demonstration is worth 10,000 words, and an interactive demonstration has to be worth 100,000 words. Doing an interactive demonstration is easy with Google Earth. The examples referenced in this article can be downloaded from the *QEX* files web site and unzipped into an empty file directory.¹⁰ Double-clicking an example file name will start Google Earth and open the KML document. It is possible to open multiple files simultaneously with the resulting KML-generated images merged. A separate entry will appear in “Temporary Places” on the left side panel for each open KML document and an entry can be deleted to remove its contents from

Listing 1 — Basic KML Document Structure

```
<?xml version="1.0" encoding="UTF-8"?>
<kml xmlns="http://www.opengis.net/kml/2.2">

  <!--                                -->
  <!--      QEX                        -->
  <!--                                -->
  <!--      Basic KML Document Structure    -->

  <Document>

  <!--      Insert KML Tags Here          -->

  <!--      End of KML Tags              -->

</Document>
</kml>
```

the map image.

If a document is changed, re-saving the document and double-clicking on the file name in the appropriate file directory will signal Google Earth to reload the document. Google Earth will then ask if the previous document should be reloaded. Click “Yes” to load the replaced document. When Google Earth is shutdown, the option to discard or save any loaded documents is presented. Reply “No” for this demonstration.

KML documents containing errors will either be rejected or possibly result in unexpected outcomes. Google Earth provides the ability to notify the user if a KML document error occurs and presents options to handle the error. This feature is activated from the toolbar by clicking “Tools/Options/General” (“Google Earth/Preferences/General” on *OS X*) and clicking “Show prompts for all errors” under “KML Error Handling.” Any detected error is displayed in a prompt that gives the document line number of the error. For debugging KML documents, a text editor with line numbering is helpful.

The example files contain several differences from the code listings that accompany this article. In the examples, the ground path is plotted in green and the signal path in red using a narrower line width than the published images, which were modified for black and white printing. Included in the examples and referenced in the article are “LookAt” elements (discussed later) that provide visual references to match the article text. They are not required for normal use.

The various KML elements making up a signal path description document may be defined in any order in the document as cre-

ation of the visual elements occur after document parsing is complete. For programming clarity and readability, however, it is best that like elements be grouped together by name or function. It is preferable to place basic elements at the beginning of the document and increasingly add complexity by building on previously defined elements in a building block fashion.

Visual elements defined by a KML document appear in the left side panel of the Google Earth window under “Temporary Places”. To aid in maintaining order, “Folder” elements can be used to group elements that describe a series of visual elements in a tree directory structure. Each folder contains a name which identifies the folder. If a description is provided the name field is highlighted to indicate it is a link that can be clicked, at which time the folder description is displayed on the Google Earth image. Folders can be expanded or collapsed by clicking the box with a plus or minus sign.

Listing 2 adds fundamental building blocks that define the drawing styles used to paint visual line elements. Three styles are defined, ground path, signal path and tower. These elements are defined with the “Style” tag where the “id” attribute provides a unique identifier for the Style and are further defined with the “LineStyle” element that defines the color and width of the line. The “color” element requires explanation as it is in reverse order from the standard Red-Green-Blue-Alpha (RGBA) sequence where the three colors combine to produce a final color and the Alpha component defines the transparency of the color from clear to opaque. The order used by the KML “color”

element is Alpha-Blue-Green-Red expressed as hexadecimal (aabbgrr) values between x’00’ — no color or for Alpha, fully transparent to x’ff’ — full color or fully opaque. The line element width is expressed in pixels. The style “tower” defines a tower image that defaults to a yellow pushpin as an identifying marker and the “LineStyle” element defines the image to be drawn. Style elements that are to be used throughout a document cannot be defined within a Folder.

Before creating folders to contain the tower and repeater definitions the “Camera” element is inserted to provide an opening viewpoint to the generated map. Listing 3 shows a “Camera” element. Four defining elements control the camera position and range. The elements “longitude” and “latitude” provide the coordinates for the camera’s view point and are expressed in decimal degrees (dd.ddddd). Altitude (“altitude”) is the distance from the map surface to the camera position, expressed in meters. The angle of the camera view (“tilt”) can be set between 0 and 90 where 0 is directly above and 90 is perpendicular to the surface at the given altitude.

Listing 4 contains the elements to draw a tower image. Towers are defined using the “Placemark” element, which as the name implies marks a place on the map. To identify the tower the “name” element is included while “styleUrl” provides a link to the style definition used to draw the tower. Note the required “#” before the tower style, which identifies the preceding text as a style identifier.

“LineString” provides the coordinates where the tower image is to be drawn on

Listing 2 — Defining KML image Styles

```
<name>Example 2</name>
  <description>KI4SBB-WA4CWI Signal Path Analysis</description>
  <open>1</open>

  <!-- Define Ground Path Line -->
  <Style id='ground'>
    <LineStyle>
      <color>ff00ff00</color>
      <width>3</width>
    </LineStyle>
  </Style>

  <!-- Define Signal Path Line -->
  <Style id='signal'>
    <LineStyle>
      <color>ff0000ff</color>
      <width>3</width>
    </LineStyle>
  </Style>

  <!-- Define Tower image -->
  <Style id='tower'>
    <LineStyle>
      <color>ffc5c6be</color>
      <width>7</width>
    </LineStyle>
  </Style>
```

Listing 3 — Camera element which will focus view when KML file runs.

```
<!-- Define initial view when file opens in Google Earth -->
<Camera>
  <latitude>33.457212</latitude>
  <longitude>-86.801737</longitude>
  <altitude>10000</altitude>
  <tilt>0</tilt>
</Camera>
```

the map and the length of the line to be drawn representing the tower's height above ground. "Tessellate" specifies that the "LineString" will follow terrain changes and for the tower image is set to "0" or no. The tower height is specified relative to the ground at the given coordinates by using setting "relativeToGround" as the element of the "altitudeMode" tag. The "coordinates" tag performs double duty, defining the location coordinates of the tower and establishing the tower height above the ground terrain. Each coordinate pair gives the longitude,

latitude and height of the drawn image above ground, expressed in meters, with the three components separated by commas and the start and end coordinates separated by at least one space. No spaces can occur between the components in each coordinate. For a tower or signal path image that seems to be drawn incorrectly, this is the first item to check. If the location coordinates are not identical the tower image will be drawn as a diagonal.

Definitions for the repeater as well as the author's location are shown in Listing 5 in a folder similar to the towers folder. [Listing

5 and subsequent Listings are available for download from the ARRL *QEX* files website. See Note 8. — *Ed.*] To form these definitions, a "Placemark" element defines a name for the point and the nested "Point" element describes the location of the point on the map image. By default, the point will be marked on the map image with a yellow pushpin.

The contents of Listings 2 through 5 can be enclosed between the Document elements of Listing 1, saved as a ".kml" suffix file then double-clicked to open Google Earth. The location entries in the left sidebar can

Listing 4 — KML statements to define a tower image.

```
<Folder>
  <name>Towers</name>
  <open>1</open>

  <!-- Red Mountain Tower Definition -->
  <Placemark>
    <name>Red Mountain Tower</name>
    <styleUrl>#tower</styleUrl>

    <!-- Draw Tower Image -->
    <LineString>
      <tessellate>0</tessellate>
      <altitudeMode>relativeToGround</altitudeMode>
      <coordinates> -86.809722,33.484167,0
-86.809722,33.484167,94</coordinates>
    </LineString>

    <!-- Set Camera to open view when tower selected -->
    <LookAt>
      <latitude>33.48424</latitude>
      <longitude>-86.80955</longitude>
      <range>500</range>
      <tilt>80</tilt>
      <heading>0</heading>
    </LookAt>
  </Placemark>
</Folder>
```

be individually double-clicked to move the map focus to the clicked image. Adding the contents of Listing 6 completes the definition process needed to analyze a signal path. In the *QEX* file, **9x13_McCullers_Examples.zip**, this is Example 1. A Folder named “WA4CWI Signal Paths” is defined to hold the path definitions. All definitions required to draw the path images have been previously described and are combined differently to define the signal paths. Two images are drawn for each signal path, a ground image and a signal image using the ground and signal styles.

When a tower entry is double-clicked, the map flies to the designated location and looks down with bird’s eye view (0 tilt). To provide a better view, a “LookAt” element can be included in the definition. “LookAt” provides a similar function as “Camera”, establishing a view of a given location. Listing 7 illustrates a “LookAt” element, which can be compared to the “Camera” element in Listing 3. The differences between “Camera” and “LookAt” are that instead of “altitude” “LookAt” uses “range” in meters

from the target location coordinates to the designated view point and adds “heading,” which is the compass heading (0-360) the view is facing, where 90 is East, 180 South, 270 West and 0 or 360 North.

The ground path definition creates a line that follows the terrain changes along the path. The combination of `<tessellate>1</tessellate>` and `<altitudeMode>clampToGround</altitudeMode>` causes the drawing engine to draw the line following the ground terrain. In “coordinates” the altitude component is set to “0” for each coordinate.

The signal path definition changes “tessellate” and “altitudeMode” to `<tessellate>0</tessellate>` and `<altitudeMode>relativeToGround</altitudeMode>`, which instructs the drawing engine to draw a straight line between the points defined by the combination of coordinates and altitude. In our use, this represents the signal path between the antennas. The altitude component in each “coordinates” element is the antenna height expressed in meters relative to the ground.

Having completed a description of the

basic mechanics for producing graphic imagery with Google Earth, the next step is to demonstrate how these design elements are combined to visually represent a line-of-site path and how to analyze these paths using the Elevation Profile function.

A Broken Path

The author lives approximately 3.79 miles (6.1 km) from the KI4SBB D-STAR repeater, which uses a triband omnidirectional antenna side mounted at an elevation of 1259 feet (384 meters) above sea level. The author has a similar triband antenna located approximately 807 feet (246 meters) above sea level. Power levels for the 2 meter and 70 cm repeaters at this site are double that of the 23 cm repeater, resulting in a 3 dB difference in effective radiated power. Communication is possible on the 2 meter and 70 cm bands, but impossible on the 23 cm band.

Using a signal path drawn with Google Earth, we will determine if terrain changes are preventing 23 cm communication. Fig-



Figure 4 — Four mile 23 cm signal path interrupted twice by terrain peaks from Example 1.



Figure 5 — Tilted view of 23 cm signal path interruption from Example 1 accompanied by Elevation Profile showing signal path drawn from antenna to antenna with cursor pointing to first interruption point.

ure 4 shows the signal path with the “Camera” view focused approximately halfway between the two coordinates with the repeater site at the top of the image and the author’s site positioned lower in the image. Figure 4 was produced by Example 1 in the QEX files. The signal path is drawn in red while the underlying ground path is green (white and black in the images printed here). Looking at the map image, two sizeable gaps in the signal path occur toward the lower end of the path, indicating an incomplete path.

The next step is to determine the cause of these gaps in the signal path. Using a combination of tilt, compass rotation, and the range function, the image can be rotated to view the signal path along its “edge” as shown in Figure 5. It is easier to manipulate an image by first tilting the image, then rotating and moving the view point and finally changing the view range to highlight all or a portion of the path.

Looking at the image in Figure 4, it is apparent the two signal path interruptions are the result of two terrain peaks visible in the image, and the possibility of an uninterrupted line-of-site path between the repeater and the author’s location does not exist. To better examine the details, the image can be manipulated to move closer to the first interruption point as can be seen in Figure 5.

Testing using a mobile 23 cm radio showed the path interruption caused by the first terrain peak effectively eliminated communication along this path even at the second terrain peak on the image. This highlights the contribution of multi-path to signal propagation at lower frequencies and the possible contribution of the higher power output of the repeaters on the 2 meter and 70 cm bands.

We might conclude from the image in Figure 4 that the laws of physics have been circumvented by Google Earth and signals can disappear into the ground and later mysteriously reappear. This simply illustrates how Google Earth draws a line that is defined to be relative-to-ground. If the line height at a given point exceeds the terrain height the line is drawn, otherwise it is hidden. It is this drawing action that enables us to discover possible interruptions in the line-of-site path.

Using the Elevation Profile

While creating a visual path, then panning and scanning to locate possible terrain or structural interruptions is useful, doing it over long distances and with precision is difficult. Fortunately, Google Earth has added the Elevation Profile function, which greatly reduces the work required to analyze a path and at the same time allows a visual view of

the path. Analyzing a path is simple. Right click on the ground path entry, in this example “KI4SBB – WA4CWI Ground Path”, then double-click “Show Elevation Profile” in the pop-up dialog box. The elevation profile, showing the terrain between the two coordinate points appears in Figure 6 with the first coordinate shown on the left (repeater) and the second coordinate on the right (the author’s location). The distance of a particular terrain feature from the first coordinate can be determined from the “X-Axis” scale expressed in meters while the terrain height can be determined from the “Y-Axis” scale, also in meters.

One negative result of opening an elevation profile is that Google Earth re-oriens the image to an overhead view (0 tilt) centered between the coordinate points. It can be frustrating to watch a carefully panned and scanned view suddenly disappear after the decision is made to view the elevation profile but this is a minor problem given the usefulness of the profile. Once the Elevation Profile is displayed, the image can be manipulated once again and will not be disturbed again. It is simpler to first open the Elevation Profile for a path then double-click on the path name to view and manipulate the path image.

A feature of Elevation Profile is matching cursors between the profile and the image

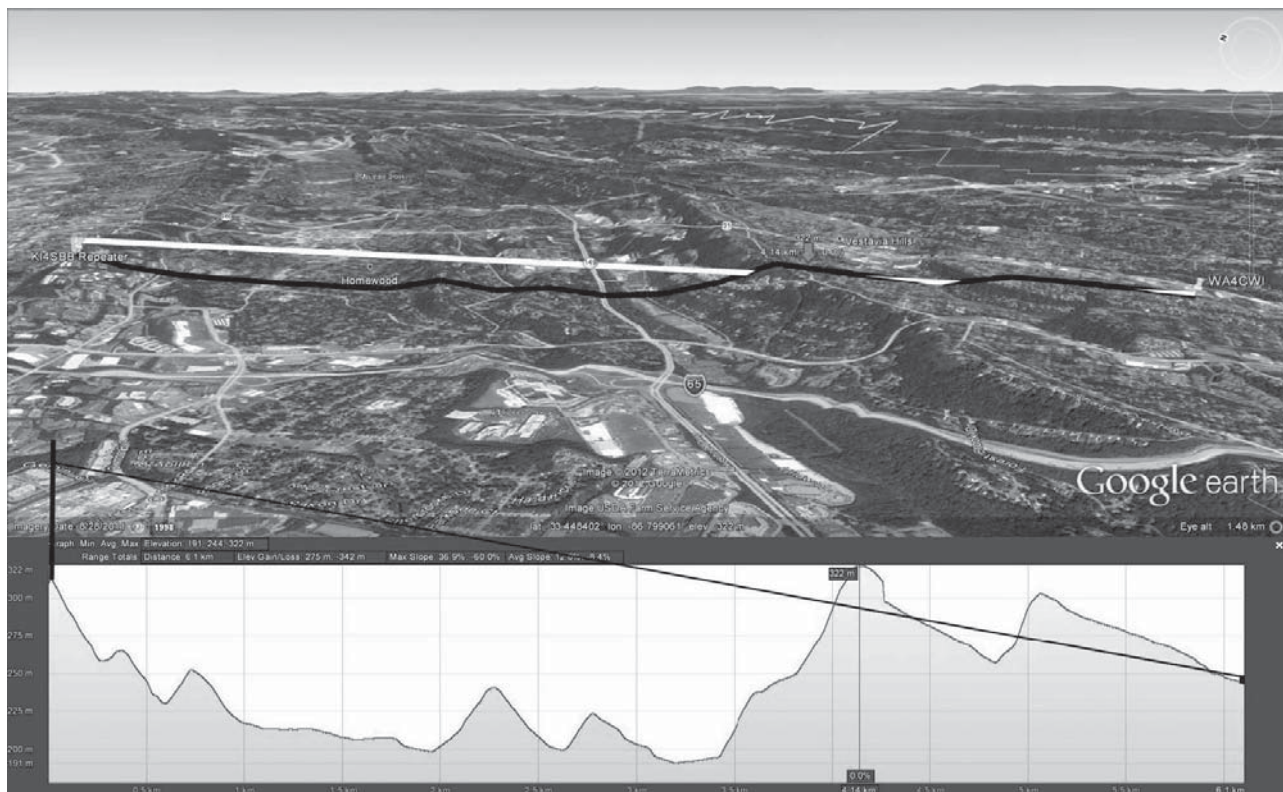


Figure 6 — Close up image of 23 cm signal path interruption. Double-click “KI4SBB – WA4CWI Signal Path” in left side panel in Example 1 to view.

path shown in Figure 6. As the mouse cursor is moved within the Elevation Profile window, data boxes follow the cursor, giving distance from the left coordinate, height at the intersection point of the cursor and terrain grade slope. Simultaneously an arrow cursor traces the path on the map surface giving the same information. As the cursor moves, the position coordinates and altitude of the map cursor are updated providing a means of determining the coordinates of any point along the path. In Figure 6, the cursor is positioned to point to the initial interruption of the line-of-site path shown in the close-up view of Figure 5.

Trust the Ground Path

When selecting a path as input to Elevation Profile, only the ground path should be selected because using the signal path will result in a false elevation profile. Unlike drawing a straight line between two points, Elevation Profile creates a terrain slice based on the given three dimensional coordinates. If a signal path is selected, the antenna heights become the terrain reference points and the created terrain slice will be in a sense an amplified representation of the true ground terrain between the points. Nothing is wasted, however, because the signal path

Elevation Profiles can be used to determine the spacing between the ground and signal path at any location along the path. With the Elevation Profile active for the signal path, move the cursor to locate a reference point to be analyzed and note the signal height at that point. Then, open the Elevation Profile for the ground path, move the cursor to the same reference point and read the ground height. The difference between the two values is the signal path height above ground at that point.

Looking at the Elevation Profile in Figure 6 the ridge interfering with the line-of-site signal path is obvious. Determination of potential path interference is not often this simple especially over longer distances, and some form of visual line representing the signal path as it crosses the terrain slice is helpful. It would be nice to draw on the Elevation Profile using KML but this is not possible. Here is where ‘ingenuity’ becomes important. The Google Earth image including the Elevation Profile can be captured and saved. Then, using either a paint or photo program or by manual drawing, the legend at each end of the path can be extended to account for the antenna height above ground level followed by drawing the line-of-site path between the antenna points.

Capturing the Google Earth image is accomplished by clicking “File” on the Toolbar

followed by “Save” then “Save Image” or “File/Save Image” if running Mac OS X. A dialog box opens allowing the image to be saved as a JPEG file. If the desire is to capture the Elevation Profile cursor at a given point along the path, the process just described will not work as moving the cursor to the Toolbar also moves the Elevation Profile cursor. To capture the image, keyboard shortcut combinations must be used to open the file save dialog. For Windows the combination is Control-Alt-S and for Mac OS X the combination is Command-Option-S. The next step is to open the resulting JPEG file using an image editor, extend the legend at both path ends by extrapolating the antenna height using the ground height legend scale as a reference, then draw the line-of-site path between the extended antenna height points. Any terrain feature that intersects with the drawn line-of-site path can be assumed to be a potential signal interference point.

The signal path line in Figure 6 demonstrates this technique. While this technique is not absolutely accurate due to the judgments required to interpret the antenna height and add the antenna heights to the vertical scale, it is accurate enough to make observations concerning terrain interference along the path. A note of warning here: The Elevation Profile height scale is not fixed and can vary based

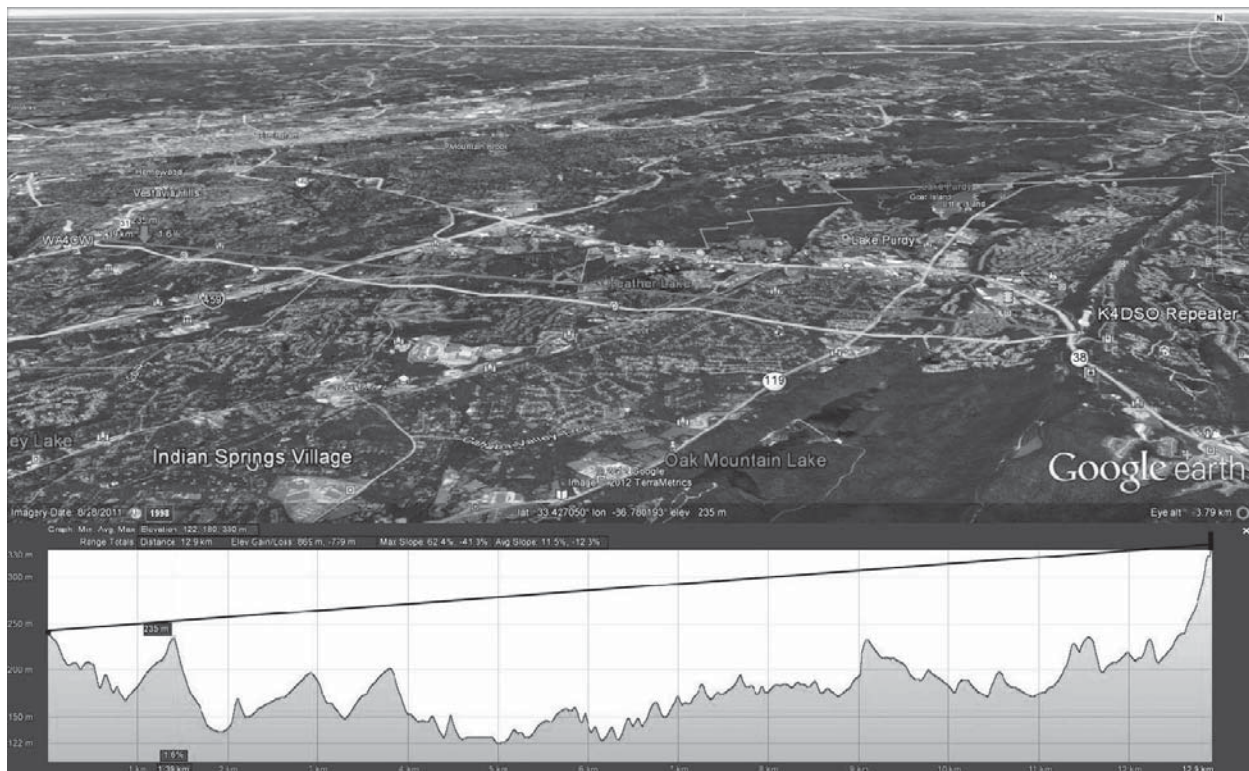


Figure 7 — Side view of clear 23 cm path showing Elevation Path with drawn signal path. Double-click on “WA4CWI – K4DSO Ground Path” in Example 3 to view.

on the relative height and height difference between the end points. The scale height, measured between the horizontal grid lines should be checked for each image and a scale factor determined. Since the vertical scale is given in meters, it is easy to measure the grid line difference in millimeters and create a meter scale factor as (grid line difference in millimeters / scale division units in meters).

If access to an image editor is not available or if there is a desire for a more accurate rendering of the path, the image can be printed, the antenna height interpolated against the elevation scale and that measurement used to extend the legend to account for the antenna height above ground and the line-of-sight path manually drawn.

While using an image editing program to draw the signal path line is fast and provides a permanent copy, if accuracy is important, the hand drawn approach is preferred.

A Path to Perfection

One of the advantages of having multiple repeater locations is the potential that if a path to a particular repeater is unusable, a path to another repeater may be available. Although the path length is double that of the previous example, a direct line-of-site path exists from the author's location to another 23 cm D-STAR repeater with power output

equal to that of the previous example. Figure 7 illustrates this path with accompanying Elevation Profile and plotted signal path. The KML source for this image is found in Example 2 in the QEX files, which replaces the tower, repeater and path definitions to create a new view. The Elevation Profile cursor in Figure 7 points to the closest intersection point between the ground and signal paths. Communication is excellent along this path as would be expected from the path analysis.

Path Planning

Having the ability to visualize and explain signal path problems resulting from terrain interference is a valuable tool for the experimenter as well as for the repeater manager who is constantly asked about areas with weak or non-existent signal coverage. Even more valuable is a tool that can provide assistance in determining if a line-of-site path is possible between two locations.

Figure 8 demonstrates an analysis of the repeaters used by BARC covering the Birmingham, Alabama area. The source code for this view is Example 3 in the QEX files. The image reveals that all three paths are intact, which should result in excellent line-of-sight communication between repeater pairs.

The closest intersection point between ground and signal occurs on the right side

of the foreground path in Figure 8 pointed to by the Elevation Profile cursor showing a ground height of 338 meters. A close up view of this point is shown in Figure 9.

This peak is interesting because it almost interrupts the signal path. This raised the question of whether communication would be possible on a path from the ground level of one of the repeater sites to the antenna height of the other. A 23 cm test was made from the access road of the KI4SBB repeater, which is situated about two meters below the base of the tower. The antenna was a mobile tri-band vertical mounted on an SUV approximately two meters above ground level. The KML source code for the path illustrated in Figure 10 is found in Example 4 in the QEX files. Figure 10 shows the signal path intersecting the ridge peak slightly below the top. Communication was possible along this path but marginal, and movement of the vehicle short distances made the differences between working and not working. Without a directional antenna, it was impossible to determine if the working and not working points were the result of "knife-edge diffraction" propagation over the interfering peak or multi-path propagation from a large water tower adjacent to the tower, the tower itself or other surrounding structures.

Figure 10 demonstrates two anomalies with Elevation Profile. The Elevation Profile

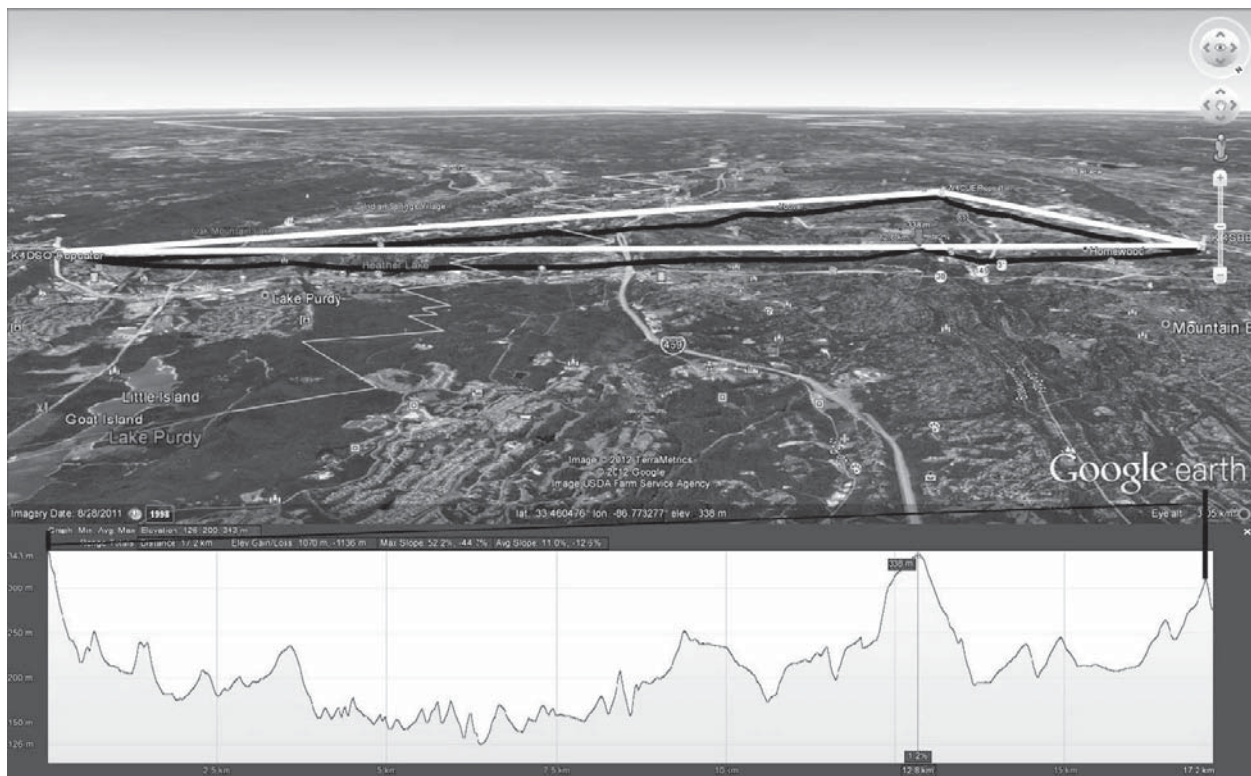


Figure 8 — Birmingham Amateur Radio Club repeater arrangement, showing clear signal paths between all repeaters. Elevation Profile cursor points to location where ground and signal paths almost intersect. In Example 3 double-click "Ground Path" under K4DSO – KI4SBB Path Analysis to view.

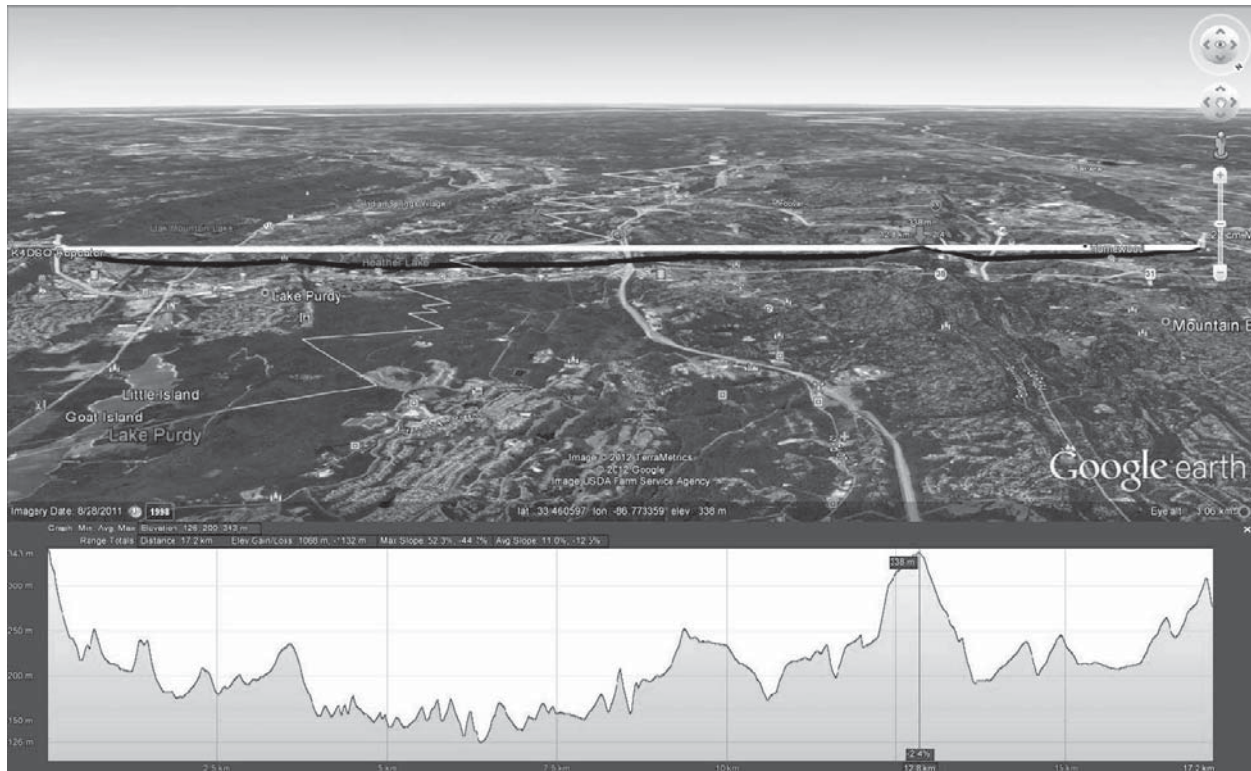


Figure 9 — Close-up view of signal and ground path intersection from Example 3. Double-click “Signal path” under “K4DSO – KI4SBB Path Analysis” to view.

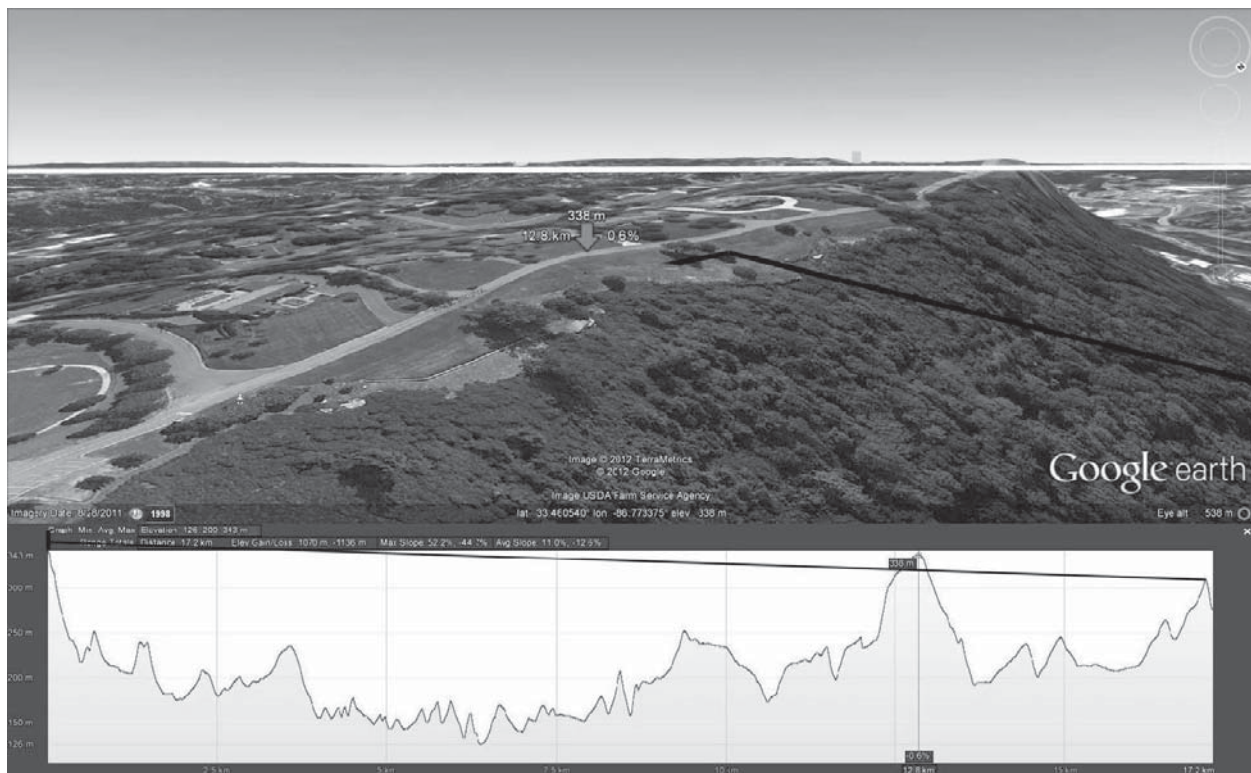


Figure 10 — Limited 23 cm mobile to repeater signal path resulting from signal path interference near the top of a mountain peak..

should begin at the first coordinate address in the path definition and end at the second. From Figure 10 one would conclude that the terrain peak on the right side of the profile is directly in front of the tower, which is not the case. The peak is the actual location of the tower. This anomaly is also visible on the Google Earth image by moving the cursor around the tower site and noting the elevation notation on the image. Three-dimensional imagery is created in Google Earth by combining aerial photography with topographic maps using contour lines to map the terrain in a given area. Variations in the coordinate to topographic map contour combine to produce the anomalies displayed in Figure 10. Having some knowledge of the coordinate location is a plus in understanding problems of this type.

Also notice the slight location difference between the peak in the plotted ground path peak, which is an averaged value, and the Elevation Profile cursor which was positioned to the highest elevation point in the viewing area. This is a combination of the explanation presented in the last paragraph and the combination of viewing position and tilt. Neither anomaly affects the effectiveness of using these techniques to analyze signal paths.

A Practical Application

Proper planning is always a requirement for any RF installation and more so for

amateur repeater installations, which must provide adequate coverage at the lowest possible cost. Not only must the cost of the repeater, controller and antenna be included but consideration must be given to the cost of feed line, tower rigging, as well as the cost to install both the feed line and the antenna. Any solution that provides the required coverage for low cost must be considered.

Figure 11 demonstrates using KML to provide analysis of optimum antenna locations to meet the requirement detailed above. The study involves providing a backup repeater site that in normal conditions provides remote receiver input to extend the coverage area of the primary repeater. This study is based on the availability of prepared antenna space at one tower site and a determination of the lowest possible antenna height on the second tower that will provide the coverage needed for the link between the sites.

Figure 11 was created by Example 5 in the QEX files and is a modification of the KML statement used to produce the three-site image in Figure 8. The third tower and path definitions were removed and three additional signal paths added, terminating at heights of five, fifteen and thirty meters on the second tower. As can be determined from running the example and viewing the paths, all four paths are more than adequate theoretically. Practically, due to foliage surrounding the tower site, the five and fifteen meter heights can be eliminated and the as-

sumption made that the optimum antenna height is somewhere between fifteen and thirty meters. All four signal paths have been drawn on the elevation profile at the bottom of Figure 11 to further illustrate the antenna height possibilities and resulting signal paths.

Conclusion

Whether a repeater manager is attempting to show an amateur why they cannot communicate with a particular repeater or a microwave group is preparing a mountain top to mountain top attempt, good path visualization and analysis tools are a necessity. Hopefully, this article demonstrates the usefulness of using Google Earth and KML as a tool to assist in predicting the possibility for successful communication using line-of-sight paths over any terrain. Once the technique is understood and a basic KML document created, changes in location and antenna height can be quickly and easily modeled, visualized and analyzed, all for the cost of a bit of time to download and learn Google Earth and KML.

Acknowledgments

Many thanks to Ken Adkisson, WB-4FAY, who chairs the Birmingham Amateur Radio Club Repeater Committee; for his contribution to the club over many years, his encouragement and assistance in preparing this article.

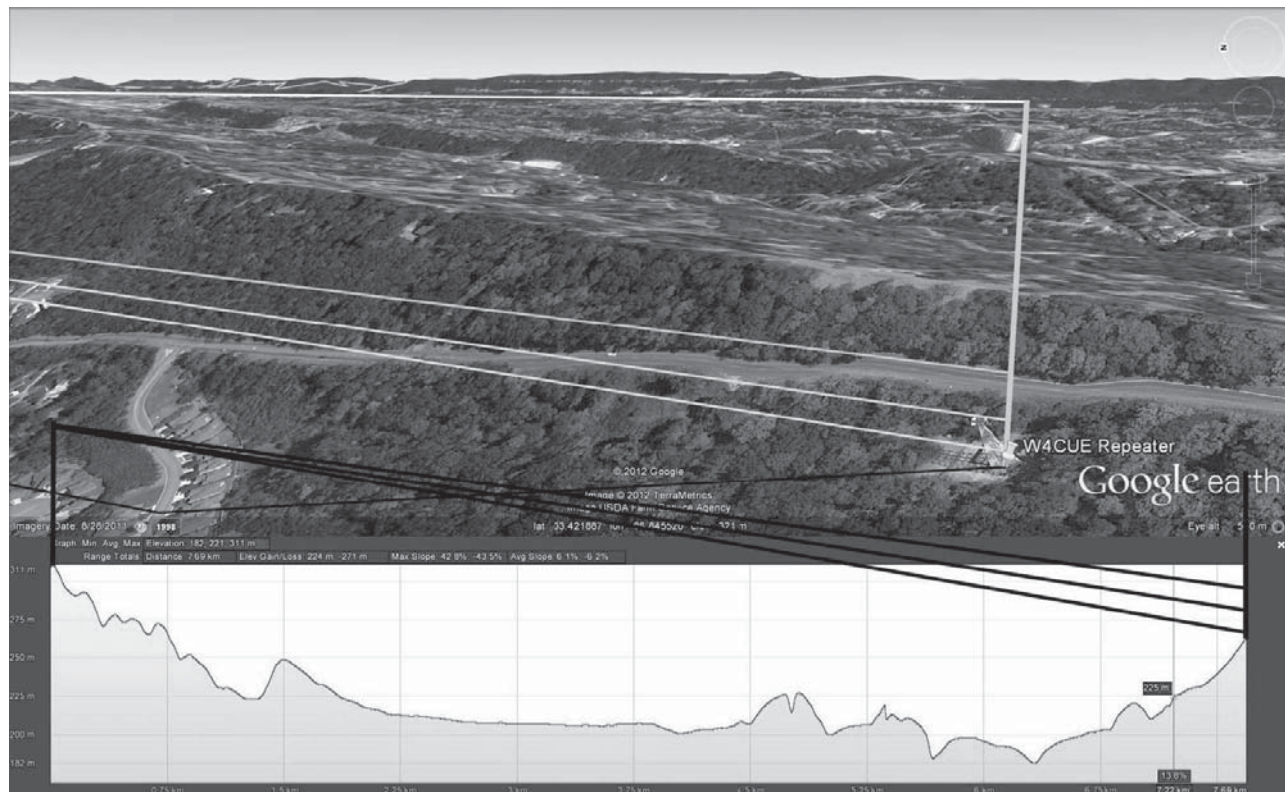


Figure 11 — Four signal plots at 5, 15, 30 and 112 meters to estimate minimum antenna height for remote receiver link antenna.

Jim McCullers, WA4CWI, is an ARRL Member and was first licensed in 1962 as WN4CWI and currently hold an Extra Class license. His primary Amateur Radio interests are homebrewing of any type and problem solving, which he does more than operate. He still enjoys working HF DX.

Jim's current interests are DSP, SDR, experimenting with higher frequencies and building test gear.

Jim holds a BA in Philosophy from Sanford University, Birmingham, Alabama. He spent a majority of his early career developing main-frame operating and communications systems. After leaving the corporate world, he became a serial entrepreneur, having started and sold a communications company and is currently developing medical products incorporating mobile and tablet devices.

Notes

¹One example of a software package that can analyze a signal path over varied terrain is the Terrain Analysis Package (TAP[®]) by Softwright. For more information, see www.softwright.com/.

²To learn more about BARC, visit their website at <http://w4cue.com/>.

³Visit the FCC website at <http://www.fcc.gov>.

⁴Color versions of the Google Earth screen shots for this article are available for download from the ARRL QEX files website. Go to www.arrl.org/qexfiles and look for the file **9x13_McCullers_Images.zip**.

⁵You can learn more about local TV and FM radio broadcast coverage, including maps at www.tvfool.com and www.fmfool.com.

⁶Learn more about Google Earth and download the program at www.google.com/earth.

⁷All images used in this article are the property of Google and providers TerraMetrics and the USDA Farm Services Agency.

⁸Complete details about Keyhole Markup Language (KLM) are available at <https://developers.google.com/kml/documentation/kmlreference>.

⁹The KLM code listings for this article are available for download from the ARRL QEX files website. Go to www.arrl.org/qexfiles and look for the file **9x13_McCullers_Listings.zip**.

¹⁰The example files for this article are available for download from the ARRL QEX files website. Go to www.arrl.org/qexfiles and look for the file **9x13_McCullers_Examples.zip**.

Array Solutions Your Source for Outstanding Radio Products

Top-ranked Measurement Equipment from Array Solutions

Announcing the: **PowerAIM 120** Vector Impedance Analyzer for Broadcast Engineers

- Patented, unique technology offers the broadcast engineer the full capabilities of a single port network analyzer
- Small, lightweight, software-driven instrument
- Easy to carry on airlines and in the field.
- Very simple to set up and use.
- Safe measurements in RF-dense broadcast environments.
- Time Domain Reflectometer (TDR) Functions.



Vector Network Analyzer Model **VNA 2180**

Measures impedance magnitude, phase and transmission parameters for antennas, filters, and discrete components - using one or two ports.

- Frequency range is 5KHz to 180MHz.
- Data plots include: impedance, SWR, return loss, S11 and S21.
- Plots can be saved for before and after comparisons.
- Dual Smith charts with zoom and rotation.
- Time Domain Reflectometer (TDR) Functions.
- New - 6 port VNA multiplexer for measuring directive arrays including Phase/Magnitude vector scope software.



Bird Wattmeter Digital Display Conversion Kits

Upgrade for your Bird analog watt meter that will transform your Model 43 into a state of the art digital meter!

AS-43A Average Power Reading Bird Wattmeter Kit Digital meter kit
AS-43AP Peak Power Reading Bird Wattmeter Kit Digital meter kit



AIM *uhf* Analyzer

- Frequency range from 5 kHz to 1 GHz.
- Data plots include SWR, RL, R + X, series and parallel, magnitude, phase, and more.
- Dual Smith charts with rotation and 20 markers.
- Plots and calibration files can be saved and used anytime in cvs and dynamic formats.
- AIM 4170C is still in production covering 5kHz to 180 MHz.
- Time Domain Reflectometer (TDR) Functions.



PowerMaster II

- New Larger, Sharp & Fast LCD Display
- Reduced Energy consumption
- USB and RS-232 interface built-in
- New - Both 3kW and 10kW couplers on one display - switched
- Hi / Lo Power Level Monitoring
- Supports 2 like couplers simultaneously (3kW & 3kW, 3kW & V/UHF, 10kW & 10kW)
- SWR Threshold Protection (with amp PTT bypass)



Single and Dual Rack Mount available
New "Power Master Basic" Software FREE!



www.arrayolutions.com

Sunnyvale, Texas USA
Phone 214-954-7140
sales@arrayolutions.com
Fax 214-954-7142

See our web site for other products and additional details.

Blood Lead Levels in Australian Amateur Radio Operators—A Pilot Study

Dr. Heinzle describes an informal study that he did with members of two Australian Amateur Radio clubs.

The 2006 Restriction of Hazardous Substances (RoHS) directive in the European Union required consumer electronics manufacturers to replace traditional 63/37 eutectic lead-tin solder (ELTS) with lead free solder (LFS) alternatives. This was prompted by concerns relating to electronic waste in landfills ultimately leaching lead into groundwater.¹

ELTS is an old but effective technology, in use for at least 2000 years. The elder Pliny described the importance of a eutectic mixture for effective soldering around AD 78 in *Naturalis Historia*.^{2,3} ELTS, being a eutectic alloy, occupies the metallurgical “sweet spot” of the lead/tin binary phase diagram, at which molten solder of minimal viscosity quickly solidifies on cooling with little or no intermediate pasty phase. The eutectic mix also melts at a lower temperature than other lead/tin compositions (183°C or 361.4°F).⁴

In contrast, LFS is usually either pure tin, or a binary, tertiary or quaternary alloy of tin, with added silver, copper, bismuth, antimony, zinc, indium or germanium, potentially posing new ecological hazards in their own right.^{1,5}

Although formulated to mimic as closely as possible the desirable characteristics of ELTS, the use of LFS can result in thermal, mechanical and metallurgical incompatibilities with existing components. Higher melting points can be incompatible

with existing soldering equipment, the components being soldered, and existing ELTS joints, as well as ELTS coatings on components and circuit boards. See Notes 1 and 5.

The absence of lead can make LFS more prone to tin whisker growth, whereby dendrites of tin can grow, altering circuit characteristics, short circuiting adjacent circuit traces, or breaking off and causing short circuits elsewhere.⁶ The absence of lead can also make soldered joints less resistant to mechanical failure from shock, and from “tin pest,” caused by temperature dependent allotropic transformation of tin with thermal cycling. See Note 4.

Concerns about LFS reliability in safety-critical and high-reliability devices in aviation, telecommunications, military and medical applications have led to continued RoHS exemptions in these areas.^{7,8}

These concerns about reliability, the difficulties in reworking defective LFS joints, the need to maintain or restore older electronic equipment, the need to terminate heat sensitive cables, the fabrication of RF tight enclosures, as well as continued use of existing soldering equipment, have led to a continued preference for ELTS among electronic hobbyists.

In addition to ongoing promotion of construction activities among Amateur Radio operators, there is similar promotion in Scouting and school environments. The rise of the “Maker” movement has also encouraged hands on electronic experimentation among budding scientists,

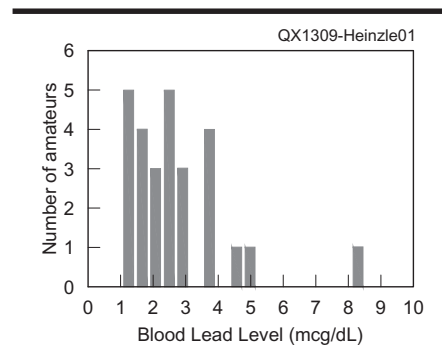


Figure 1 — Distribution of blood lead levels in the 27 test subjects.

engineers and programmers, with cheap and flexible development platforms such as the Arduino, PICaxe, and Stellaris Launchpad.

This ongoing use of ELTS among Amateur Radio operators and the potential for lead exposure while soldering by Amateur Radio operators and electronic hobbyists generally, was the motivation for this pilot study.

A literature review found that electronic soldering has not been associated with geometric mean blood lead levels (BLL) in excess of 10 mcg/dL in the occupational context, although hypersensitivity to soldering flux constituents and other pyrolysis products such as isocyanates from nearby plastics is well described.⁹⁻¹⁷ No published studies of BLLs in electronic hobbyists were found.

[Note that the abbreviation “mcg/dL”

¹Notes appear on page 43.

would be read as “microgram per deciliter.” Many readers would expect that to be written as µg/dL, which would follow standard usage of the Metric System prefixes. We have left it as mcg/dL in this article because that seems to be the way it is specified in the medical community. — *Ed.*]

This is in contrast to the elevated BLLs frequently found with ELTS use in radiator repair work, which typically employs far higher temperatures, using oxygen-acetylene or oxygen-propane torches, with the potential for metal vaporization, along with grinding, grit blasting or brushing of the ELTS joints.^{18, 19}

Amateur Radio operators, particularly those of the homebrewing persuasion, were thought to be representative of the most avid recreational users of ELTS. In contrast to commercial premises, the typical environment in which Amateur Radio operators solder is without engineered exposure controls such as local exhaust extraction, and no formal safety management systems bringing attention to and managing the lead hazard. Amateur Radio operators were therefore considered to reflect a worst case recreational exposure to ELTS in electronics.

The current study aimed to establish if radio amateurs in the home environment using ELTS were likely to have a BLL at or above the World Health Organization (WHO) recommended exposure limit of 10 mcg/dL, thereby helping to inform routine hygiene practices when soldering, and as an aside, determine the likelihood of hobby electronics influencing the results of occupational BLL monitoring in lead industry workers.

Methods

I approached the organizing committees of two metropolitan Amateur Radio clubs in Adelaide, South Australia, to see if the clubs would be interested in participating in the proposed pilot study. Both clubs, the Adelaide Hills Amateur Radio Society (AHARS) and the North Eastern Radio Club (NERC), expressed interest in participation.

Participation of members was voluntary, and the research adhered to the principles espoused in the Declaration of Helsinki (2008 revision). Results of the research were shared with the participants to foster understanding among club members of the lead hazards associated with soldering.

In order to select the most active solder-using subgroup of the Amateur Radio community, 16 AHARS members were sampled at a construction night attended by members intending to construct a club project that evening. Similarly, 11 NERC members were sampled at a technical meeting attended by members who often

Table 1
Summary of Results

<i>Parameter</i>	<i>AHARS</i>	<i>NERC</i>	<i>Pooled</i>
Sample Size (n)	16	11	27
Minimum BLL (mcg/dL)	1.04	1.04	1.04
Geometric Mean	2.39	2.09	2.26
Median BLL (mcg/dL)	2.28	2.28	2.28
Arithmetic Mean BLL (mcg/dL)	2.77	2.53	2.68
Maximum BLL (mcg/dL)	8.07	3.73	8.07
Standard Deviation (SD)	1.77	1.00	1.50
Geometric SD	1.70	1.60	1.65

engage in project construction on these technical meeting nights.

At each of the radio club meetings, I obtained informed consent from interested members, after which blood was taken in 4 ml K-EDTA tubes, stored at ambient temperature overnight, and couriered the morning after the respective meetings to the Institute of Medical and Veterinary Science (IMVS) in Adelaide, South Australia. All samples were tested using inductively coupled plasma mass spectrometry (ICPMS) on a PerkinElmer ELAN DRC II.

Results

The statistical analysis of environmental or biological variables in the field of occupational hygiene is often complicated by log-normal data distributions, detection limits for contaminants that may cause zero values among data sets, and small sample sizes.^{20, 21}

In addition, approaches usually employed for large log-normally distributed datasets, such as the generalized confidence interval (GCI) method, or modified Cox method, can be computationally complex, yet can over or under estimate confidence intervals in smaller datasets.²²

The method described by Zou and others was chosen to determine a 99% confidence interval (CI) for the geometric mean of the BLL data, which was found to range from 2.18 mcg/dL to 2.32 mcg/dL.²²

At the 99.9% confidence level, this resulted in a left tail error, demonstrating some of the statistical difficulties associated with the interpretation of log normal data distributions in similar contexts.

Discussion

In keeping with screening for environmental and occupational exposures generally, the results of this study were in the form of a small, log-normally distributed data set. Despite the small sample size, analysis of the results using the method described by Zou suggests that ELTS use among active

radio amateurs is associated at a 99% level of confidence with a geometric mean BLL of between 2.18 mcg/dL and 2.32 mcg/dL. This is well below the WHO recommended threshold of 10 mcg/dL.

Interpretation of the results was simplified by the absence of BLLs below the detection limit and by the study group coming from a wider population with low BLLs generally, thereby allowing meaningful conclusions to be made without requiring statistical comparison with a non ELTS using control group.

Conclusions

Based on the results of this study, recreational use of ELTS in electronics can be considered unlikely to cause geometric mean BLLs at or above the WHO recommended exposure threshold of 10 mcg/dL (99% CI: 2.18 mcg/dL to 2.32 mcg/dL).

By extension, activities encouraging electronic construction in schools or Scouting can be considered unlikely to pose a significant risk of lead exposure.

Recommendations

The study results suggest that recreational use of ELTS in electronics can be considered unlikely to significantly confound interpretation of BLL results in workers undergoing routine BLL surveillance for occupational exposure, where exposure thresholds are typically greater than 10 mcg/dL.

If the traditional hierarchy of controls is applied to the risk of lead toxicity posed by ELTS use among Amateur Radio operators and electronic hobbyists generally, the metallurgical and thermal issues affecting LFS at present make outright prohibition or replacement of ELTS impractical.

Given that the risk of lead toxicity in Amateur Radio operators from electronic ELTS use appears to be low, ongoing attention to simple ventilation and hand washing would appear to be proportionate and sufficient controls for electronic hobbyists using ELTS.

Acknowledgements

I would like to thank the organizational committees of AHARS and NERC, who allowed their members to be approached about involvement in the study, the members who subsequently volunteered, and Dr Alex Kutlaca, for statistical advice.

This work was funded solely by the author.

Dr Erich Heinzle, VK5HSE, is working towards specialist qualifications in industrial and environmental medicine, an area which provides an interesting mix of physics, chemistry, engineering and medicine. Erich enjoys designing and building electronic equipment, with a bit of microcontroller programming thrown in for fun; the "i-kaktuss" iambic keyer and Morse trainer is a recent example.

Notes

- ¹O.A. Ogunseitan. "Public Health and Environmental Benefits of Adopting Lead-Free Solders," *The Journal of the Minerals Metals and Materials Society (TMS)*, Vol 59(7), pp 12-17 (2007).
- ²E. Paparazzo. "Pliny the Elder on the Melting and Corrosion of Silver With Tin Solders," *prius liquescat argentum ... ab eo erodi argentum* (HN 34.161). *Classical Quarterly*, Vol 53(2), pp 523-529 (2003).
- ³E. Paparazzo. "Pliny the Elder on Metals: Philosophical and Scientific Issues," *Classical Philology*, Vol 103(1), pp 40-54 (2008).
- ⁴W. Plumbridge. "Tin Pest Issues in Lead-Free Electronic Solders," *Journal of Materials Science: Materials in Electronics*, Vol 18(1), pp 307-318 (2007).
- ⁵E. P. Wood and K. L. Nimmo. "In Search of New Lead-Free Electronic Solders," *Journal of Electronic Materials*, Vol 23(8), pp 709-713 (1994).
- ⁶K. Zeng. "Lead-Free Soldering: Materials Science and Solder Joint Reliability," *Journal of Minerals, Metals and Materials Society*, Vol 61(6), pp 28 (2009).
- ⁷K. J. Puttlitz and G. T. Galyon. "Impact of the ROHS Directive on High-Performance Electronic Systems: Part I: Need for Lead Utilization in Exempt Systems," *Journal of Materials Science: Materials in Electronics*, Vol 18(1), pp 331-346 (2007).
- ⁸K. J. Puttlitz and G. T. Galyon. "Impact of the ROHS Directive on High-Performance Electronic Systems: Part II: Key Reliability Issues Preventing the Implementation Of lead-Free Solders," *Journal of Materials Science: Materials in Electronics*, Vol 18(1), pp 347-365 (2007).
- ⁹C. D. Barrett and H.D. Belk. "Blood Lead Study of Long Term Hand Soldering Operators." *Journal of Occupational Medicine*, Vol 19(12), pp 791-794 (1997).
- ¹⁰K-R. Kim, S-W Lee and N-W Paik. "Cross-Sectional Analysis of Blood Lead Level of Entire Korean Lead Workers," *Industrial Health*, Vol 44(2), pp 318-327 (2006).
- ¹¹P. S. Burge, M. G. Harries, I. M. O'Brien and J. Pepys. "Respiratory Disease in Workers Exposed to Solder Flux Fumes Containing Colophony (Pine Resin)," *Clinical Allergy*, Vol 8, pp 1-14 (1978).
- ¹²I. W. Fawcett, A. J. Newman Taylor, and J. Pepys. "Asthma Due to Inhaled Chemical Agents — Fumes From 'Multicore' Soldering Flux and Colophony Resin." *Clinical Allergy*, Vol 6(6), pp 577-585 (1976).
- ¹³C. L. Goh and S. K. Ng. "Airborne Contact Dermatitis to Colophony in Soldering Flux," *Contact Dermatitis*, Vol 17(2), pp 89-91 (1987).
- ¹⁴I. A. Greaves, D. H. Wegman, T. J. Smith and D. L. Spiegelman. "Respiratory Effects of Two Types of Solder Flux Used in the Electronics Industry," *Journal of Occupational Medicine*, Vol 26(2), pp 81-85 (1984).
- ¹⁵G. M. Liss, W. E. Halperin and P. J. Landrigan. "Occupational Asthma in a Home Pieceworker," *Archives of Environmental Health* Vol 41(6), pp 359-362 (1986).
- ¹⁶D. P. G. Paisley. "Isocyanate Hazard From Wire Insulation: An Old Hazard in a New Guise," *British Journal of Industrial Medicine*, Vol 26(1), pp 79-81 (1969).
- ¹⁷W. H. Perks, P. S. Burge, M. Rehahn and M. Green. "Work Related Respiratory Disease in Employees Leaving an Electronics Factory," *Thorax*, Vol 34(1), pp 19-22 (1979).
- ¹⁸R. H. Goldman, E. L. Baker, M. Hannan and D. B. Kamerow. "Lead Poisoning in Automobile Radiator Mechanics," *New England Journal of Medicine*, Vol 317(4), pp 214-218 (1987).
- ¹⁹D. H. Lussenhop, D. L. Parker, A. Barklind and C. McJilton. "Lead Exposure and Radiator Repair Work," *American Journal of Public Health*, Vol 79(11), pp 1558-1560 (1989).
- ²⁰K. Krishnamoorthy, T. Mathew and G. Ramachandran. "Generalized P-Values and Confidence Intervals: A Novel Approach for Analyzing Lognormally Distributed Exposure Data," *Journal of Occupational Environmental Hygiene*, Vol 3(11), pp 642-650 (2006).
- ²¹K. Krishnamoorthy, and T. Mathew. "Inferences on the Means of Lognormal Distributions Using Generalized P-Values and Generalized Confidence Intervals," *Journal of Statistical Planning and Inference*, Vol 115, pp 103-121 (2003).
- ²²G. Y. Zou, C. Y. Huo and J. Taleban. "Simple Confidence Intervals for Lognormal Means and their Differences with Environmental Applications," *Environmetrics*, Vol 20(2), pp 172-180 (2008).

From MILLIWATTS
To KILOWATTSSM
More Watts per DollarSM

In Stock Now!
**Semiconductors
for Manufacturing
and Servicing
Communications
Equipment**

- **RF Modules**
- **Semiconductors**
- **Transmitter Tubes**

Se Habla Español • We Export

Phone: **760-744-0700**
Toll-Free: **800-737-2787**
(Orders only) **800-RF PARTS**
Website: **www.rfparts.com**
Fax: **760-744-1943**
888-744-1943
Email: **rfp@rfparts.com**



RF PARTS
COMPANY
From Milliwatts to KilowattsSM

A Model for Sporadic E: Meteors+ Wind Shear+Lorentz Force

The author describes a possible explanation for sporadic E propagation conditions.

At the moment the most accepted theory to explain the formation of the sporadic E (E_s) region of the ionosphere is wind shear, but this theory does not fully explain the formation of the E_s region. I have conducted further studies and hypothesized another model, always connected to wind shear, but that introduces the contribution of meteors that ionize at the 100 km altitude, with the electrons concentrated in a dense layer by Lorentz Forces. I will call this model “Wind Shear and Lorentz Force.” The previous models and theories considered an accumulation of ions. How is this theory different? The change concerns the concentration of free electrons, not positive ions, because the electrons are responsible for ionospheric refraction, as we will see.

[Others have described similar or related explanations of enhanced E_s propagation. See, for example, the articles by Jim Kennedy, KH6/K6MIO, and Gene Zimmerman, W3ZZ (SK), in *DUBUS*.¹ — Ed.]

The Zonal Winds

The key to understanding Sporadic E is given by meteorology, and specifically the mesospheric winds. The “raw material” is provided from meteorites entering the atmosphere and burning due to friction caused by their very high speed as they enter the atmosphere. The result of this vaporization is both ions and oxidized ions, by combination with oxygen ions present at that altitude (created by UV rays). A metal atom from the meteorite loses an electron and becomes a positive ion. In the short term, wind speed varies the most, but it is also the most difficult parameter to predict

and control. It shows significant variations in amplitude on a local scale. There is a significant seasonal trend, due to a complex mechanism of large-scale atmospheric circulations, (Consider that the Polar Vortex is the system that virtually governs the weather in middle latitudes). These winds in summer months show a clear trend, with a trend from west to east, on top (about 110 km) and an opposite direction to the lowest height (90 km), in other words, from east to west. See Figure 1.

Meteor Stream

In the E Region of the ionosphere, in addition to the gas composing the atmosphere, there is a continuous flow of particles of various sizes (meteor dust, mostly metal) from outer space with high kinetic energy, which collide with the particles in the atmosphere. The collisions cause the transformation of their kinetic energy into heat energy, consequently we have their vaporization and ionization

The gas present in these areas, has been enriched with metal ions and their electrons. In the case of pressure differences, all the component particles move like the wind, electrons included.

Lorentz Force

In physics the force acting on an electrically charged object that moves in a magnetic field is called the Lorentz Force. The main feature of the Lorentz Force is that it is always directed perpendicularly to the direction of motion and perpendicular to the magnetic field. Therefore it does not do mechanical work (change of kinetic energy), but it only affects the trajectory of the charged particle, since it is a deflecting force.

The Lorentz Force is the force, F , exerted by the electric field, E , and the magnetic field, B , on the charge, q . It is proportional to the vector product between velocity, v , and magnetic field, B , according to the equation:

$$F = q(E + V \times B)$$

where:

F = Lorentz Force

q = electric charge

V = instantaneous velocity

E = electric field

B = magnetic field

\times is the vector cross product

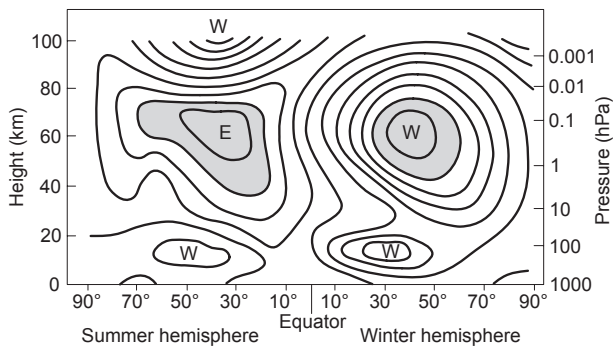
All boldface variables are vector quantities

The Lorentz Force Applied to the Ionosphere and to the Direction of the Zonal Winds

The rule of the force acting on an electric current immersed in a magnetic field is very clear and has no exceptions, if electrons and positive ions move in the same direction, the forces on them are of opposite sense. The Earth’s magnetic field, oriented South-North, is orthogonal to the direction of the reverse winds. The Lorentz Force separates the positive ions from the electrons, accumulating electrons in the central region and dispersing the positive ions outward.

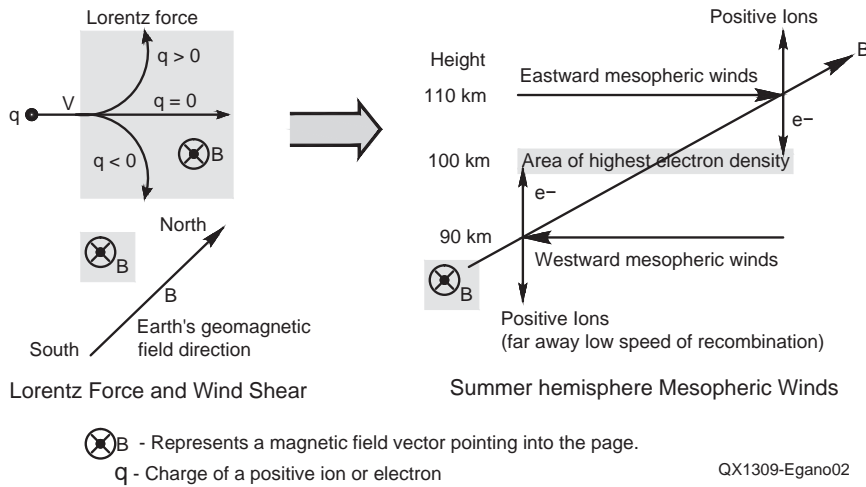
During the winter months, the wind circulation is reversed and this case is the reverse phenomenon, where the electrons are scattered and the positive ions focused. The refraction of the electromagnetic wave is due to electrons. This factor, combined with the higher contribution of meteors in summer, is the cause of the pronounced summer occurrence. Then, when the upper wind goes in one direction (and the lower one

¹Notes appear on page 48.



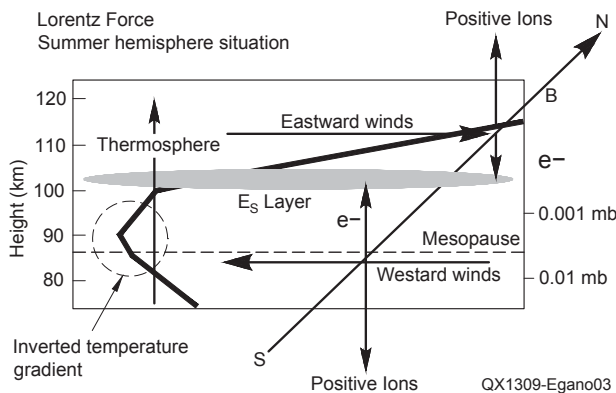
QX1309-Egano01

Figure 1 – The general circulation of winds: The zonal currents in the stratosphere (below) and in the Mesosphere (above) are subject to a seasonal reversal process. From the graph we can see that in the summer hemisphere, the prevailing winds have a trend from west to east, above 100 km of altitude, and from east to west, below. (W = Winds from the west, E = winds from the east). Image source : Department of Atmospheric Sciences and Climate – CNR, Italy.



QX1309-Egano02

Figure 2 — Schematic model of Wind Shear and Lorentz Force, responsible for the concentration of the layer of electrons. This scheme applies to the summer months, where the dominant trend is eastward winds (above) and westward (below). The accumulation of free electrons is possible only with this composition of the zonal wind. The refraction of radio waves in the ionosphere is due to the concentration of free electrons, N.



QX1309-Egano03

Figure 3 — This diagram describes what happens at an altitude of around 100 km. The Lorentz Force is associated with the winds and with the force lines of magnetic field, B, which flow from south to north.

From **MILLIWATTS**
To **KILOWATTS**
More Watts per Dollar



Transmitting & Audio Tubes



COMMUNICATIONS
BROADCAST
INDUSTRY
AMATEUR

Immediate Shipment from Stock

3CPX800A7	4CX1000A	810
3CPX1500A7	4CX1500B	811A
3CX400A7	4CX3500A	812A
3CX800A7	4CX5000A	833A
3CX1200A7	4CX7500A	833C
3CX1200D7	4CX10000A	845
3CX1200Z7	4CX15000A	6146B
3CX1500A7	4CX20000B	3-500ZG
3CX3000A7	4CX20000C	3-1000Z
3CX6000A7	4CX20000D	4-400A
3CX10000A7	4X150A	4-1000A
3CX15000A7	572B	4PR400A
3CX20000A7	805	4PR1000A
4CX250B	807	...and more!

Se Habla Español • We Export

Phone: **760-744-0700**

Toll-Free: **800-737-2787**

(Orders only) **RF PARTS**

Website: **www.rfparts.com**

Fax: **760-744-1943**

888-744-1943

Email: **rfp@rfparts.com**



in the other), positive ions are concentrated; when it goes in the opposite direction (and vice versa for the lower one), the electrons are concentrated. Since the electrons are the cause of refraction of the electromagnetic wave, we have E_s layer formation when there is accumulation of electrons, and this occurs with a specific condition of Zonal winds, as shown in Figure 1. In practice, the combined action of winds and the Lorentz Force creates a separation between the positive ions and electrons. Figure 2 shows a model of how the Lorentz Force acts on the positive ions and the free electrons in the ionosphere.

The Ionospheric Refraction Depends on the Electron

When an electromagnetic wave enters the ionosphere, the electric field of the wave produces a displacement of the electrons and positive ions; the displacement of the ions is much more limited than the electrons, because the electrons weigh much less than the ions (about 2000 times less in the case of hydrogen, the lighter gas), thus we consider only the movement of electrons.

Figure 4 — A comparison of the probability of Sporadic E (upper panel) with the daily ft E_s— top frequency for E_s (lower panel). The graphs reveal a significant correspondence between the curve of E_s of Rome Ionosonde and probabilistic graph above. (Source: IK3XTV elaboration on data of GFZ German Research Centre for Geosciences and INGV Rome Ionosonde.)

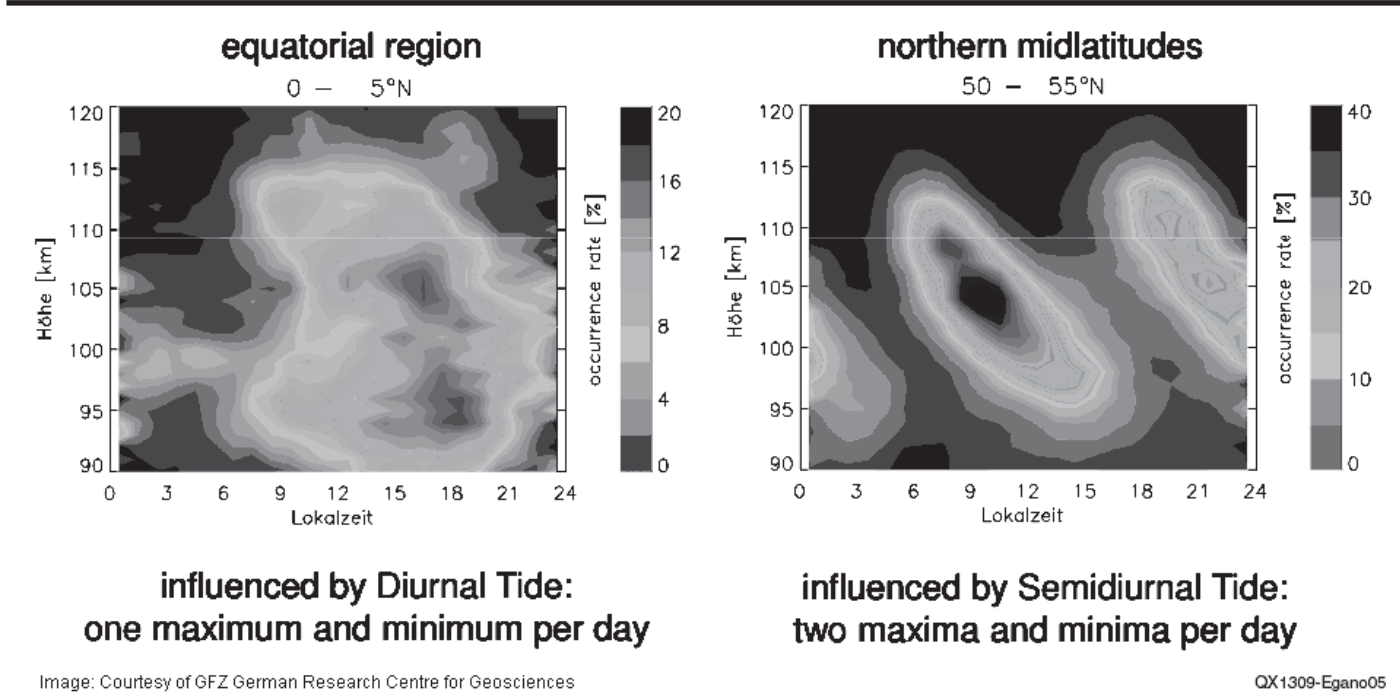
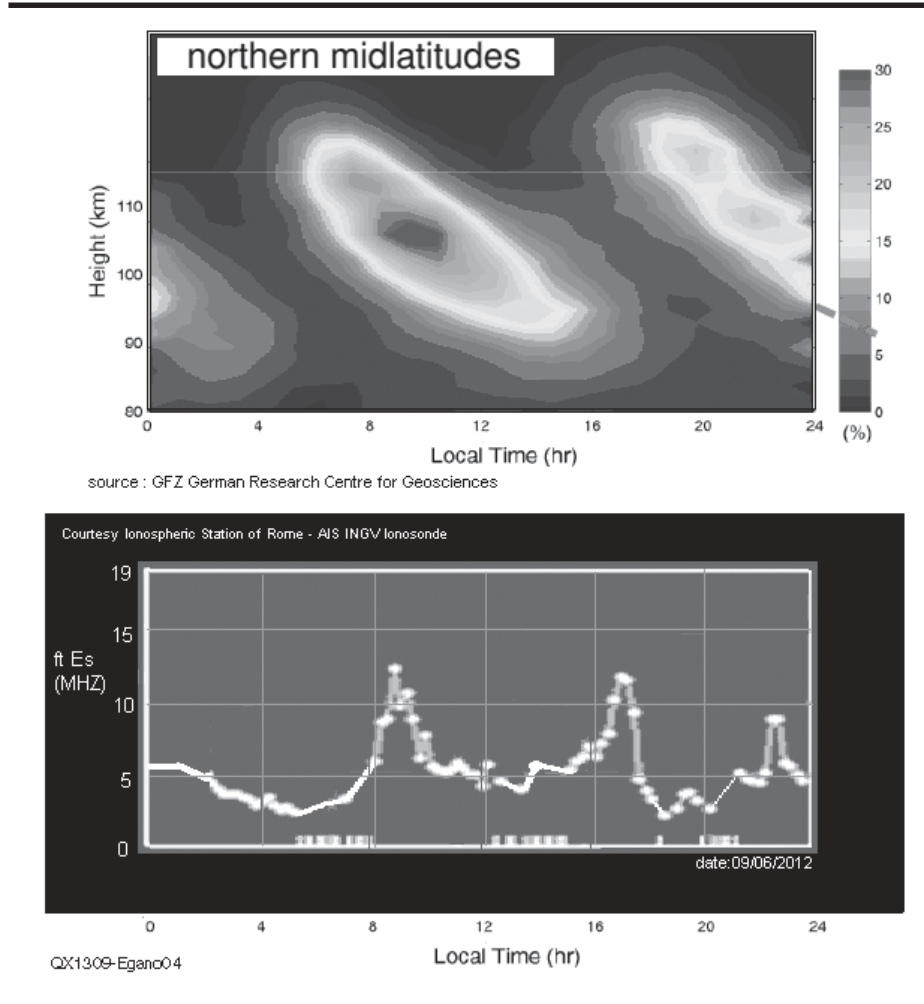


Figure 5 — These graphs illustrate the probability of E_s, with one maximum and minimum per day in equatorial regions and two maxima and minima per day for midlatitudes during the summer (northern latitudes shown here). Image courtesy of GFZ German Research Centre for Geosciences.

The refractive index is proportional to the density of free electrons expressed as N . The wave is refracted as a result of interaction with free electrons.

1) If an ion is dragged away by the wind, this represents an electric current. If there is a magnetic field perpendicular to this current, and it creates a force that acts on the ions in the direction perpendicular to the plane containing the velocity vector, v , and the magnetic field vector, B . If this plane is horizontal, the force is vertical.

2) Since there are periodic winds at an altitude of about 80-90 km in one direction, and winds in the opposite direction at an altitude of about 110-120 km, electrons (negative charges) present in these altitudes are concentrated in a layer at an altitude of about 100 km because those electrons in the lower wind current undergo an upward force, and the electrons of the upper wind current are subject to a force in the opposite direction. See Figure 3. Positive ions (positive charges) undergo the reverse process.

3) At this altitude you can see some of the electrons and ions, especially metal ones, which burn at an altitude of about 80 km; in the summer months a minimum E_s layer is always there. This is also confirmed by recent studies at the University of Crete, that with very sensitive instruments detected the presence of E_s layer that is not detected by Ionosonde (less sensitive). The density of the layer is proportional to the velocity, magnetic field and ion density, which may help explain why the phenomenon varies so much from day to day.

The daily wind variations have distinctly stronger amplitudes. Daily variations result from atmospheric tides with periods that are equal to, or multiples of a solar day. While the magnetic field is influenced by solar events, and the number of meteorites varies over time. One possible explanation is that of these three variables (wind velocity, magnetic field, presence of ions) the only one that varies more in a short time is the speed of the wind.

Some Observations

A) When the winds create a shear, a certain concentration arises in the middle. When the winds have the opposite shear, thinning occurs instead of concentration, because the forces are reversed. This is consistent with the observed temporal duration of the layer.

B) The wind blows in the same direction on the electrons and positive ions, but the force due to the magnetic field that acts on the positive ions has the opposite direction to that which acts on the electrons. So, the electrical balance is valid not only locally but also for a global scale. In the sense that the dense E_s layer is formed only by electrons, while the positive ions are moved above and below. This is also the most logical explanation of the

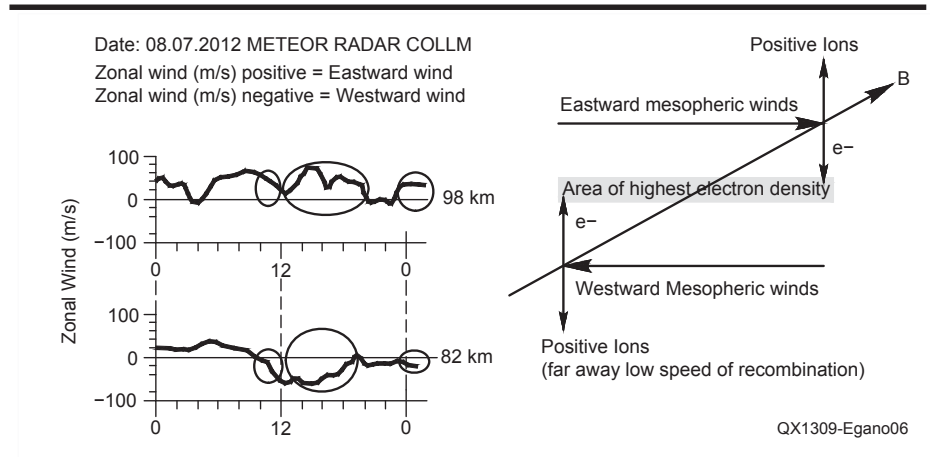


Figure 6 — This is an example of practical use with meteor radar Collm that records the speeds of the zonal winds at high altitude. The height is listed on the right of the diagram. Image elaborated by IK3XTV on data from meteorologic radar of Collm. http://www.uni-leipzig.de/~meteo/de/wetterdaten/radar_wind.php.

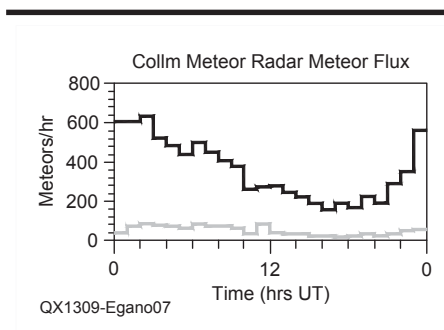


Figure 7 — Flow curve of the meteors from the Meteor Radar-Collm Germany.

long time of recombination.

In the normal ionospheric layers, for example (the highest layers), which are formed as a result of UV radiation, there is no separation of positive ions and electrons, and in fact, given the proximity, there is a continuous process of recombination, slowed only by the intense solar ionization process. When the sun sets the recombination is fast, no matter what type the ions are. Also, if they were metallic, recombination would be quick, since the force of attraction between an electron and a positive ion depends only on the square of the distance between both particles, independent of the nature of the ions.

Forecasting Model

A reliable prediction is currently not possible because we cannot have real-time data on the amplitude and phase of the winds at high altitude. It is possible to create a probabilistic model starting from the crucial fact that the time of possible openings is governed by atmospheric tides, or the amplitude of the diurnal variation of winds. Figure 4 shows the Sporadic E occurrence rate at 40-45° Latitude. The wind

shear exhibits two daily peaks. Near these peaks, there is the best chance of sporadic E (Semidiurnal Tides). We highlight two maxima and two minima per day (24 hours).

Sporadic E Expectation Model

Figure 5 illustrates the probability of E_s on local time. These graphs are divided by latitude.

Therefore, the atmospheric tides are the important thing, since their amplitudes can be larger than the mean wind, they will form negative (from eastward to westward) shear also, and then E_s can form. In fact, if one could predict the tidal shear correctly it would be possible to predict the diurnal E_s maximum. With some uncertainty this is already possible, but there is no good model for the intensity (mean fo E_s or critical frequency for E_s propagation) and also for the exact time since tides are variable from day to day. A comparison was published in *Annales Geophysicae* 2009.²

Figure 6 is an example of the practical use of the meteor radar Collm, which records the speeds of the zonal winds at high altitude.

Variation of Meteor Stream

The Meteor stream is not constant but has some variation. There is a seasonal variation (the mean meteor stream is about 6 times higher in summer months) and there is a diurnal variation (peak in the morning followed by gradual decrease) and an hourly variation.

Figure 7 shows the flow curve of the meteors from the Meteor Radar-Collm Germany. The peak flow occurs early in the morning followed by a gradual decrease during the day. Note the time difference between the arrival of the larger amount of mass weathering and the hours

of occurrence of E_s due to migration by the Lorentz Force. The dispersion of meteoric material depends on size. There is a wide dispersion of particles, because the dimensions are very different. The larger particles vaporize at lower altitudes, while the smaller particles vaporize at higher altitudes. The accumulation is subsequently created by the Lorentz Force.

Some Considerations

The Lorentz Force deflects the electron trajectory until it moves horizontally; when an electron moves vertically the Lorentz Force ceases to act and the electron continues to coast with the speed reached. The fewer the positive ions in its path, the greater the probability that the wind will be reversed, and again the Lorentz Force will act to slow down the electron. Since the central area that will vaporize the meteoric dust is about 90 km, and this coincides with the inversion region of the winds, the bulk of the contribution by meteors remains neutral. If we consider that the larger corpuscles vaporize farther down, in the lower level of the winds, there is a possibility that the formation of the E_s layer is predominantly a phenomenon from the bottom upwards. In

this case the electrons will cross the back-end neutral reversal of the winds and would be concentrated by slowing down within the upper band of wind. This could explain the difference in height between the E_s layer and the neutral band inversion.

Conclusion

This model is well suited to explain the pronounced summer seasonal occurrence of the E_s phenomenon, and the slow process of ion recombination. It also shows that we can have occurrence of E_s only when the reverse winds exhibit a precise vector (the winds above moving to east and winds below moving to west). If these vectors change direction, we have a dispersion of electrons and then E_s formation is not possible. In the summer hemisphere, the prevailing direction of the mesospheric winds is favorable to the accumulation of free electrons. During the winter months, the prevailing wind direction is reversed. The difficulty at the moment is to predict the amplitude and direction of the winds, and this is a big problem for the prediction.

Note: Hypotheses and models are valid for the middle latitudes.

1) Formation of the Winds.

The local heating causes a decrease

in density because the increased thermal agitation causes increased distance between the particles, in other words there is a decrease of the local pressure (tide). Particles of lower density, being immersed in the Earth's gravitational field, rise to higher altitudes and cool for expansion.

A lower central area of low pressure and an upper central of high pressure is formed. This causes a flow of particles towards the centre of low pressure (lower zonal wind) and an increased distance between particles in the center of the high pressure area (zonal wind above).

2) Hypothesis of Asymmetric E_s Layer

The hypothesis discussed so far provides a symmetrical pattern with winds above and below. Also, an asymmetric formation is possible. Even this case depends on the meteorological day and particle size. In fact, even in the "symmetrical E_s " case, electrons must be stopped by an opposite wind, otherwise they would be lost to dispersion. In the symmetric case, I think they are stopped by electrostatic forces of repulsion, but especially for braking by the opposite wind. It is not necessary, for the formation of an E_s layer, that the electrons must come from above and below together. They could be lifted up by the lower wind and then stopped by the opposite upper wind.

I want to thank Giorgio Marchi, IK1UWL, for his collaboration on this study.

Flavio Egano, IK3XTV, has been an Amateur Radio operator since 1993, with a Class A license. He is an ARRL member and a member of ARI, the Italian Amateur Radio Association). For many years he has been committed to radio propagation studies.

Flavio is an electronic engineering technician in Italy, and he works as a technical salesman for a multinational company.

He lives with his wife and their daughter in Thiene (Vi) Italy.


Notes


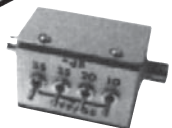


¹Jim Kennedy, KH6/K6MIO, Gene Zimmerman, W3ZZ (SK), "Extreme Range 50 MHz E_s : East-West (EWEE)," *DUBUS*, Hamburg, Germany, Issue I, 2012, p 51 and "Extreme Range 50 MHz E_s : North-South (TEFE)," *DUBUS*, Issue III, 2012, p 63.

These articles are included in *Technik XII* (2011-12), available from the *DUBUS* website: www.dubus.org/.

²C. Arras, C. Jacobi, and J. Wickert, "Semidiurnal Tidal Signature in Sporadic E Occurrence Rates Derived from GPS Radio Occultation Measurements at Higher Midlatitudes," *Annales Geophysicae*, 27, 2555-2563, 2009. Arras and Wickert with the Helmholtz Centre Potsdam, German Research Centre for Geosciences (GFZ), Department 1: Geodesy and Remote Sensing, Germany and Jacobi with The University of Leipzig, Institute for Meteorology, Germany.

NATIONAL RF, INC.



 <p>VECTOR-FINDER Handheld VHF direction finder. Uses any FM xcvr. Audible & LED display VF-142Q, 130-300 MHz \$239.95 VF-142QM, 130-500 MHz \$289.95</p>	 <p>ATTENUATOR Switchable, T-Pad Attenuator, 100 dB max - 10 dB min BNC connectors AT-100, \$89.95</p>
 <p>TYPE NLF-2 LOW FREQUENCY ACTIVE ANTENNA AND AMPLIFIER A Hot, Active, Noise Reducing Antenna System that will sit on your desk and copy 2200, 1700, and 600 through 160 Meter Radio Signals! Type NLF-2 System: \$369.95</p>	 <p>DIAL SCALES The perfect finishing touch for your homebrew projects. 1/4-inch shaft couplings. NPD-1, 3 1/2 x 2 3/4, 7:1 drive \$34.95 NPD-2, 5 1/8 x 3 5/8, 8:1 drive \$44.95 NPD-3, 5 1/8 x 3 5/8, 6:1 drive \$49.95</p>

NATIONAL RF, INC
7969 ENGINEER ROAD, #102
SAN DIEGO, CA 92111

858.565.1319 FAX 858.571.5909
www.NationalRF.com

Down East Microwave Inc.

We are your #1 source for 50MHz to 10GHz components, kits and assemblies for all your amateur radio and Satellite projects.

Transverters & Down Converters, Linear power amplifiers, Low Noise preamps, coaxial components, hybrid power modules, relays, GaAsFET, PHEMT's, & FET's, MMIC's, mixers, chip components, and other hard to find items for small signal and low noise applications.

We can interface our transverters with most radios.

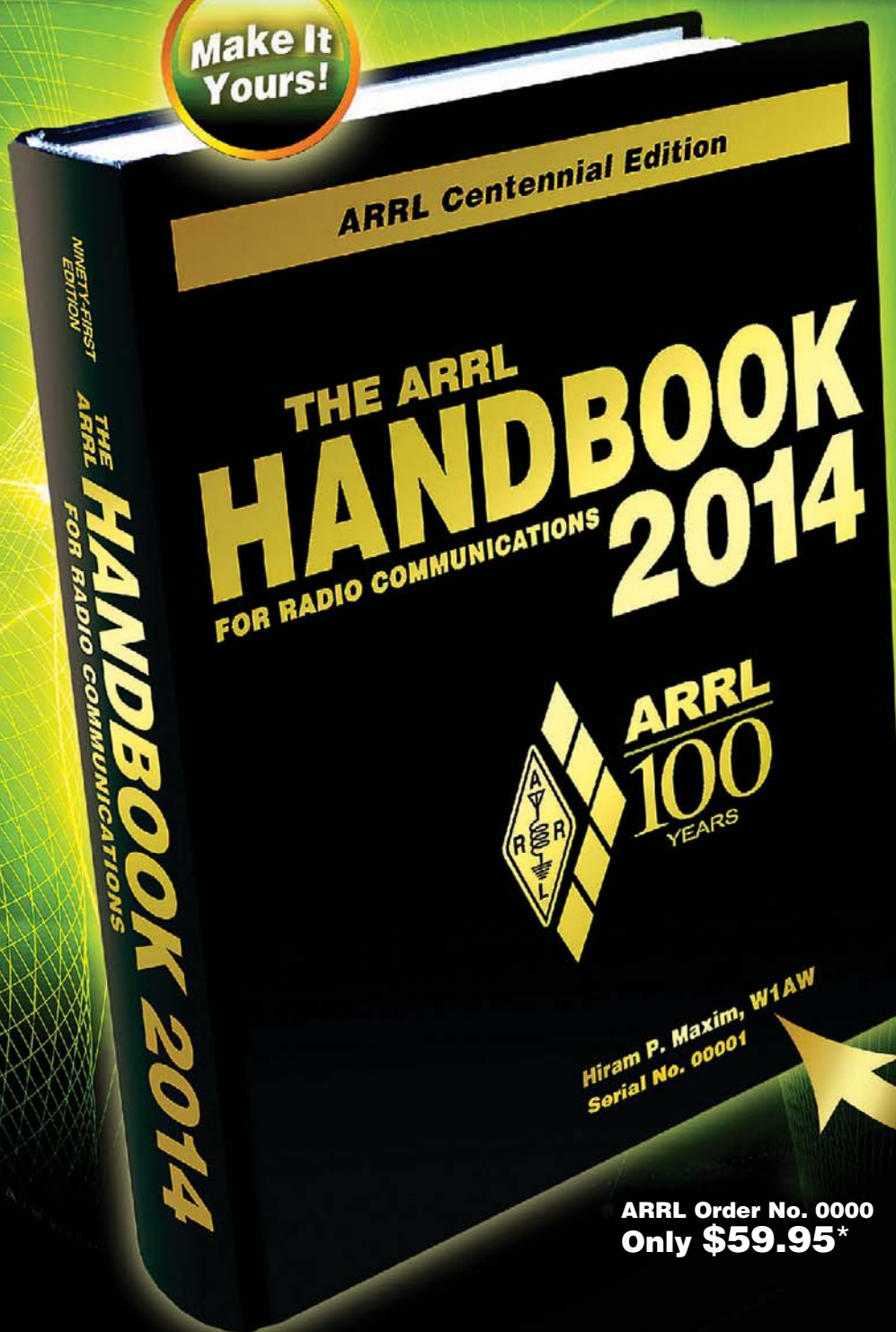
Please call, write or see our web site
www.downeastmicrowave.com
for our Catalog, detailed Product descriptions and interfacing details.

Down East Microwave Inc.
19519 78th Terrace
Live Oak, FL 32060 USA
Tel. (386) 364-5529

ARRL Centennial Edition

Celebrate 100 years of ARRL with the 2014 Handbook!

Make It Yours!



NEW! The 2014 ARRL Handbook

Celebrate ARRL's first 100 years of advancing the art and science of radio with this commemorative **ARRL Centennial Edition of The Handbook**. Always updated, this edition has been extensively revised to reflect the latest technology and innovation in the field of applied electronics and communications. Written by radio amateurs...for radio amateurs, and other experimenters, engineers and students.

Order your personalized copy today!

Features:

- Gold foil/embossed hardcover
- Personalized with your NAME and CALL SIGN
- Serial numbered commemorative edition
- Major new edition: components, new projects, latest technology
- Fully searchable CD-ROM included

The perfect gift for any ham!

YOUR HANDBOOK. MAKE IT YOURS.

Personalize the cover with your NAME and CALL SIGN (optional). Pre-orders begin shipping in October!

**ARRL Order No. 0000
Only \$59.95***

* Shipping and handling charges apply. Sales Tax is required for all orders shipped to CT, VA, and Canada. Prices and product availability are subject to change without notice.

** Actual book appearance may vary slightly from the representation in this ad.

ARRL The national association for
AMATEUR RADIO®



www.arrl.org/shop

Toll-Free US 888-277-5289,
or elsewhere +1-860-594-0355

Discrete Component Analyzer

Identifies and measures transistors, MOSFETs,
J-FETs, diodes, LEDs and more.
Pocket sized and battery powered.
Visit our Web Site for more details.



RED GREEN BLUE
Gate Srce Drn +

Gate threshold
 $V_{GS}=0.25V$ +



LCR Analyzer

Identifies and measures
inductors, capacitors,
and resistors. Optional
tweezers for SMD
components
More info and
downloadable manuals
on our Web Site.



Inductance
16.3μH +

Capacitance
72.50μF +



Quicksilver Radio Products

Sign up on our Web Site for your free newsletter.
Ham Radio news, articles, & special discounts.